

IMPACT OF HUMAN ACETYLCHOLINESTERASE'S STEREOSELECTIVITY FOR
NERVE AGENTS & SUBSEQUENT REACTIVATION

by

STEPHANIE MARIE BESTER

(Under the Direction of Scott Pegan)

ABSTRACT

The intentional use of organophosphate (OP) nerve agents and pesticides pose a significant health threat through their inhibition of human acetylcholinesterase (hAChE), which serves a critical role in neurotransmission. Their recent use in the assassination of the half-brother of the North Korean leader, the ongoing Syrian Civil War, and the United Kingdom has reaffirmed their relevant toxicity. Inhibition of AChE occurs when the catalytic serine becomes covalently modified by the nerve agent adduct. AChE displays stereoselectivity for OP nerve agent binding resulting in stereospecific toxicities of these agents. Oxime reactivators are one of the current treatments for OP exposure, which seek to reverse nerve agent conjugation of the hAChE active site serine prior to aging. However, the therapeutic efficacy of these agents varies based on the OP used, the stereochemistry of the OP, and the origin species of AChE. Currently the factors that influence reactivator efficacy are not well-understood including the influence of AChE's stereoselectivity on the accommodation of OP nerve agent stereoisomers and their impact on subsequent reactivation. Due to these issues, there is a strong need to develop novel reactivators. However, until now there were lingering questions about the mechanism of

reactivation. In addition, the means to accommodate certain nerve agents and reactivators into the active site is potentially due to the flexibility of certain regions of hAChE, but these dynamics are not well-understood. This study aims to fill these major gaps in knowledge to provide insight into the dynamics of the active site and its ability to accommodate a wide variety of OP nerve agents and reactivators. Through modified Ellman's assays and X-ray crystallography, this study examines the impact of hAChE's stereoselectivity on inhibition and reactivation, the influence of different nerve agents and their subsequent reactivation on hAChE's active site, and the structural and biochemical effects of monomerizing hAChE via site-directed mutagenesis. These studies provided the first structural insight into the ability of hAChE's active site to accommodate nerve agents and reactivators, elucidated some of the factors that influence this accommodation, and developed a tool for assessing the flexibility and dynamics of the active site.

INDEX WORDS: Acetylcholinesterase, Nerve Agent, Organophosphate, Reactivator, Inhibitor, Hydrolase

IMPACT OF HUMAN ACETYLCHOLINESTERASE'S STEREOSELECTIVITY FOR
NERVE AGENTS & SUBSEQUENT REACTIVATION

by

STEPHANIE MARIE BESTER

B.A., Rollins College, 2015

A Dissertation Submitted to the Graduate Faculty of The University of Georgia in Partial
Fulfillment of the Requirements for the Degree

DOCTOR OF PHILOSOPHY

ATHENS, GEORGIA

2019

© 2019

Stephanie Marie Bester

All Rights Reserved

IMPACT OF HUMAN ACETYLCHOLINESTERASE'S STEREOSELECTIVITY FOR
NERVE AGENTS & SUBSEQUENT REACTIVATION

by

STEPHANIE MARIE BESTER

Major Professor:	Scott Pegan
Committee:	William Lanzilotta
	Shelley Hooks
	Y. George Zheng

Electronic Version Approved:

Suzanne Barbour
Dean of the Graduate School
The University of Georgia
May 2019

DEDICATION

I would like to dedicate my dissertation first and foremost to my family. I recognize the distance between us has taken its toll on all of us. However, all of you have helped and supported my decisions at every step. Mum, you have always and forever will be my greatest advocate and inspiration. You taught me to be my own person and always set an example for the woman I want to be one day. I will never NOT need you, no matter the time or distance. My niece and nephew, CeCe and Leo, I have missed you every moment of every day. You two are the light of my life. Lou & Cassandra, I love you both and thank you for always putting up with me. Dad, thank you for believing in me, knowing that you are so proud of me means a lot. Nana, you are my partner in crime and I am always flattered when people say how similar we are. You taught me that no matter what happens, you keep moving forward. To my Papa, it breaks my heart that you cannot be here to see this moment. You were always there with a snarky comment and a sly smile. I know you were always so proud of me and bragged about my every accomplishment. I hope you knew how much I loved and respected you and how my life was forever changed for you being in it.

And for my loving partner, Brendan, who wakes up every day and looks at me with a sleepy smile, just happy I am still there, thank you for making every day better, every accomplishment more meaningful, and every second worth living. I know you would disagree, but you do not know the extent that you have helped me get through all this. I can be the worst at times, with my fangs, horns, and claws out, and yet you are still

here. You have been such a source of motivation to me because I want to succeed not only for myself, but also for you, for us.

ACKNOWLEDGEMENTS

I would like to acknowledge my advisor, Dr. Scott Pegan. The last four years have without a doubt been challenging, but I always knew it would be worth it and that you always had my best interest at heart. You taught me so much about science, the real world, and myself. You pushed me past the limits I thought I had and my true capabilities have shined through.

I would also like to acknowledge my committee, Dr. Hooks, Dr. Zheng, Dr. Lanzilotta, and Dr. Cummings, although he is no longer on my committee. Thank you for your belief in me despite some rough patches and for leading and guiding me through this process.

I would also like to acknowledge my lab mates, John Dzimianski, Brendan Freitas, Caroline Langley, Jack McGuire and our fantastic undergraduate students Isabelle Williams, Kailee Baker, and Ashton Clary. A lot of us are moving on to the next stage in our lives, but I hope our time together has made a difference to all of you as it has to me. Thank you for all the advice, help with troubleshooting, and often just giving me someone to soundboard at or complain to about my life.

TABLE OF CONTENTS

	Page
ACKNOWLEDGEMENTS.....	vi
LIST OF TABLES.....	x
LIST OF FIGURES.....	xi
LIST OF SCHEMES.....	xiv
CHAPTER	
1 INTRODUCTION.....	1
The development and use of organophosphate nerve agents.....	1
Acetylcholinesterase as a biological target for OP nerve agents.....	6
Reactivation of nerve agent inhibited AChE.....	12
Acetylcholinesterase structure.....	17
2 STRUCTURAL INSIGHTS OF STEREO SPECIFIC INHIBITION OF HUMAN ACETYLCHOLINESTERASE BY VX AND SUBSEQUENT REACTIVATION BY HI-6.....	21
Abstract.....	22
Introduction.....	23
Experimental Procedures.....	26
Results.....	33
Discussion.....	47
References.....	55

3	INSIGHTS INTO INHIBITION OF HUMAN ACETYLCHOLINESTERASE BY NOVICHOK, A-SERIES NERVE AGENTS.....	61
	Abstract	62
	Introduction	63
	Results	66
	Discussion & Conclusions.....	77
	Experimental Section	83
	References	90
4	THE STRUCTURAL AND BIOCHEMICAL IMPACT OF MONOMERIZING HUMAN ACETYLCHOLINESTERASE	93
	Abstract	94
	Introduction	95
	Results	96
	Discussion.....	105
	Materials and Methods.....	107
	References	111
5	DISCUSSION.....	115
	AChE's stereoselectivity for OP nerve agents	115
	Influence of the small hydrophobic pocket upon potency	117
	Recognition of structural features involved in reactivation	119
	Future Directions	122
	REFERENCES	127
	APPENDICES	

A SUPPLEMENTARY MATERIAL FOR CHAPTER 2	135
B SUPPLEMENTARY MATERIAL FOR CHAPTER 3.....	139
C SUPPLEMENTARY MATERIAL FOR CHAPTER 4.....	142
D ADDITIONAL MATERIAL ON THE ENZYME KINETICS OF INHIBITION.....	144

LIST OF TABLES

	Page
Table 2.1: Inhibition of hAChE and Reactivation of hAChE by HI-6	34
Table 2.2: Crystallography data of hAChE structures.	35
Table 3.1: Data collection and refinement statistics	89
Table 4.1: Enzymatic activity of dimer hAChE and hAChE L380R/F535K.	97
Table 4.2: Data collection and refinement statistics	99
Table 4.3: Inhibition of hAChE, Reactivation of inhibited hAChE by HI-6	105

LIST OF FIGURES

	Page
Figure 1.1: Chemical structures of organophosphate nerve agents	2
Figure 1.2: Overall scheme of disulfide bond cleavage of Ellman's Reagent, DTNB.....	9
Figure 1.3: Overall scheme of the inhibition and aging of hAChE by a nerve agent including reactivation by an oxime reactivator	12
Figure 1.4: Chemical Structures of Oxime Reactivators.....	14
Figure 1.5: Active site of human acetylcholinesterase.....	19
Figure 2.1: Crystal structures of human acetylcholinesterase in complex with stereoisomers of nerve agent, VX.....	36
Figure 2.2: Crystal structures of acetylcholinesterase in complex with HI-6	41
Figure 2.3: The active site of human acetylcholinesterase with stereoisomers of VX and the reactivator, HI-6	44
Figure 2.4: The active site of human acetylcholinesterase with post-catalysis HI-6 and a byproduct, EMPA	47
Figure 2.5: Binding modes of HI-6 in human acetylcholinesterase active site	52
Figure 2.6: Structural Diversity in Specific Residues surrounding the Active Site between Acetylcholinesterase Species.....	54
Figure 3.1: The chemical structures of nerve agents	64
Figure 3.2: Crystal Structures of Human Acetylcholinesterase in complex with Stereoisomers of Nerve Agent, A232	68

Figure 3.3: Comparison of Crystal Structures of Human Acetylcholinesterase in complex with A-series agents	70
Figure 3.4: Accommodation of HI-6 in A230 and A232 bound hAChE active sites	73
Figure 3.5: Multiple Orientations of HI-6 in A234 bound hAChE active site	75
Figure 3.6: Comparison of HI-6 accommodation with the A-series inhibited hAChE active site	76
Figure 3.7: Comparison of nerve agent accommodation in hAChE active site	81
Figure 4.1: Comparison of the crystal lattice of hAChE L380R/F535K and dimeric hAChE	100
Figure 4.2: Global structural comparison of monomeric hAChE L380R/F535K and dimeric hAChE	101
Figure 4.3: Comparison of the 491-499 loop of monomeric hAChE L380R/F535K and dimeric hAChE	102
Figure 4.4: Comparison of the active sites and acyl loop of monomeric hAChE L380R/F535K and dimeric hAChE	103
Figure S2.1: Crystal Structures of Human Acetylcholinesterase in complex with Stereoisomers of Nerve Agent, VX	136
Figure S2.2: Crystal structures of HI-6 bound in the active site of hAChE.....	137
Figure S2.3: Overlay of the Acyl Loop Region of Human Acetylcholinesterase Inhibited by VX-Pr	137
Figure S2.4: The Active Site of human Acetylcholinesterase with Stereoisomers of VX and the Reactivator, HI-6	138

Figure S2.5: The Active Site of human Acetylcholinesterase with Post-Catalysis HI-6 and a by-product, EMPA	138
Figure S3.1: Comparison of Crystal Structures of Human Acetylcholinesterase in complex with A-series agents.....	140
Figure S3.2: Crystal Structures of Human Acetylcholinesterase in complex with A-series agents and HI-6.....	141
Figure S4.1: Sedimentation velocity analysis studying the oligomeric state of hAChE L380R/F535K and hAChE in solution.....	143
Figure A2.1: Double reciprocal plot for the inhibition of hAChE by racemic VX	145
Figure A2.2: Double reciprocal plot for the inhibition of hAChE by P _S -VX	145
Figure A3.1: Double reciprocal plot for the inhibition of hAChE by racemic A-232....	146
Figure A3.2: Double reciprocal plot for the inhibition of hAChE by P _S -A-232	146
Figure A3.3: Double reciprocal plot for the inhibition of hAChE by racemic A-230....	147
Figure A3.4: Double reciprocal plot for the inhibition of hAChE by racemic A-234....	147
Figure A4.1: Double reciprocal plot for the inhibition of hAChE L380R/F535K by racemic VX.....	148

LIST OF SCHEMES

	Page
Scheme 2.1: Inhibition and Aging of VX in hAChE	24
Scheme 2.2: Schematic of nerve agent, VX, in complex with reactivator, HI-6, and potential manner for the removal of VX from AChE S203	49
Scheme 3.1: Inhibition of hAChE by A-series with transition state of S_2N concerted substitution.....	65

CHAPTER 1

INTRODUCTION

The development and use of organophosphate nerve agents

The first organophosphorus cholinesterase inhibitor was synthesized in 1854^{1, 2}. Beyond this first agent, there was a general focus in the 1930s of developing novel organophosphorus insecticides to combat the debilitating effects of insect- and louse-borne diseases (malaria³, trench fever⁴, and typhus⁴) witnessed in World War I (WWI). These efforts and issues would continue into World War II (WWII). In pursuing these original aims, Dr. Gerhard Schrader and his team at IG Farben Industries in Germany accidentally discovered the first nerve agent, tabun (GA; ethyl N, N-dimethylphosphoramidocyanidate) in 1936⁵. Between 1934 and 1944, Schrader and his team also generated about 2,000 organophosphorus compounds including di-isopropyl phosphorofluoridate (DFP), octamethylpyrophosphorotetramide (OMPA), and well-known OP pesticides, diethyl-p-nitrophenylphosphate (paraoxon) and diethyl-p-nitrophenylthiophosphate (parathion)^{1, 6}. Due to a Reich Ordinance of 1935, which required that all inventions of possible military relevance be reported to the Ministry of War, a sample of tabun was sent to the Chemical Warfare section of the Army Weapons Office⁵. The value of this accidental discovery for chemical warfare was recognized immediately and the Nazi government of Germany relocated Schrader and his team and redefined their major aim to the development of OP nerve agents^{5, 7}. Two years after the initial discovery of tabun, he and his team synthesized sarin (GB; 2-fluoro-

methylphosphoryloxypropane) and in 1944 soman (GD; 3-fluoromethyl-phosphoryloxy-2, 2-dimethyl-butane) was also discovered ⁵. These OP nerve agents came to be known as the G-series agents (G referencing German). The G-series agents are one of the two major series of OP nerve agents. This group includes GA, GB, GD, and cyclosarin (GF; fluoromethylphosphoryloxycyclohexane), which was first synthesized in 1949 (Figure 1.1). There are other lesser known G-series agents such as GP, GE (ethylsarin), GC (chlorosarin), and GV. G-series agents are mostly known for their fluoride leaving group, excluding GA who has a cyanide leaving group, as well as being odorless, colorless, and slightly volatile ⁸. At the end of World War II, Allied forces found that Germany had large stockpiles of these agents with estimates at 30,000 tons of tabun and 500 tons of sarin, but they were never used during the war ^{5,9}.

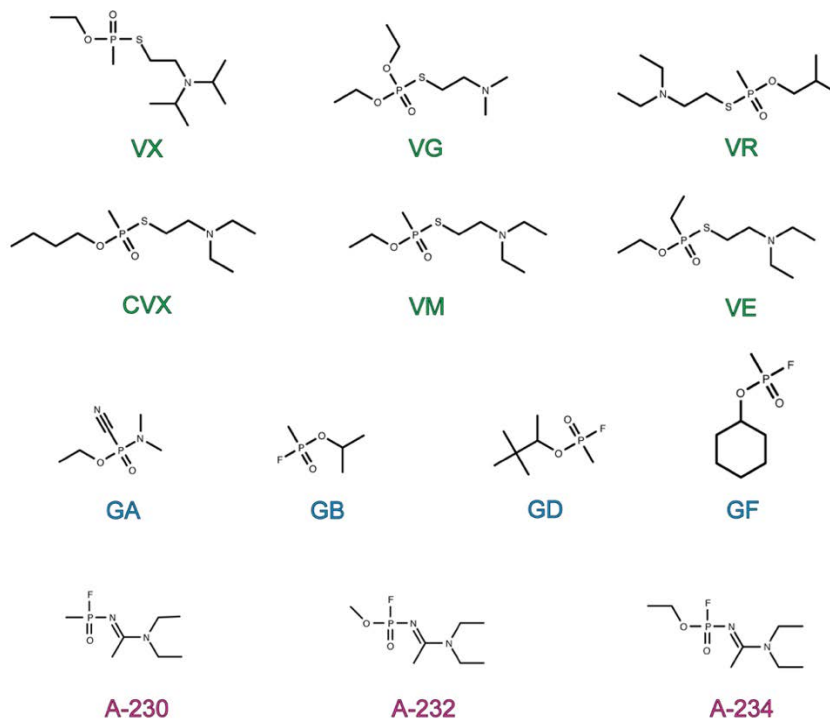


Figure 1.1. Chemical structures of organophosphate nerve agents. The chemical structure of OP nerve agents with colored labels corresponding to either the V-series (green), G-series (blue) or Novichok (pink) class.

Not long after WWII ended, Ranajit Ghosh, a researcher at Imperial Chemical Industries in Great Britain also stumbled across OP nerve agents while researching OP insecticides and pesticides in the 1950s ^{10, 11}. VG (2 diethoxyphosphorylsulfanyl-N,N-diethylethanamine), known as ‘Amiton’, was marketed as an insecticide in 1954, but was withdrawn after its toxicity became apparent ¹¹⁻¹³. Once the government and military became aware that the toxicity of these compounds was too high to be agriculturally relevant, they shut down research into these agents altogether in 1956 ⁵. These compounds are part of the second major OP nerve agent class, V-series agents (V referencing either victory, venomous, virulent, or viscous) ¹⁴. This class includes VX (S-2 diisopropylamino O-ethylmethylphosphonothioate), VG, VR (Russian VX; N,N-diethyl-2-methyl-2-methylpropoxy phosphorylsulfanylethanamine), VE (S-2-diethylaminoethyl O-ethylethylphosphonothioate), VM (2-ethoxy-methylphosphoryl sulfanyl-N,N-diethylethanamine) and CVX (Chinese VX; O-Butyl S-[2-(diethylamino)ethyl] methylphosphonothioate). Overall, the V-series agents are more toxic than the G-series in addition to being less volatile due to their thiol leaving group ¹⁵. Unlike G-series agents that evaporate quickly, V-series agents are persistent, which means they can potentially remain around for weeks after dispersal ⁸. Research into these agents continued in the 1950s and 1960s by the United States, who determined that VX was the most promising chemical warfare agent of the group ^{5, 9, 10}. Countries including the United States and Russia as well as Iraq and Syria at a smaller scale began to mass stockpile VX and other nerve agents at this point in time. The Chemical Weapons Convention (CWC) went into force in 1997, which prohibits the development, synthesis, use and stockpiling of chemical weapons, including all known nerve agents at the time ^{8, 16-18}. According to the

CWC, countries agreed to destroy their stockpiles by 2012, nonetheless many countries are still destroying their very sizable stashes ^{8, 19-21}.

The third lesser known class of nerve agents are the A-series or Novichok (meaning Newcomer in Russian) agents. Information on these agents is limited and within the information available there is an extensive amount of contradiction. The Soviet Union developed these agents toward the end of the Cold War under a program codenamed FOLIANT. At the beginning of the 1970s, the design and development of new nerve agents was ordered, but specific requirements for the substances were imposed including that they must be: undetectable using standard chemical detection instruments used by NATO member states, unmentioned in lists of CWC, able to get around protection measures and access enemy's body, and safer to store and prepare than previous nerve agents ^{9, 14, 22}. In the late 1980s and early 1990s, Russia chemists did produce several OP nerve agents that fit these parameters including A-230 (E-[1-(diethylamino)ethylidene]amino](methyl)phosphinoyl fluoride), A-234 (N'-[ethoxy(fluoro)phosphoryl]-N,N-diethylethanimidamide), and A-232 (methyl N-[1-(diethylamino)ethylidene]phosphoramidofluoridate). There is uncertainty surrounding the toxicity of these agents with some suggesting the toxicity of these agents is 10 to 100 times higher than VX ^{7, 22, 23}. This program and the existence of these nerve agents was revealed when two chemists published an article in the weekly *Moskovskie Novosti* in 1992²³. One of the two scientists, Mirzayanov now lives in the US and wrote an autobiography in 2008 where he goes more in depth about working with these agents ²³. Despite all this information, many mysteries about these agents has still remained.

While OP nerve agents were never used during WWII, they have been utilized in both warfare and terrorism since then. GA was the first recorded OP nerve agent to be employed on the battlefield during the Iraq-Iran conflict in 1984²⁴. From 1983-1988, Iraq used nerve agents and other chemical weapons, such as sarin, tabun, and possibly VX, against Iranian combatants and civilians²⁴⁻²⁶. Iraqi Kurdish civilians were also exposed to these agents in 1988 by the Iraqi government²⁵. Only a few years later in 1994, the Japanese Aum Shinrikyo cult released GB in Matsumoto, which was followed by another attack in March 1995 where sarin was released in a Tokyo subway²⁷⁻³⁰. These two events resulted in about 5,800 people exposed and 19 dead.^{29, 30} Nearly two decades later in the midst of the still ongoing Syrian Civil War (2011-present), sarin and other chemical weapons were released during major attacks^{17, 31}. There were confirmed reports from the United Nations that GB was utilized in at least four major attacks spanning 2013 to 2017 including the Ghouta incident in August 2013 where several thousand were exposed and potentially 1,500 people died^{17, 31, 32}. In 2017, VX was used in the assassination of Kim Jong-nam, the half-brother of the North Korean Leader Kim Jong-un, in a Malaysian airport³³. Unlike these previous events, the nerve agent attack in the United Kingdom in 2018 involved the use of a Novichok agent. A former Russian military intelligence officer, Sergei Skripal and his daughter Yulia Skripal had been exposed to a Novichok agent in what was likely an attempted assassination³⁴. Both survived the attack, but months later two more UK citizens became exposed to the same substance found in a perfume bottle and this incident resulted in one fatality³⁵. These attacks brought OP nerve agents back to the cover of newspapers and the forefront of people's minds.

Acetylcholinesterase as a biological target for OP nerve agents

The toxicity of OP nerve agents and pesticides is primarily due to their ability to irreversibly inhibit acetylcholinesterase (AChE; E.C. 3.1.1.7). Acetylcholinesterase is a serine hydrolase primarily located at neuromuscular junctions (NMJ) of all innervated organs, the autonomic ganglia, and cholinergic brain and spinal synapses in a wide variety of species³⁶. The enzyme exists in multiple molecular forms that possess similar catalytic properties including monomers, dimers, and tetramers, but differ in their mode of cell surface attachment as well as their oligomeric assembly³⁷⁻³⁹. AChE's principal biological role is terminating impulse transmission at cholinergic synapses by hydrolyzing the neurotransmitter, acetylcholine (ACh) into choline and acetate. ACh is released into the synaptic cleft following a nerve impulse, where it binds to cholinergic receptors on the post-synaptic cell membranes, triggering a response, such as a muscle contraction⁴⁰. Once released from the receptor, AChE hydrolyses ACh. The specific catalytic activity of AChE is exceptionally high, especially for a serine hydrolase, functioning at a rate that approaches a diffusion-controlled reaction^{40,41}.

The active site of AChE includes as Ser-His-Glu catalytic triad⁴⁰. The hydrolysis of ACh has two major steps. The catalytic serine attacks ACh, before separating into choline and an acetylated AChE. After the acetylated serine is attacked by a water molecule, acetate is produced and the enzyme is regenerated. OP nerve agents and pesticides interact with the catalytic serine in a similar manner to ACh. With the exception that once the catalytic serine attacks the electrophilic phosphorus of the organophosphate core and the leaving group comes off, the

enzyme is irreversibly inhibited. OP nerve agents and pesticides make use of the same organophosphate chemical scaffold to covalently modify the catalytic serine, which leads to inhibition ⁴². The phosphorylated serine can undergo further dealkylation to an anionic phosphorylated serine also known as the “aged” state ^{43, 44}. In the aged state, the modified serine is resistant to nucleophilic attack in part due to the stabilization that occurs when the anionic oxygen and nearby histidine of the catalytic triad form a salt bridge ^{44, 45}. In either of these states, the enzyme can no longer break down ACh.

When AChE is inhibited, ACh accumulates in the synaptic cleft and continues to interact with the nicotinic and muscarinic ACh receptors (nAChR; mAChR). The constant signal firing can cause overstimulation of these receptors, which can be observed as continuous muscle spasms or seizures. This condition is referred to as cholinergic crisis ⁷. Eventually the receptors become desensitized and will stop responding to the bombardment of ACh, which can lead to numerous signs and symptoms including the most severe: paralysis, respiratory failure, increased bronchial secretions, coma, and potentially death depending on the nerve agent and how quickly treatment is sought.

OP nerve agents and pesticides vary greatly in their ability to inhibit AChE as well as how quickly they age. From a molecular standpoint, there are still many unanswered questions regarding why the inhibition and aging rates of OP nerve agents differ so significantly ^{46, 47}. Although a few studies have made progress on answering these lingering questions including a prior study that recognized the inhibitory ability of some G-series agents appeared to be influenced by the size of their alkoxy (group) group

⁴⁷. In addition, the aging kinetics of certain organophosphonate nerve agents were found to be dependent on the structure of the alkoxy side chain of the phosphorylated AChE with branched alkoxy groups showing the most pronounced aging rates ^{43, 47-49}. Nevertheless, only a portion of the OP nerve agents and pesticides follow these trends, which suggests there are additional factors influencing the rate of inhibition and aging of these agents. Additionally, the driving force(s) behind AChE's stereoselectivity for OP nerve agents and pesticides require further research as they are also still not well-understood.

The ability of individual nerve agents to inhibit AChE is assessed through modified Ellman's assays. In general, Ellman's assays are a colorimetric method for determining AChE and butyrylcholinesterase (BChE; EC 3.1.1.8) activity by measuring the increase of yellow coloration (2-nitro-5-thiobenzoate anion; TNB²⁻) that is produced when thiocholine (TCh) reacts with Ellman's agent (5,5'-dithiobis-(2-nitrobenzoic acid) or DTNB) by a plate reader or photometer (Figure 1.2) ⁵⁰. Thiocholine (TCh) is produced when acetylthiocholine (ATCh) is hydrolyzed by AChE. When DTNB, the chromogen, reacts with the thiol group of TCh under mild alkaline conditions (pH 7-8), its disulfide bond is cleaved and produces TNB²⁻. Ellman's assays indirectly measure the activity of AChE by measuring the increase of absorbance from TNB²⁻ at 412 nm over time ^{50, 51}. This reaction rate is equated with the rate of ATCh hydrolysis by AChE and therefore the activity of the enzyme.

Ellman's assays have been modified over the years to suit the types of experiments being run including alterations for the sample type ⁵²⁻⁵⁴. For example, assays run on membrane bound AChE in erythrocytes had issues as hemoglobin also has high

absorption at 412 nm ⁵¹. To avoid this issue, hemolyzed erythrocytes, known as erythrocyte ghosts, began to be employed in Ellman's assays ⁵³. Through hemolysis, AChE activity is maintained, but the majority of the erythrocytes' internal contents including hemoglobin are eliminated ⁵³. Additionally, the recognition that BChE is present within blood plasma led to the addition of a BChE inhibitor to assays on blood, erythrocytes, and erythrocyte ghost samples. In general, the use of erythrocyte ghosts in Ellman's assays became common, but the results of these assays are sometimes called into question due to the possibility of residual hemoglobin or BChE artificially elevating the measured activity. Most recently, Ellman's assays are utilizing purified protein rather than blood, tissue, or erythrocyte ghost samples to ensure the accuracy of the assays.

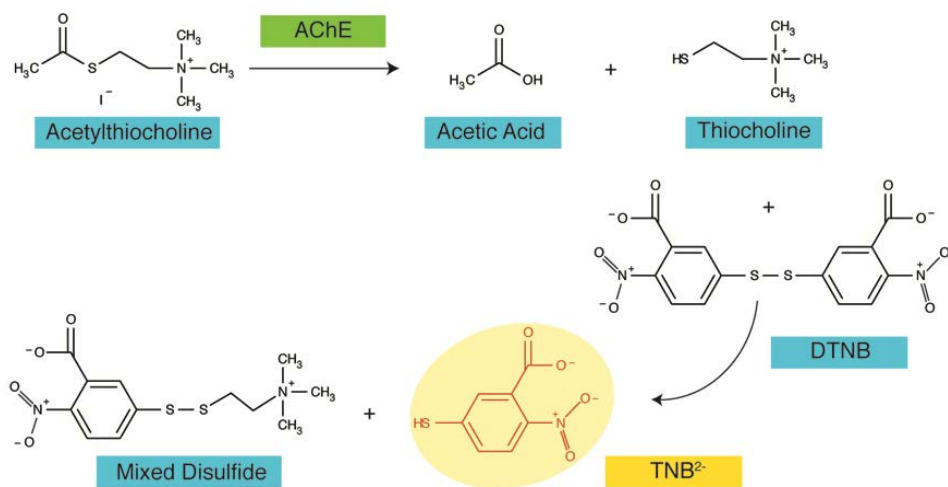
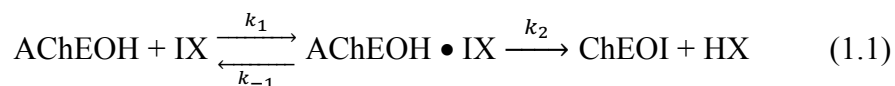


Figure 1.2. Overall scheme of disulfide bond cleavage of Ellman's Reagent, DTNB.

Other modifications of Ellman's assays allow for the assessment of a nerve agent's ability to inhibit AChE. Their inhibitory ability is often expressed as the k_i , the bimolecular rate constant ^{55, 56}. Overall, there are two main generally accepted methods of collection for determining the k_i , continuous ^{55, 56} and discontinuous ⁴⁷. Both methods

involve the addition of an inhibitor to the components of a standard Ellman's assay and measuring the slowing increase in absorbance over time. The continuous collection method measures the absorbance every few seconds for the entire measurement time for multiple inhibitor concentrations, while the discontinuous collection method stops the reaction at specified times to record the absorbance. The continuous method of collection is especially useful for inhibitors with fast inhibition rates as it ensures significant changes are recorded despite the speed at which they occur ⁵⁵. The discontinuous method is favorable for slower inhibiting agents as the absorbance changes should be less dramatic over short spans of time ⁴⁷. In addition, these methods for the most part differ in their manner of calculating the nerve agents' inhibitory ability.

Of the two methods, the calculations for the continuous method are utilized more frequently within the field. These assays are run under pseudo-first-order reaction conditions by using sufficiently high inhibitor concentration(s), which allows the simple bimolecular inhibitor binding interaction to be linearized. The calculations for the continuous method are based on the premise that inhibition of AChE proceeds in two steps with a reversible Michaelis complex forming before the irreversible step (Eq. 1.1) ⁵⁷. The ratio between the two parameters characterizing inhibition, the dissociation constant (K_d ; k_{-1}/k_1) and the unimolecular bonding constant, k_2 , gives the overall rate of inhibition, k_i ^{55, 56}. This method does assume in its analysis that the initial binding step is an equilibrium, which cannot be proven, but the k_1 would have to be quite small for this assumption to be invalid ⁵⁵.



The standard assay components with varying concentrations of inhibitor are recorded alongside negative (no ACTI) and positive controls (no inhibitor). The slopes of the tangents of the progressive inhibition curves for each concentration are calculated and any residual activity is subtracted. The corrected slopes of multiple runs at the same inhibitor concentration are averaged at this point to plot the corrected averaged slopes of each inhibitor concentration in a semilogarithmic plot against time. The slopes ($\Delta \ln v / \Delta t$) of these linear plots are determined by least-squares method and then utilized in applying the double-reciprocal method⁵⁶ which takes advantage of the relationship in Eq. 1.2:

$$\frac{\Delta t}{\Delta \ln v} = \frac{K_d}{k_2} \times \frac{1}{[IX](1-\alpha)} + \frac{1}{k_2} \quad (1.2)$$

In this equation: [IX] is the concentration of inhibitor, t stands for the time when assay solution are added to inhibited AChE, and α represents $[S]/(K_m + [S])$ where [S] is the consistent substrate concentration and K_m is the Michaelis constant which is determined separately before running inhibition experiments. Plotting ($\Delta t / \Delta \ln v$) against $1/([IX](1-\alpha))$ with the least-squares method allows the determination of k_2 as the reciprocal of the y-intercept and K_d as the reciprocal of the x-intercept. k_i is then determined from Eq. 1.3.

$$k_i = k_2 / K_d \quad (1.3)$$

The calculation for the discontinuous method also occurs under pseudo-first order reaction conditions and utilizes Eq. (1.4)⁴⁷ with v_0 and v_t as the reaction rates at time zero and t, respectively.

$$k_i = \frac{1}{[IX]t} \ln \frac{v_0}{v_t} \quad (1.4)$$

Unlike the continuous method of calculation that utilizes the least-squares method to minimize the sum of squared residuals, the discontinuous method of calculation calculates the standard error of several replicates to determine the quality of the data. The

ability to accurately assess the k_i of OP nerve agents and pesticides enables a proper understanding of their toxicities and how they compare to one another. This information is invaluable in understanding the role of toxicity in treatment of OP agent exposure as well as the influence OP agents can have upon therapeutics.

Reactivation of nerve agent inhibited AChE

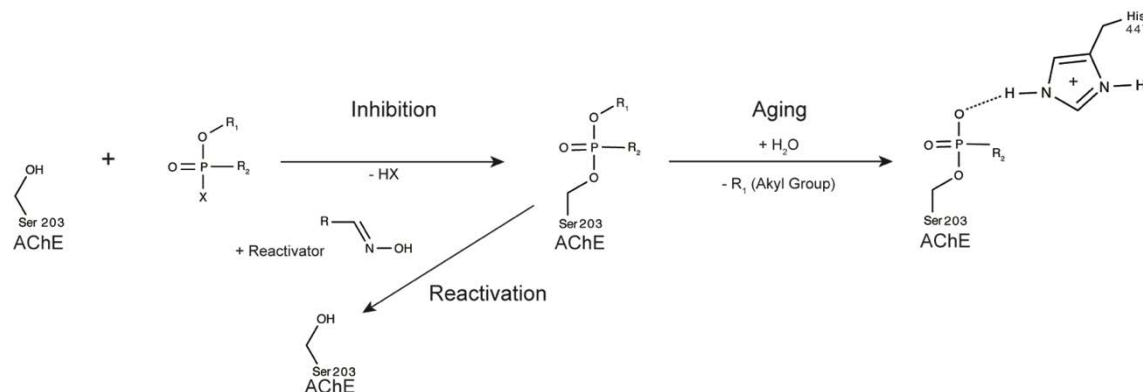


Figure 1.3. Overall scheme of the inhibition and aging of hAChE by a nerve agent including reactivation by an oxime reactivator.

The current treatments of OP nerve agent and pesticide exposure includes a mixture of atropine, benzodiazepine, and oxime reactivator⁵⁸. Atropine and benzodiazepine treat the symptoms of ACh accumulation in the synaptic cleft by acting as a muscarinic AChR antagonist and a minor tranquilizer that reduces nerve sensitivity to stimulation, respectively⁵⁹. Oxime reactivators can remove the phosphonyl moiety from the inhibited serine through a strong nucleophilic attack by the oxime (Figure 1.3)⁶⁰⁻⁶³. However, once the enzyme becomes aged, oxime reactivators are ineffective in part due to their inability to approach the bound serine because of the charge of the aged moiety's anionic oxygen^{43, 44, 64}. Thus, treatment with oxime reactivators is only effective for use immediately after exposure to ensure AChE is still in an inhibited state. Other

types of reactivators and therapeutics have been developed, but thus far oxime reactivators have demonstrated the greatest potential as therapeutic agents ^{65, 66}.

The development and search for reactivators began in 1952 when Wilson determined that hydroxylamine was a more efficient reactivator than water against the OP pesticide, tetraethylpyrophosphate (TEPP) inhibited AChE ⁶⁷. As the hydroxylamine is the simplest compound with an N-OH group, this finding started efforts into developing reactivators with an oxime (C=NOH) functional group ⁶⁵. These initial studies also examined hydroxamic acids, whereas ketoximes and aldoximes were explored later ^{60, 61, 65, 68-70}. While other compounds were utilized in animal studies, mono-pyridinium oxime 2-pyridine aldoxime methiodide (pralidoxime; 2-PAM) was the first successful reactivator used against human OP poisoning (Figure 1.4) ^{60, 61, 65, 71, 72}. While moderately successful with certain agents, there appeared to be room for improvement with 2-PAM thus, researchers attempted combining the structures of two effective reactivators hoping that it would increase reactivation ability ⁷³. The bispyridinium oxime reactivator, trimedoxime (1,1'-Trimethylenebis(4-aldoximinopyridinium); dipyroxime; TMB-4) was developed as one of these compounds in 1958 ⁷³. Coincidentally, another group of researchers independently developed TMB-4 within the same year ⁷⁴. TMB-4 appeared to be an improvement as it was the first effective oxime reactivator against tabun ^{75, 76}, however TMB-4 was found to be potentially toxic within the body ⁷⁷. An analogue of TMB-4, MMB-4 (1,1'-Trimethylenebis[4-(hydroxyimino)methyl]pyridinium; methoxime), was synthesized in 1959 ⁷⁸ and observed to have a greater potency than TMB-4 towards several nerve agents including sarin ⁷⁹ and soman ^{80, 81}. Another bispyridinium oxime reactivator, Obidoxime (LüH-6; 1,3-Bis(4-hydroxyiminomethyl-1-

pyridinium), was discovered by German scientists, Lüttringhaus and Hagedorn in 1960⁸². Obidoxime was the most effective against OP pesticides at this point in oxime reactivator development⁸³.

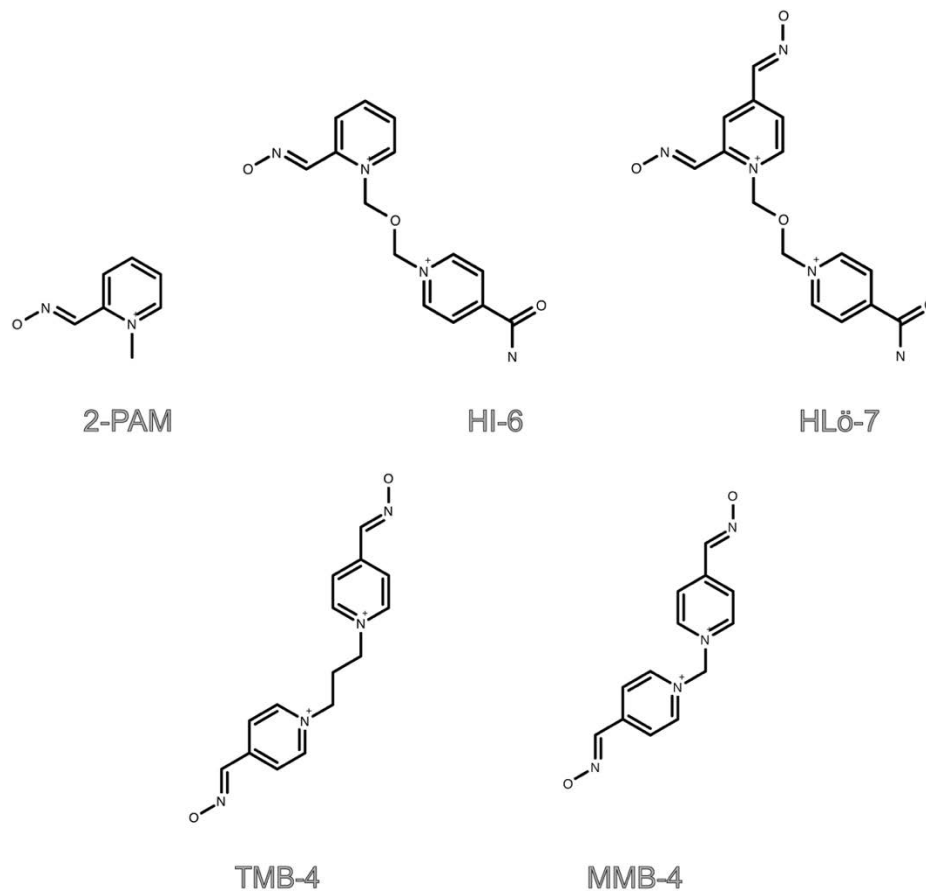
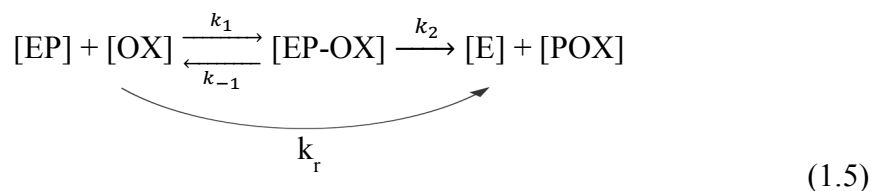


Figure 1.4. Chemical Structures of Oxime Reactivators.

The reactivators developed by 1960 were still fairly ineffective towards soman. As a result Hagedorn's group continued to synthesize numerous oxime reactivators including the development of HI-6 (1-(2-hydroxyiminomethyl-1'-pyridinium)-3-(4'-carbamoyl-1-pyridinium; asoxime) in 1969^{84, 85} and HLö-7 ((1-[[[4-(aminocarbonyl)pyridinio]methoxy]methyl]-2,4-bis [(hydroxyimino)methyl]pyridinium) in the 1970s⁸⁶. Both HLö-7 and HI-6 are considered superior reactivators compared to 2-

PAM, obidoxime, and MMB-4 as they both have remarkable reactivation potency towards most OP nerve agents and pesticides⁸⁵⁻⁸⁹. As some reactivators have shown toxicity and inhibitory side effects, HI-6's relatively low toxicity when compared to other oxime reactivators is an attractive quality when considering usage for human OP exposure^{88,90}. A major drawback of HI-6 is its near to complete ineffectiveness towards tabun-inhibited AChE, although HLö-7 is considerably more effective towards tabun-inhibited AChE^{87,89,91}. In general, HI-6 and HLö-7 are considered the most promising of these current oxime reactivators. However, there is still room for improvement as variations in reactivator effectiveness based on the bound nerve agent were a major reason for further development between the 1950s and 1970s and still is today. Currently, little is known on the reason(s) for the variation in the ability of oxime reactivators or which structural components of AChE may contribute to this.

Parts of the oxime reactivation mechanism have been studied over the past sixty years, but the complete mechanism had yet to be fully discerned until now. Previously the evidence supported that reactivation proceeds by a two-step reaction (Eq. 1.5)^{84, 86, 92-94}. Initially the oxime reactivator [OX] will form a Michaelis-type bipyramidal trigonal intermediate [EPOX] with phosphorylated AChE [EP]. Afterwards, the phosphoryl moiety becomes displaced from the intermediate by the oxime, leading to the reactivation of the enzyme [E] and the phosphorylation of the oxime [POX]⁴⁷. Some gaps within this suggested reaction still remained, including when and how quickly the phosphorylated oxime separate. The efficacy of oxime reactivators can potentially be attributed to the nucleophilicity of their oximes, the scaffold of the reactivator as well as the rate of separation from the phosphorylated oxime intermediate.



K_{OX} (k_{-1}/k_1) approximates the dissociation constant, which is inversely proportional to the oxime's affinity to the phosphorylated oxime reactivator. The rate constant, k_2 , expresses the reactivity of the oxime reactivator. The second order reactivation rate constant, k_r , characterizes the specific activity and is calculated from Eq. 1.6⁴⁷.

$$k_r = k_2/K_{\text{OX}} \tag{1.6}$$

When reactivation is complete, pseudo-first order rate equations can be derived for the reactivation process⁹⁵ where k_{obs} is the first-order rate constant of reactivation observed at any used oxime reactivator concentration.

$$k_{\text{obs}} = \frac{k_2[\text{OX}]}{K_{\text{OX}} + [\text{OX}]} \tag{1.7}$$

k_{obs} is not proportional to the oxime concentration, but underlies a saturation kinetics⁹⁶ and k_2 and K_{OX} adhere to Michaelis-Menten kinetics according to Eq. 1.7⁹⁷. This generally accepted approach enables the efficacy of reactivators towards OP nerve agent and pesticide inhibited AChE to be assessed through running modified Ellman's assays. These determinations are a valuable tool in the development and improvement of oxime reactivators.

Despite the development of numerous oxime reactivators over the years including those aforementioned, novel and improved therapeutic agents are highly sought. As of now, oxime reactivators are still the best treatment option available, but they also have considerable limitations. In addition to being ineffective once the bound serine is in an aged state^{44, 59, 64}, the therapeutic effect appears to vary not only depending on the OP

nerve agent and pesticide ^{47, 98}, but also based on the stereochemistry of the bound agent ⁹⁹ as well as the species of AChE ^{100, 101}. However, little significant progress has been made in further improving oxime reactivators until recently due to the lack of access to authentic agents and hAChE. As a result instead of authentic agent and hAChE, nerve agent surrogates and other AChE species were often studied, but it was discovered that the results were not translatable to hAChE likely due to species-species differences ⁴². Consequently, most of the reactivators utilized today are the same prominent few developed before the mid-1970s. For instance, the treatment cocktail provided by the US government to their soldiers in auto-injectors includes atropine with 2-PAM ⁵⁹. Whereas other countries utilize different oxime reactivators with atropine in their treatment cocktails including HI-6 in Canada and Sweden, obidoxime in Germany and the Netherlands, and TMB-4 in Israel ⁵⁹. Due to the use of OP nerve agents occurring with frequency over the past few years, attempts are being made to develop oxime reactivators that work more broad-spectrum with significant reactivation towards all OP nerve agent and pesticide exposures.

Acetylcholinesterase structure

The first AChE x-ray crystal structure was published in 1991. The *Torpedo californica* AChE (tAChE) structure provided the first insight into the relationship between structure and function in AChE ¹⁰². This revealed that AChE like other α/β hydrolases has central β -sheets surrounded by α -helices. Specifically, AChE consists of 14 α -helices and 12 stranded β -sheets ^{102, 103}. The most remarkable feature of this structure was the visualization of a narrow 20 Å gorge into the center of the enzyme with

the active site near the bottom of the gorge ¹⁰². The majority of the active site gorge is lined with aromatic residues (14 in total) and contains only a few acidic residues ^{102, 104}.

AChE is a rather ubiquitous enzyme, occurring within numerous species including humans, vertebrates, and insects ¹⁰⁵. The ease of access to tAChE at this time compared to other species was likely the reason tAChE was the first species crystallized. Following the initial crystallization of tAChE, tAChE was crystallized in complex with several different inhibitors to discern their mechanism of inhibition as well as the behavior of the active site ^{42, 106-108}. Eventually more species of AChE began to be crystallized and studied including *Electrophorus electricus* (electric eel; eAChE) ¹⁰⁹, *Mus musculus* (mouse; mAChE) ^{94, 110, 111}, *Drosophila melanogaster* (fruit fly; dAChE) ¹¹², *Anopheles gambiae* (mosquito; AgAChE) ¹¹³, *Bungarus fasciatus* (BfAChE) ¹¹⁴, and eventually *Homo sapiens* (human; hAChE) ^{42, 104, 115}. hAChE, mAChE, and tAChE have been crystallized in complex with a potent AChE inhibitor, fasciculin-II (green mamba venom), however the inhibitor was observed near the entrance to the active site gorge in an area known as the peripheral anionic site (PAS), rather than near the catalytic triad ^{114, 116-118}. This led to the recognition of the PAS as a potential allosteric binding site for inhibitors, but substrate and other inhibitors can potentially still enter the active site depending on the position of the inhibitor ^{111, 117, 118}. Due to their easier availability and chemical similarity to OP nerve agents, crystal structures of different species of AChE with OP pesticides and surrogates were utilized instead of OP nerve agents ^{45, 119, 120}. While these structures helped to provide a foundational understanding of AChE inhibition by OP agents, the shift to using real OP nerve agents, including racemic mixtures and stereoisomers, enabled a better characterization of how these agents influence the active

site of AChE via inhibition and aging^{15, 43, 45, 97, 120, 121}. Subsequently, structures including reactivators as well as OP nerve agents were determined to elucidate the mechanism of reactivators on removing the phosphonyl moiety as well how the reactivator is accommodated within the active site^{92, 94, 115}.

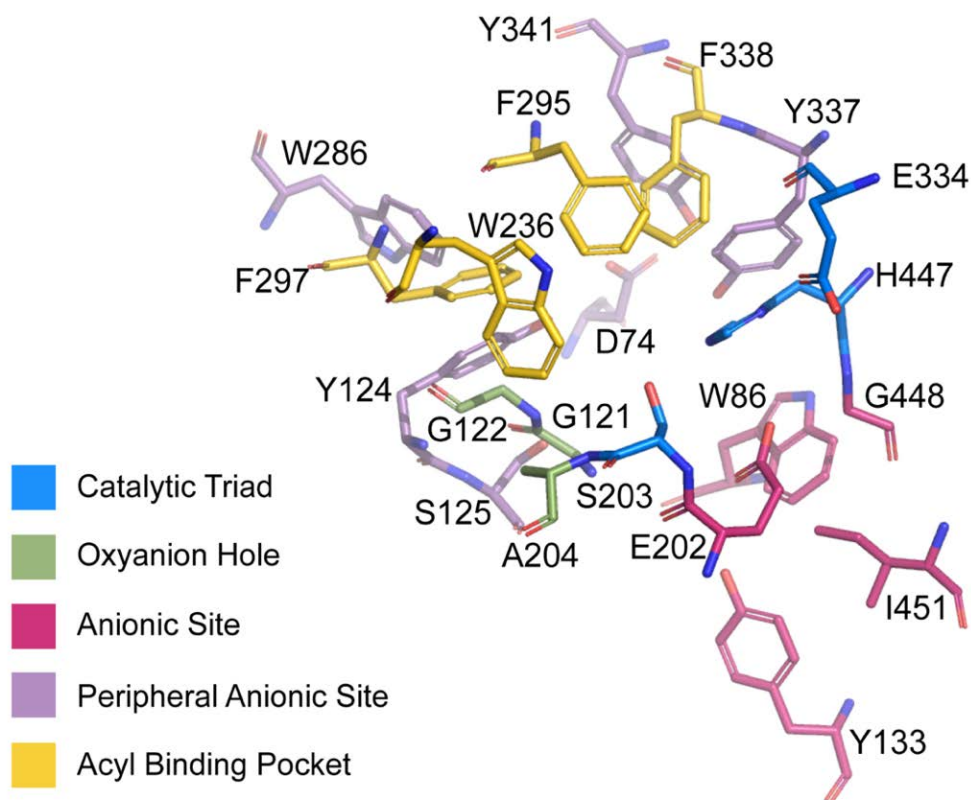


Figure 1.5. Active site of human acetylcholinesterase. The subsites of the hAChE active site are each denoted by a different residue color (PDB 4EY4).

Overall, the structure of hAChE⁴² shows marked similarity to the original tAChE structure¹⁰² as well as to other species. Most of the active site gorge residues are the same between the tAChE, mAChE and hAChE including residues within key sites. There are several subsites within the AChE active site including the catalytic triad (Ser203, His447, and Glu334; numbered in hAChE), the oxyanion hole (Gly121, Gly122, Ala204), anionic site (Trp86, Tyr133, Glu202, Gly448, Ile451), peripheral anionic site (PAS; Asp74, Tyr124, Ser125, Trp286, Tyr337, Tyr341), and acyl binding pocket (Trp236,

Phe295, Phe297, Phe338) (Figure 1.5) ^{102, 105}. The active site residues of AChE tend to remain fairly conserved across species, especially those that are closely related ^{42, 105}. However, the residues just outside the active site, known as second shell residues, show much greater variance, which could influence AChE's ability to accommodate certain inhibitors and reactivators ¹⁰⁵. These species-species differences may explain the wide variation in OP nerve agent and reactivator potency between AChE species ^{100, 101}. Thus, the inability to translate species-species and lack of reliable animal model systems has heightened the need for authentic hAChE to use in structural and enzymatic characterizations.

However, there are still many unanswered questions surrounding AChE's accommodation of nerve agents and reactivators in the active site. Specifically, the influence of AChE's stereoselectivity on the accommodation of OP nerve agent stereoisomers and their impact on subsequent reactivation is not fully discerned. In addition, the means to accommodate certain nerve agents and reactivators into the active site is potentially due to the flexibility of certain regions of hAChE, but these dynamics are not well-understood. Currently, the development of novel therapeutic agents is somewhat hindered by the lingering questions surrounding the mechanism and manner of reactivation by oxime reactivators. To provide insight into the dynamics of hAChE's active site, the impact of hAChE's stereoselectivity on inhibition and reactivation, the influence of different nerve agents and their subsequent reactivation on AChE's active site, and the structural and biochemical effects of monomerizing hAChE were examined. The following studies further elucidate the dynamics of the active site and its ability to accommodate a wide variety of OP nerve agents and reactivators.

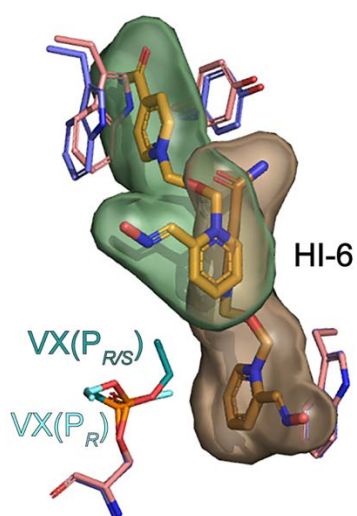
CHAPTER 2

STRUCTURAL INSIGHTS OF STEREO SPECIFIC INHIBITION OF HUMAN
ACETYLCHOLINESTERASE BY VX AND SUBSEQUENT REACTIVATION BY
HI-6¹

¹Bester, S.M., M.A. Guelta, J. Cheung, M.D. Winemiller, S.Y. Bae, J. Myslinski, S.D. Pegan, and J.J. Height. 2018. *Chemical Research in Toxicology*. 31(12): 1405–1417. Reprinted here with permission of the publisher.

Abstract

Over 50 years ago, the toxicity of irreversible organophosphate inhibitors targeting human acetylcholinesterase (hAChE) was observed to be stereospecific. The therapeutic reversal of hAChE inhibition by reactivators has also been shown to depend on the stereochemistry of the inhibitor. To gain clarity on the mechanism of stereospecific inhibition, the X-ray crystallographic structures of hAChE inhibited by a racemic mixture of VX ($P_{R/S}$) and its enantiomers were obtained. Beyond identifying hAChE structural features that lend themselves to stereospecific inhibition, structures of the reactivator HI-6 bound to hAChE inhibited by VX enantiomers of varying toxicity, or in its uninhibited state, were obtained. Comparison of hAChE in these pre-activation and postre-activation states along with enzymatic data reveals the potential influence of unproductive reactivator poses on the efficacy of these types of therapeutics. The recognition of structural features related to hAChE's stereospecificity toward VX shed light on the molecular influences of toxicity and their effect on reactivators. In addition to providing a better understanding of the innate issues with current reactivators, an avenue for improvement of reactivators is envisioned.

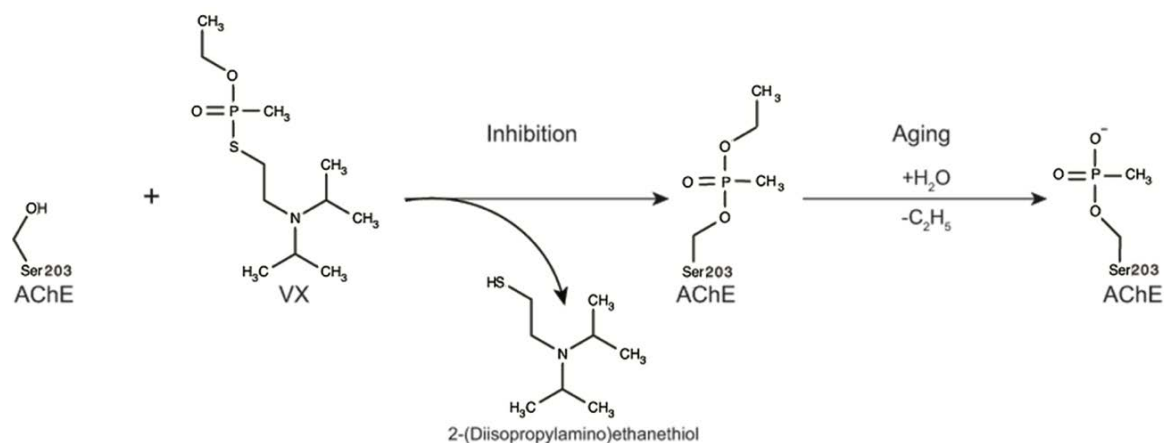


Introduction

The intentional use of organophosphate (OP)-based nerve agents and pesticides poses a significant health threat through their irreversible inhibition of human acetylcholinesterase (E.C. 3.1.1.7, UNIPROT: P22303, hAChE). Their relevant toxicity has recently been reaffirmed by the recent assassination of the half-brother of North Korean leader, Kim Jong-un, with the chemical nerve agent VX,¹ the continued use of chemical nerve agents in Syria,² and recent use in the United Kingdom.³ Acetylcholinesterase catalyzes the hydrolysis of the neurotransmitter acetylcholine (ACh) and regulates nerve signaling. It is found in the neuromuscular junction (NMJ) of all autonomic ganglia and innervated organs and in the brain and spinal cholinergic synapses.⁴ Due to its essential role in the nervous system, AChE is the biological target of pesticides and chemical warfare agents. Conventional OP nerve agents and pesticides employ the same organophosphate chemical scaffold to covalently modify acetylcholinesterase catalytic serine leading to inhibition and in most cases can result in additional processes that age the enzyme.⁵ For example, G-type nerve agents such as soman (O-pinacolyl methylphosphonofluoridate) possess the same fluorophosphate moiety as the pesticide mipafox (N,N'-diisopropyldiamidofluorophosphate; DDFP).⁶ In the case of V-type nerve agents that have been used recently,⁷ the fluoride of the organophosphate core is substituted with a thiol leaving group,⁸ yielding a more stable molecule with greater toxicity to hAChE (Scheme 2.1).

Intriguingly, straightforward assessment of the underlying factors that lead to inhibition of hAChE by V-series agents such as VX (ethyl({2-[bis(propan-2-yl)amino]ethyl}sulfanyl)-(methyl)phosphinate) have traditionally proven difficult due in

part to the availability of hAChE. Although structures of AChE from species other than human inhibited by VX, such as mouse and *Torpedo californica*, exist the toxicity of nerve agents to include those of the V-series have been known to vary in a species-dependent manner.⁹ This has made direct comparisons of nerve agent toxicity measured in homologues to hAChE difficult. Adding further complexity, the toxicity of nerve agents including the V-series agents, such as VX, has been historically observed to be stereospecific.^{10,11} Utilizing human erythrocyte ghosts, previous reports have suggested a 13-fold difference in toxicity between VX enantiomers, with the (–) or P_S enantiomer being the more toxic of the two.¹¹ Similar trends have been observed for other G- and V-series agents using similar techniques with other species AChE.^{12,13} Understanding the molecular basis for this stereospecific phenomenon of nerve agents, especially in humans, has been in part limited due to lack of structural data of hAChE with the nerve agents themselves.



Scheme 2.1. Inhibition and Aging of VX in hAChE.

Currently, the preferred treatment for organophosphate agent poisoning involves a combination of atropine, benzodiazepine, and pralidoxime.¹⁴ The latter, also known as 2-PAM, belongs to a class of nerve agent antidotes classified as reactivators. These

therapeutics seek to reverse nerve agent conjugation of the hAChE active site serine prior to further dealkylation of that moiety, or aging.¹⁵⁻¹⁹ Intriguingly, therapeutic efficacy appears to vary not only with the OP used but also the stereochemistry of originating OP and species origin of the AChE.^{9,13,20-22} For example, HI-6 (asoxime) (1-(2'-hydroxyiminomethyl-1'-pyridinium)-3-(4'- carbamoyl-1-pyridinium)) is currently being considered a next-generation reactivator-based therapeutic by certain nations²³ and is preferred due to its ability to robustly reactivate AChEs inhibited by V-series agents and others across the chemical warfare spectrum compared to 2-PAM and its low toxicity compared to other reactivators.^{9,22,24-26} Similar to the scarcity of structural information surrounding inhibition of hAChE by V-series agents, limited structural information is also available in regards to how HI-6 is accommodated within the apo hAChE active site and the hAChE active site inhibited by nerve agents. Attempts to observe HI-6 within AChE have occurred with some success utilizing apo or sarin inhibited mouse acetylcholinesterase (mAChE), particularly in observing the core pyridinium ring system. Regrettably, density for the catalytically relevant and flexible oxime-containing side chain of HI-6 in these structures was absent, or limited.^{8,27} Some more recent attempts have been able to assemble a density functional theory (DFT)-based computational model of the oxime-containing arm with the aid of X-ray crystallographic information.²⁸ However, with species-species differences among AChEs already known to effect reactivator efficacy and recent reports finding that other AChE therapeutic relevant ligands interact with the hAChE differently than other AChEs, the structural understanding of how HI-6 is accommodated within the most pertinent AChE, hAChE, is limited.

Here, we illuminate hAChE's molecular mechanism related to stereospecificity toward VX and similar agents and subsequent reactivation. To this end, VX and its associated stereoisomers' ability to inhibit hAChE were directly assessed as well as its potential relation to their toxicity. Additionally, the efficacy of HI-6 to reactivate these stereospecifically inhibited hAChEs was explored. Utilizing X-ray crystallography, seven structures of hAChE were obtained with conjugates of $P_{R/S}$ -VX, P_R -VX, and P_S -VX, and with these VX conjugates and HI-6 (hAChE-VX-HI-6), and hAChE bound solely with HI-6. Furthermore, a post-reactivation structure of a VX-hAChE conjugate was elucidated illuminating the products of reactivation by HI-6. Through these structures and accompanying enzyme kinetic information, critical insights into the hAChE active site features that drive hAChE stereoselectivity for certain VX stereoisomers and impact their reactivation were obtained.

Experimental Procedures

Materials.

Acetylthiocholine, 5,5'-bis-dithio-2-nitrobenzene (DTNB), HI-6, sodium carbonate, monosodium phosphate, and disodium phosphate were purchased from Sigma-Aldrich (St. Louis, MO USA). HEPES, KNO₃, and PEG-3350 solutions were purchased from Hampton Research, Aliso Viejo, CA. Laboratory deionized water >17 MΩ was used for all assays. Hexane and isopropyl alcohol were purchased from Fisher Scientific (Waltham, MA).

Agent Enantiomers.

Nerve agent VX (>95% purity) was synthesized by the Agent Chemistry Team from the Research and Technology Directorate of the U.S. Army Edgewood Chemical

Biological Center (Aberdeen Proving Ground, MD). VX enantiomers were prepared, and the purity characterized by HPLC methods. Analytical samples were prepared at 100 $\mu\text{g}/\text{mL}$, preparative samples were prepared at 22 mg/mL , and all reagents and solvents were high- performance LC grade. The enantioselective preparative-scale separation of agents was achieved using an Agilent 1100 series preparative-scale LC system equipped with a diode array detector. Injections were monitored at 210 nm. Separation was through a Phenomenex Lux Cellulose-1 Axia packed column ($250 \times 30 \text{ mm}$) with an isocratic condition of 96/4 (v/v %) A/B, a flow rate of 20 mL/min , and a sample volume of 1000 μL . Both VX enantiomers were baseline separated within 23 min. The Agilent 1200 Infinity series fraction collector was configured using the peak-time-based collection protocol, and the separated enantiomers were combined into 500 mL round-bottom flasks for solvent removal by rotary evaporation. Individual enantiomers were confirmed by polarimetry using an Autopol I (Rudolph Research Analytical, U.S.) and a 100 mm optical cell.

The analytical separations of the enantiomers were characterized using an Agilent 1200 Infinity series LC system (Agilent Technologies; Santa Clara, CA), with an Agilent TOF-MS and APCI source using TIC; 5–500 m/z with the molecular ion at 268.1505 was performed on a Lux Cellulose-1 column ($250 \times 4.6 \text{ mm}$, 5 μm ; Phenomenex; Torrance, CA). The mobile phase consisted of *n*-hexane (A) and isopropyl alcohol (B), and the sample volume was 10 μL . Separation was achieved using isocratic conditions of 96/4 (v/v %) A/B for VX with a flow rate of 0.6 mL/min .

Cloning, Expression, and Purification of hAChE.

Expression and purification of hAChE were as previously described^{5,29} by transfecting recombinant octahistidine (His₈)-tagged hAChE amino acid sequence 1–574 (preprocessed protein numbering which includes the native secretion signal) encoded construct into HEK- 293-H cells (Invitrogen). Purified protein was dialyzed into storage buffer C (10 mM HEPES pH 7.0, and 10 mM NaCl) overnight and concentrated to 16 mg/mL for crystallization.

Measurement of Inhibition Rate Constants.

hAChE samples were prepared in 50 mM phosphate buffer, pH 8.0 containing BSA (5%) aliquoted (900 μ L) and stored at -80 °C. An Ellman assay was adapted to assess the inhibitory properties of P_{R/S}-VX and each of its stereoisomers.³⁰ Two methods were utilized for calculation of inhibition rate constants: (1) a continuous method³¹ for isomers that react with AChE quickly, and (2) a discontinuous method²² for isomers that react slowly. The continuous method was utilized for P_{R/S}-VX and P_S-VX. Briefly, the stabilized hAChE solution was thawed on ice, and about 0.48 μ M was dispensed into the desired well on a 96-well flat-bottomed polystyrene microplate, which contained varying concentrations of P_{R/S}-VX (94.4, 37.8, 18.9, 13.2, 7.6, 3.8, 0.38, 0.038, 0.0038, 0.00038, 0.000038, and 0 nM) or P_S-VX (37.8, 34.0, 28.3, 22.7, 17.0, 11.3, 5.7, 3.8, 0.38, 0.11 0.038, 0.0038, and 0 nM), DTNB (0.3 mM), and acetylthiocholine (1 mM) (final volume 250 μ L) at $t = 0$. Hydrolysis of acetylthiocholine was monitored as the increase in absorbance of the TNB²⁻ chromophore at 412 nm, which was recorded every 7 s on a plate reader (BioTek Synergy4) for 30 min. Due to the long inhibition times required, the discontinuous method was utilized for P_R-VX. Briefly, the stabilized hAChE solution was

thawed on ice, and 0.48 μM was dispensed into eight wells of a 96-well flat-bottomed polystyrene microplate, which contained a range of concentrations of $\text{P}_R\text{-VX}$ ranging from 378 to 0.038 nM (final volume 50 μL) at $t = 0$. The plate reader was equilibrated to 37 $^\circ\text{C}$; a solution of DTNB and acetylthiocholine (210 μL) injected immediately before monitoring the absorbance (412 nm) over a period of 30–60 s. The absorbance was measured at time points of 0, 0.1, 1, 2, 3, 4, 5, 6, 7, 10, and 15 min. The Beer's Law plot ($\epsilon = 14150 \text{ M}^{-1} \text{ cm}^{-1}$, $b = 0.79 \text{ cm}$) yielded the rate of hydrolysis of acetylthiocholine for each set of reaction conditions. All experiments were done in at least triplicate.

Measurement of Reactivation of VX Inhibited hAChE.

Inhibited hAChE was prepared by diluting AChE into 50 μL of 50 mM phosphate buffer, pH 8.0 containing BSA (5%), and 10 μL of VX (1 mg/mL), incubated on ice for 30 min, then excess inhibitor was removed by centrifugation through a Centri-Sep spin column, at 750xG for 2 min, prior to dilution in the same buffer (pH 8.0 containing 0.1 mg/mL BSA), aliquoted (900 μL), and stored at $-80 \text{ }^\circ\text{C}$. The same modified Ellman's assay as for determining the inhibition kinetics of $\text{P}_{R/S}\text{-VX}$ and its individual stereoisomers was utilized to observe reactivation kinetics of HI-6. Briefly, the assay solution was dispensed via the plate reader into 96-well flat-bottomed polystyrene microplate containing the desired concentration of reactivator. Reactivation of inhibited AChE was determined by adding a reactivator (1500, 1000, 500, 250, 150, or 15 μM , final concentration) to the VX inhibited AChE immediately prior to inserting into the plate reader. The activity was measured at 30 s, 1, 2, 3, 4, 5, and 30 min. The change in percent reactivated AChE was proportional to the rate of hydrolysis of acetylthiocholine relative to uninhibited AChE. The rate of reactivation (k_{obs}) at each concentration is

given by eq 2.1, which assumes complete inhibition. All experiments were performed in triplicate.

$$-k_{obs}t = \ln\left(\frac{v_o - v_t}{v_o - v_{ox}}\right) \quad (2.1)$$

Percent reactivated was determined according to eq 2.2:

$$(E_{react})_t = \frac{v_t - v_{ox}}{v_o - v_{ox}} \quad (2.2)$$

where v_t is the rate of reaction of thiocholine with DTNB at time t , v_{ox} is the rate of reaction of oxime with DNTB at each concentration measured, and v_o is the rate of reaction of thiocholine with DTNB at time t for uninhibited AChE. The rate of reaction of thiocholine with DTNB was taken as the rate of the hydrolysis of acetylthiocholine to thiocholine and acetate.

$$(E_{react})_t = A(1 - e^{-k_{obs}t}) \quad (2.3)$$

where k_{obs} is the first-order reactivation rate constant, t is the time at which the assay solution was added to the reactivated AChE; and A is the theoretical percent of maximum reactivation.

$$k_{obs} = \frac{k_2}{1 + K_{OX}/[ox]} \quad (2.4)$$

$$k_r = \frac{k_2}{K_{OX}} \quad (2.5)$$

where K_{OX} and k_2 were determined from the second-order plot of k_{obs} and oxime concentration, where k_2 is the intrinsic reaction constant; K_{OX} is the apparent equilibrium constant; and k_r is the second-order reactivation rate constant³².

Human Acetylcholinesterase Crystallization and Inhibitor Soaking.

Crystallization of hAChE for ligand soaks occurred following the general procedures communicated in recent studies.^{5,33} In short, purified protein concentrated to

16 mg/mL and apo hAChE crystals were grown by sitting drop vapor diffusion at 22 °C against 5 μ L crystallization buffer. The crystallization buffer contained 15–21% polyethylene glycol 3350 (PEG) and 0.17–0.21 M potassium nitrate. The hexagonal rod-shaped crystals generally nucleated within 5 days and finished their growth after an additional 3 days. Crystals of a ligand in complex with hAChE were obtained by soaking apo crystals at 22 °C in crystallization buffer accompanied by 20–25% ethylene glycol and specific concentrations of each ligand for individually designated periods of time. In order to obtain AChE-HI-6 apo complex, the apo AChE crystals were soaked in crystallization buffer with a concentration of 11.1 mM of HI-6 for 1 min. For AChE- $P_{R/S}$ -VX complex, the apo AChE crystal was soaked in a 22.47 mM $P_{R/S}$ -VX mixture for 5 min, while to achieve AChE- P_S -VX, the apo crystals were soaked in buffer with 3.74 mM P_S -VX for 5 min. For AChE- P_R -VX complex, the crystals were soaked in buffer with 3.74 mM P_R -VX for 2 min. To obtain the AChE- $P_{R/S}$ -VX-HI-6 complex, the crystal was soaked in a 3.94 mM $P_{R/S}$ -VX solution for 30 min and an 11.1 mM HI-6 solution for 2 min. For the AChE- P_R -VX-HI-6 complex, the apo crystals were soaked in buffer with a concentration of 22.47 mM P_R -VX for 1 min and then buffer with 11.1 mM concentration of HI-6 for 2 min. The AChE-EMPA-HI-6 complex was achieved via soaking the crystals in buffer with a $P_{R/S}$ -VX mixture concentration of 3.94 mM for 6 min and in 11.1 mM HI-6 buffer for 10 min. The crystals were then mounted onto liquid nitrogen flash-cooled nylon loops.

Data Collection, Reduction, and Refinement.

Data sets were collected for AChE- $P_{R/S}$ -VX, AChE- P_S -VX, AChE-VX-HI-6, AChE- P_R -VX-HI-6, and AChE-EMPA-HI-6 complexes with a resolution of 2.22, 2.27,

2.28, 2.60, and 2.45 Å, respectively, on the 22ID beamline of SERCAT at the Advanced Photon Source, Argonne National Laboratory using a monochromic X-ray beam with a Rayonix (Mar) 300HS high-speed CCD detector. Data sets were collected for AChE-HI-6 apo and AChE- P_R -VX complexes with a resolution of 2.31 and 2.40 Å, respectively, on the 22BM beamline of SERCAT at the Advanced Photon Source, Argonne National Laboratory using a monochromic X-ray beam with a Mar300 CCD detector. X-ray images were indexed, strategized, integrated, and scaled processed, using HKL2000.³⁴ CCP4 software suite was employed to create a cross-validation set from a random 5% of the reflections, and the same test set was employed throughout the structural refinement.³⁵ The initial phase solutions for the structures were established using molecular replacement via Phaser with 4EY4⁵ as an initial mode.³⁶ The refinement of the structures was performed using repetitive cycles of model building and refinement using COOT and Phenix to refine, respectively. TLS motion determination (TLSMD) was utilized to analyze the structure for flexibility, and this analysis was employed for TLS parameters in Phenix Refine to aid in refining anisotropic displacements in the structures.³⁷ Water molecules were originally added to $2F_o - F_c$ density peaks of $>1\sigma$ using the Find Water COOT program function, and then were assessed individually.³⁸ Subsequently, carbohydrates, PEGs, and other ligands were individually placed into structures based on $F_o - F_c$ density at 3σ and refined with Phenix.Refine after which the structures are positioned to fit the $2F_o - F_c$ density at 1σ . The final model of each structure was examined via Molprobit to confirm the quality of the structures. The data collection and refinement statistics for each structure are listed in Table 2.2.

Results

Stereospecific Inhibition of hAChE by VX Stereoisomers.

A number of values for the kinetics surrounding AChEs and their inhibition by OPs have been determined and used to highlight not only that AChE rates differ between species but also that other variables impact these values.^{9,13,32,39} These variables include purification, assay conditions, differing standardization of erythrocyte ghosts, need to address residual butyrylcholinesterase activity, and other confounding factors.^{39,40} Only recently, the option of using of mammalian recombinant hAChE for enzyme has become available and allows for more direct assessment of hAChE kinetics. However, kinetic assessment of recombinant hAChE has been limited to racemic mixtures of nerve agents.³³ To obtain kinetic values related to the stereospecific inhibition of recombinant hAChE by VX, hAChE was expressed and purified from HEK-293 cells and treated with pure enantiomers of VX. Utilizing a modified Ellman's assay, hAChE's k_{cat} toward acetylcholine was determined to be 9204 s^{-1} . Subsequently, the potency of $P_{R/S}$ -VX as well as its pure P_S and P_R enantiomers was obtained. Due to the high potency of $P_{R/S}$ -VX and its P_S enantiomer, a continuous method³¹ was utilized. This yielded a k_i of $7.7 \times 10^7 \text{ M}^{-1} \text{ min}^{-1}$ and $1.6 \times 10^8 \text{ M}^{-1} \text{ min}^{-1}$ for $P_{R/S}$ -VX and the P_S -VX enantiomer, respectively (Table 2.1). For P_R -VX, which was observed to react generally slower than $P_{R/S}$ -VX and the P_S -VX, a discontinuous method was employed.²² This revealed a k_i of $1.6 \times 10^5 \text{ M}^{-1} \text{ min}^{-1}$ for P_R -VX that is about 480- and 1000- fold less than that observed for $P_{R/S}$ -VX and P_S -VX, respectively (Table 2.1A). The relatively low k_i of P_R -VX toward hAChE when compared to that of $P_{R/S}$ -VX and P_S -VX as well as the nearly double potency of P_S -VX over $P_{R/S}$ -VX and P_R -VX further supports previous findings that the

presence of P_S-VX is the main driving force behind hAChE inhibition by VX and its toxicity.¹¹

Table 2.1. A. Inhibition of hAChE and B. Reactivation of hAChE by HI-6

A				
	k_2 (min ⁻¹)	K_d (M)	k_i (M ⁻¹ min ⁻¹)	
(P _S /P _R)-VX	4.5×10^{-2}	5.9×10^{-10}	7.7×10^7	
(P _S)-VX	3.5×10^{-2}	2.3×10^{-10}	1.6×10^8	
(P _R)-VX			1.6×10^5	
B				
OP	k_2 (min ⁻¹)	K_{OX} (μM)	k_r (μM ⁻¹ min ⁻¹)	max%
(P _S /P _R)-VX	0.63 ± 0.04	7.50 ± 2.1	0.084 ± 0.02	>100
(P _S)-VX	0.71 ± 0.06	23.3 ± 8.0	0.031 ± 0.01	92
(P _R)-VX	n.c. ^a	n.c. ^a	n.c. ^a	n.c. ^a

^an.c. refers to noncalculable.

Structural Basis of hAChE Stereospecific Inhibition of VX.

With the significant preference of hAChE for one stereoisomer of P_S-VX over P_R-VX readily apparent, the molecular underpinnings of this preference were investigated. To this end, hAChE was crystallized and then soaked in a solution containing P_{R/S}-VX for 5 min prior to freezing. These crystals lead to obtaining a 2.2 Å data set in space group *P*3₁21 that was subsequently solved using apo hAChE (PDB 4EY4)⁵ as a molecular replacement search model (Table 2.2). As expected, two monomeric subunits were found in the asymmetric unit. Upon examination of the active sites, significant $F_o - F_c$ simulated annealing omit map density was observed at the OG atom of Ser203 in both active sites of the dimeric hAChE (Figure S2.1a). Initial placement of a phosphonate or P_R-VX did not fully account for density. Only upon refinement with S_N2 reaction derived adduct of P_S-VX placed within the difference map density of each monomer accounted for additional density observed off Ser203 (Figure 2.1a). To confirm the nature of the adduct found in the P_{R/S}-VX, a data set to 2.3 Å was obtained in crystals soaked in the P_S-VX isomer. Density within the active site of hAChE-P_S-VX is consistent to that observed in

the hAChE-P_{R/S}-VX structure (Figures 2.1a,b and S2.1b). Intriguingly, as P_S-VX is reported to be the more toxic of the two isomers, the presence of the hAChE reaction P_S-VX appears to lend further evidence that P_S-VX's toxicity is linked to hAChE preference for the P_S-VX.¹¹

Table 2.2. Crystallography data of hAChE structures.

	AChE HI-6 Apo (PDB 6CQU)	AChE P _{R/S} -VX (PDB 6CQZ)	AChE P _S -VX (PDB 6CQT)	AChE P _R -VX (PDB 6CQX)
Data Collection				
space group	P3 ₁ 21	P3 ₁ 21	P3 ₁ 21	P3 ₁ 21
cell dimensions				
<i>a</i> , <i>b</i> , <i>c</i> (Å)	105.1, 105.1, 324.1	104.6, 104.6, 323.8	104.4, 104.4, 323.2	104.9, 104.9, 323.9
<i>α</i> , <i>β</i> , <i>γ</i> (°)	90, 90, 120	90, 90, 120	90, 90, 120	90, 90, 120
resolution (Å)	50.0–2.31 (2.31–2.35) ^a	50.0–2.22 (2.22–2.26) ^a	50.0–2.27 (2.27–2.31) ^a	50.0–2.40 (2.40–2.44) ^a
completeness (%)	97.5 (97.2) ^a	99.5 (91.9) ^a	99.5 (97.3) ^a	99.6 (95.3) ^a
<i>R</i> _{merge} (%) ^b	8.2 (60.5) ^a	10.2 (31.4) ^a	7.1 (31.0) ^a	7.0 (36.2) ^a
<i>R</i> _{pim} (%)	6.1 (46.7) ^a	4.8 (16.5) ^a	3.2 (15.0) ^a	4.4 (24.1) ^a
<i>I</i> / <i>σI</i>	12.4 (2.1) ^a	16.6 (5.2) ^a	25.8 (3.6) ^a	13.6 (3.2) ^a
redundancy	2.5 (2.6) ^a	5.1 (5.1) ^a	6.0 (6.0) ^a	3.4 (3.4) ^a
Refinement				
resolution (Å)	34.75–2.31 (2.39–2.31)	37.11–2.22 (2.30–2.22)	45.19–2.27 (2.36–2.27)	36.98–2.40 (2.49–2.40)
no. reflections	90115	94142	94419	81622
<i>R</i> _{work} (%) ^c / <i>R</i> _{free} (%) ^c	17.0/20.7	17.0/19.6	15.1/18.2	16.6/19.0
no. atoms (protein/ligand/water)	8296/191/807	8267/102/1143	8352/158/1184	8323/161/917
B-Factors				
protein	43.51	34.2	34.1	44.9
ligands	92.31	87.0	81.8	106.9
water	53.57	52.0	49.9	55.7
Deviations				
bond lengths (Å)	0.005	0.008	0.008	0.012
bond angles (°)	0.92	0.96	1.07	1.40
	AChE P _{R/S} -VX HI-6 (PDB 6CQW)	AChE P _R -VX HI-6 (PDB 6CQV)	AChE EMPA HI-6 (PDB 6CQY)	
Data collection				
space group	P3 ₁ 21	P3 ₁ 21	P3 ₁ 21	
cell dimensions				
<i>a</i> , <i>b</i> , <i>c</i> (Å)	105.0, 105.0, 324.6	104.4, 104.4, 323.6	105.2, 105.2, 324.3	
<i>α</i> , <i>β</i> , <i>γ</i> (°)	90, 90, 120	90, 90, 120	90, 90, 120	
resolution (Å)	50.0–2.28 (2.28–2.32) ^a	50.0–2.60 (2.64–2.60) ^a	50.0–2.45 (2.45–2.49) ^a	
completeness (%)	99.6 (93.9) ^a	98.7 (99.7) ^a	100.0 (100.0) ^a	
<i>R</i> _{merge} (%) ^b	10.4 (42.7) ^a	5.9 (40.4) ^a	7.0 (59.0) ^a	
<i>R</i> _{pim} (%)	4.6 (20.8) ^a	2.7 (18.7) ^a	3.1 (27.5) ^a	
<i>I</i> / <i>σI</i>	12.43 (2.0) ^a	26.8 (4.1) ^a	20.0 (2.1) ^a	
redundancy	5.7 (5.7) ^a	5.6 (5.4) ^a	6.1 (6.1) ^a	
Refinement				
resolution (Å)	39.67–2.28 (2.36–2.28)	39.5–2.60 (2.69–2.60)	43.84–2.45 (2.54–2.45)	
no. reflections	95417	62304	77474	
<i>R</i> _{work} (%) ^c / <i>R</i> _{free} (%) ^c	18.0/20.5	16.6/20.9	17.2/20.0	
no. atoms (protein/ligand/water)	8379/172/683	8268/172/718	8318/160/510	
B-Factors				
protein	54.6	43.5	57.4	
ligands	100.3	77.5	89.9	
water	60.2	48.0	61.9	
RMS Deviations				
bond lengths (Å)	0.006	0.006	0.005	
bond angles (°)	0.86	0.95	0.80	

^aData for the last resolution shell are provided in parentheses. ^b $R_{\text{merge}} = \frac{\sum h \sum i |\Pi(h) - \langle I(h) \rangle|}{\sum h \sum i \Pi(h)}$, where $\Pi(h)$ is the *i*th measurement and $\langle I(h) \rangle$ is the weighted mean of all measurements of *I*(*h*). ^c R_{work} and $R_{\text{free}} = \frac{h[|F_{(h)\text{obs}}| - |F_{(h)\text{calc}}|]}{h|F_{(h)\text{obs}}|}$ for reflections corresponding to the working and test sets.

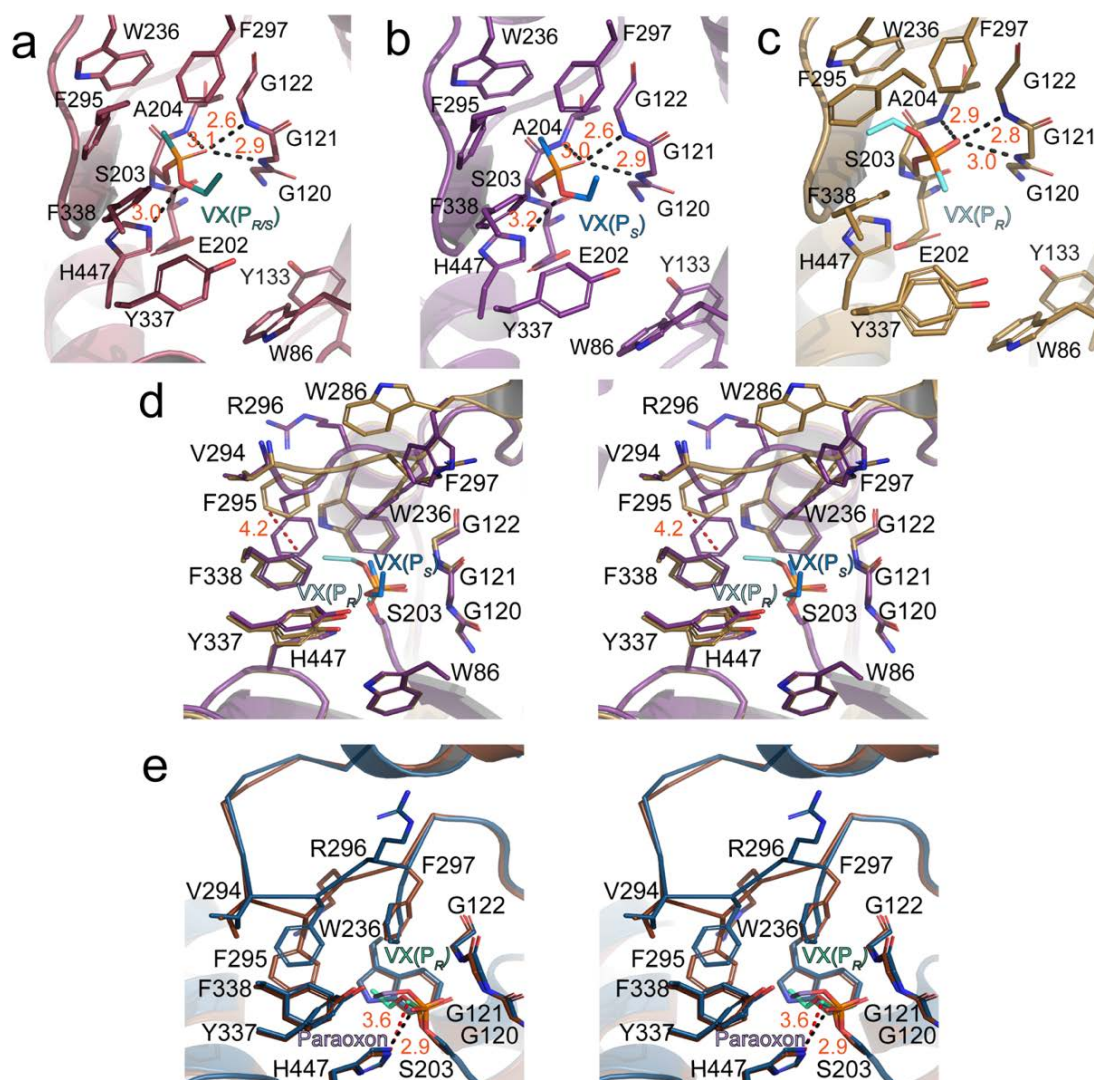


Figure 2.1. Crystal structures of human acetylcholinesterase in complex with stereoisomers of nerve agent, VX. (a) Wall-eyed stereo view of $P_{R/S}$ -VX (dark teal) bound to the active site of hAChE (raspberry) (PDB 6CQZ). (b) Wall-eyed stereo view of P_S -VX (marine blue) bound to the active site of hAChE (violet purple) (PDB 6CQT). (c) Wall-eyed stereo view of P_R -VX (aquamarine) bound to the active site of hAChE (sand brown) (PDB 6CQX). (d) Wall-eyed stereo view of an overlay of the active sites of hAChE containing P_S -VX and P_R -VX. (e) Wall-eyed stereo view of an overlay of the active sites and acyl loops of hAChE (chocolate) inhibited by P_R -VX (sea foam green) and hAChE (Prussian blue) inhibited by paraoxon in an aged state (purple heather) (PDB 5HF6). The red dashed line represents the distance between two atoms, while the black lines represent hydrogen bonds. The AChE residues are represented by black letters, while the red letters are the distances.

The P_S -VX adduct appears to adopt an orientation that illustrates how P_S -VX capitalizes on the cavities present in not only in the apo hAChE structure but also other

AChEs.^{41,42} In detail, the methyl group Ps-VX points into a small hydrophobic pocket consisting of Trp236, Phe297, and Phe295, whereas the ethoxy group points in the opposite direction into a substantially larger hydrophobic pocket formed by Tyr133, Trp86, Tyr337, and Phe338 (Figure 2.1a,b). In the hAChE oxyanion hole, the backbone amines of Gly122, Gly121, and Ala204 form hydrogen bonds with the carbonyl oxygen in the Ps-VX adduct. Additionally, the ethoxy oxygen forms a hydrogen bond with a nitrogen on the His447 side chain, which forms part of the catalytic triad with Ser203 and Glu334 of the active site. Intriguingly, the hydrogen bonds made by Ps- VX largely mirror the bonds expected to form between hAChE and its natural substrate, ACh.⁴³

With the snug and well-coordinated fit of the Ps-VX adduct within the active site pocket, biochemical data illustrating hAChE ability to be inhibited, albeit slower, by P_R-VX are surprising, given the spatial constraints of the hAChE active site. To gain insight into how the hAChE active site can accommodate the P_R-VX isomer with enough affinity for hAChE to react, hAChE was soaked for 2 min in solution containing the P_R-VX isomer. As with hAChE complexes formed with P_{R/S}-VX and P_S-VX, the structure of hAChE in complex with P_R-VX showed an inhibited state, refined to 2.4 Å (Figures 2.1c and S2.1c). Although at first glance the global structure obtained from these crystals largely mirrored those of the P_{R/S}-VX and P_S-VX bound hAChE structures, notable differences were observed within the hAChE active site. Not surprisingly, the placement of the alkyl chains of the P_R-VX adduct within the catalytic site is different from the other two structures, but hydrogen bonding between the carbonyl oxygen of the adduct with backbone nitrogen atoms of Gly122, Gly121, and Ala204 is preserved. This proposes that the oxyanion hole of hAChE has a similar role with both enantiomers and that the overall

inhibition of hAChE is likely similar between the two VX enantiomers. In the structure of hAChE inhibited by P_R-VX, the methyl group points to the larger hydrophobic pocket formed by Tyr133, Trp86, Tyr337, and Phe338 (Figure 2.1c,d), and the larger ethoxy group points toward the small pocket created by Trp236, Phe297, and Phe295, and a hydrogen bond between the oxygen of the ethoxy and His447 is not formed. Excitingly, despite the small steric volume observed previously within the VX bound hAChE structures for the pocket of Trp236, Phe297, and Phe295, the ethoxy group of the P_R-VX was accommodated.

Comparison of hAChE-P_R-VX and hAChE-P_S-VX structures reveals that this accommodation occurs through the ability of Phe295 to shift up to 4.2 Å to enlarge this pocket (Figures 2.1d and S2.1d). This accommodation also leads to the movement of Trp286, Phe297, and Arg296 as well as shifts in the surrounding residues (286–297), which encompasses the majority of the acyl loop (287–299). The side chain of Arg296 shifts 4.3 Å at C α between the structures of the enantiomers. In the hAChE-P_S-VX structure the side chain is positioned outward from the active site and directed into the active site in the hAChE-P_R-VX structure. In the active site the side chain of Arg296 is positioned into the peripheral anionic site, resulting in the displacement of Trp286. A similar shift, resulting in Phe295 moving 3.4 Å is observed in the other asymmetric unit active site albeit with Arg296 retaining a more wild-type confirmation (Figure S2.3). Shifting of the acyl loop has been observed recently upon inhibition and aging of hAChE by paraoxon.³³ Although the P_R-VX and the aged paraoxon adducts share the similarity of an ethoxy group pointing toward Phe295, the aged paraoxon adduct has an oxygen available to form a hydrogen bond with His447. Divergent from the P_R-VX inhibited

active site, the paraoxon adduct projects its ethoxy group more toward Phe338 than observed in P_R-VX (Figure 2.1E). Given the same space group and crystal conditions along with the large resulting movement of Phe295 compared to hAChE-P_S-VX and hAChE aged by paraoxon, hAChE-P_R-VX appears to highlight how sensitive the acyl loop can be to even minor differences between OPs.

Influence of VX Stereoisomer-Specific Inhibition of hAChE on HI-6 Reactivation.

To examine the influence of a nerve agent's stereochemistry on the efficacy of therapeutic intervention by reactivators, the ability of a next-generation reactivator, HI-6, to reverse recombinant hAChE's inhibition by P_{R/S}-VX or its individual stereoisomers was examined. Making use of hAChE and employing a modified Ellman's assay, the k_r of HI-6 for hAChE inhibited by P_{R/S}-VX and P_S- VX were revealed to be 0.084 ± 0.02 and $0.031 \pm 0.01 \mu\text{M}^{-1} \text{min}^{-1}$ respectively, while the k_r of HI-6 for hAChE inhibited by P_R-VX was not appreciable (Table 2.1B). Comparing with previous studies using the erythrocyte-based assays, the general trend was the same.^{13,22} The k_r values of the P_{R/S}-VX and its P_S enantiomer mirrored each other, further highlighting that P_S- VX is principally responsible for the inhibition of AChE. Intriguingly, the k_r for hAChE inhibited by P_R-VX was not appreciable, suggesting it is significantly lower than the k_r of P_S- VX, which underscores the impact the stereochemistry of the nerve agent has on the potency of reactivators.

HI-6 Bound to the Active Site of hAChE.

Given the striking divergence between the ability of HI-6 to rehabilitate hAChE inhibited by different stereoisomers of VX, atomic level insight into how the stereospecific inhibition of hAChE impacts the ability of the enzyme to be reactivated by

HI-6 was sought. With no hAChE-HI-6 structure to serve as a baseline, apo hAChE crystals were soaked in a solution containing HI-6, and data sets were subsequently collected. Using molecular replacement, a 2.3 Å structure was obtained. Unlike previous reports with mAChE that revealed density attributed to only part of HI-6 in the absence of a nerve agent adduct,⁴⁴ both active sites possessed $F_o - F_c$ simulated annealing omit map density that readily accommodated the entire HI-6 ligand (Figures 2.2 and S2.2).

Interestingly, the placement of HI-6 differed between active sites. Specifically, the HI-6 (HI-6₁) in chain A is oriented in the peripheral anionic site (PAS) with the hydroxyl oxime arm orthogonal to the oxygen on the side chain of Ser203 (Figure 2.2a). This is facilitated by the significant conformational rearrangement of Trp286 in the hAChE-HI-6 structure leading to 3.0 Å widening of the PAS that enables HI-6₁ to access the active site (Figure 2.2a). The tail-end pyridinium ring of HI-6₁, which is the ring nearest to the entrance of the active site, is sandwiched via multiple π - π stacking interactions with Trp286 and Tyr72. There is a hydrophobic interaction between the tail-end pyridinium ring of HI-6₁ with Tyr124 as well as further hydrogen-bond interactions between the amine group of the HI-6₁ tail-end acetamide-containing pyridinium ring and one of the side chain oxygens of both Val282 and Glu285. At the opposite oxime-containing end of the HI-6₁ molecule, which is submerged further into the active site, the oxime-pyridinium ring placement appears to be driven by π - π stacking interactions with Tyr341 and additional hydrophobic interactions with Tyr337. The HI-6₁ oxime arm is further stabilized by a hydrogen-bond network involving the hydroxyl group of Tyr124 and a couple of water-mediated hydrogen bonds with Asn87 (Figure 2.2a).

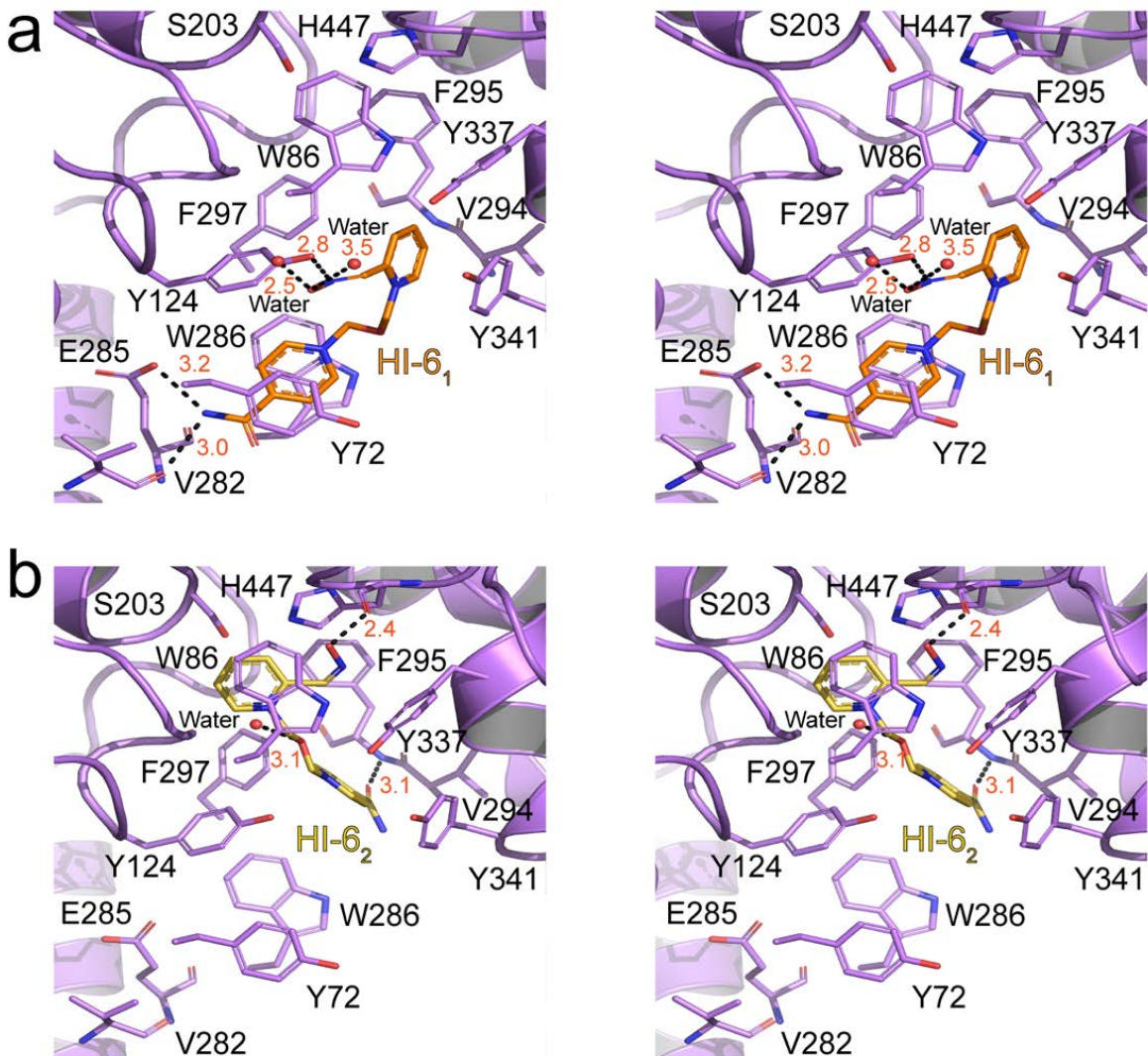


Figure 2.2. Crystal structures of acetylcholinesterase in complex with HI-6. Wall-eyed stereo view of the active site of chains A (a) and B (b) of hAChE (bright purple) in complex with HI-6 (orange and dark yellow, respectively) (PDB 6CQU). Waters are shown as red spheres, and black dashed lines indicate hydrogen bond interactions.

On the contrary to the HI-6 placement in chain A, the entire molecule of HI-6 in chain B is submerged deeper into the active site than HI-6 binding observed in chain A. The HI-6 in this conformation, HI-6₂, is positioned transversely between the Ser203 and Trp86 with the oxime arm inserted in a pocket near Ser203 formed by His447, Trp86, Tyr337, and Tyr449. The arm is further stabilized via a hydrogen-bond interaction with

the carboxyl group of His447. The tail-end pyridinium ring is located within a hydrophobic cluster created by Tyr341 and Phe297. The tail of the HI-6₂ conformation is also stabilized by a hydrogen bond between its acetamide oxygen and the amine of Phe295. Furthermore, the hydroxyl of Tyr124 forms an electrostatic interaction with the nitrogen on the acetamide-containing pyridinium ring of the HI-6₂ conformation (Figure 2.2b).

HI-6 Bound to VX Enantiomer Inhibited hAChE.

With distinctly different conformations of HI-6 observed in the absence of a reagent, further examination of how the stereospecific inhibition of hAChE affected the accommodation of HI-6 or favored a particular conformation within the active site was sought. Crystals of apo hAChE were soaked in a solution containing P_{RS}-VX and were subsequently placed in a solution containing HI-6 before freezing. Using molecular replacement, a 2.28 Å structure was obtained. As expected, Ser203 was found to be bound covalently to the P_S-VX adduct. Additionally, $F_o - F_c$ simulated annealing omit map density was apparent for one HI-6 within each of the asymmetric unit AChE active sites (Figure S2.4a,b).

Surprisingly, both of the HI-6 ligands observed within the structure are oriented in the same manner. This orientation, HI-6₃, is similar to that observed for HI-6₁ in proximity to the PAS. However, the oxime arm is rotated ~180° from orientation found in HI-6₁ (Figure 2.3a,b). Even though the arm of the oxime-containing pyridinium ring is flipped relative to the HI-6₁ position, Tyr341 still serves as a platform through π - π stacking interactions with the oxime-containing pyridinium ring. The oxime-containing pyridinium ring position is also influenced by hydrophobic interactions with Tyr337 as

well as the ethyl side chain of the P_S-VX adduct. This appears to draw the ring closer to the P_S-VX adduct. The oxime- containing arm itself is stabilized by a hydrogen-bond interaction between the hydroxide on the oxime arm, the amine of Phe295, and a water molecule. The divergent orientation of the oxime-containing pyridinium ring in the HI-6₃ conformation appears to translate only into minimum changes in how hAChE accommodates the acetamide- containing pyridinium ring in comparison to that of the HI-6₁ orientation. Despite the noticeable flexibility of Trp286, strong hydrophobic and π - π stacking interactions still fix the acetamide-containing pyridinium ring of HI-6₃ between two Tyr72 and Trp286 (Figure 2.3a,b). In addition, a stabilizing hydrogen-bond network involving the HI-6 acetamide group, Val282, Glu285, and a water molecule is observed.

At first blush, this places the oxime arm of the HI-6 bound to the inhibited form of hAChE in a position ~ 10 Å away from the phosphate contained in the P_S-VX adduct. This raises the possibility that rotation around the linker between the pyridinium rings plays an important role in allowing the HI-6 to strike at the phosphate from this pose of HI-6. With the presence of the P_S-VX adduct appearing to stabilize a unique orientation of HI-6, the impact of active site changes caused by P_R-VX inhibition of hAChE on HI-6 accommodation was investigated. To this end, hAChE crystals were soaked in a solution containing the P_R-VX isomer and moved to a solution containing HI-6 before freezing. A 2.6 Å structure was subsequently obtained using molecular replacement. As seen in the hAChE-P_S-VX structure, electron density around the side chain of Ser203 was clearly recognizable as the P_R-VX adduct. Beyond this additional density, clear $F_o - F_c$ simulated annealing omit map density was apparent for one HI-6 molecule within each of the asymmetric unit AChE active sites (Figures 2.3c and S2.4).

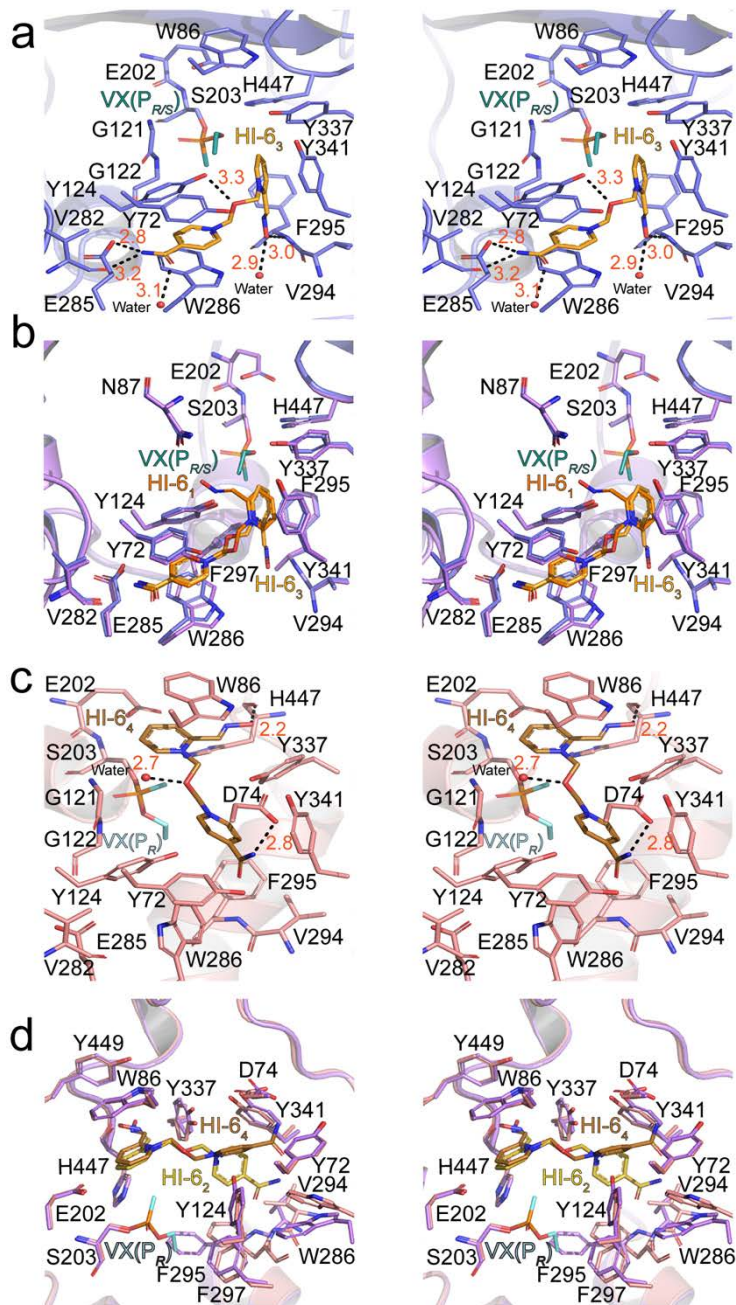


Figure 2.3. The active site of human acetylcholinesterase with stereoisomers of VX and the reactivator, HI-6. (a) Wall-eyed stereo view of P_{R/S}-VX (dark teal) with reactivator HI-6 (bright orange) bound to the active site of hAChE (indigo) (PDB 6CQW). (b) Wall-eyed stereo view of an overlay of the active sites of hAChE (bright purple) of apo HI-6 (PDB 6CQU) and hAChE of P_{R/S}-VX and HI-6 (PDB 6CQW). (c) Wall-eyed stereo view of P_R-VX (aquamarine) with the reactivator HI-6 (copper-colored) bound to the active site of hAChE (salmon pink) (PDB 6CQV). (d) Wall-eyed stereo view of an overlay of the active sites of hAChE (lavender purple) of apo HI-6 (PDB 6CQU) and hAChE of P_R-VX and HI-6 (PDB 6CQV). The dashed black lines represent hydrogen bonds and the red spheres signify water molecules. The AChE residues are represented by black letters, while the red letters denote distances.

As with the hAChE-P_S-VX-HI-6 structure, only one orientation of HI-6 is observed in both asymmetric unit active sites of AChE. Surprisingly, this conformation is markedly divergent from the previously observed HI-6₃ orientation found within the hAChE-P_S-VX-HI-6 structure. Specifically, HI-6₄ inserts its oxime-containing pyridinium ring deeper into the active site by capitalizing on the space between Trp86 and P_R-VX that was made available by the group in P_S-VX (Figure 2.3c). Concurrently, the amine of the acetamide group of HI-6 in the HI-6₄ conformation positions itself to optimize hydrogen-bonding interactions with Asp74 and Tyr72. This positioning of the acetamide group and connected pyridinium ring is intriguing as the oxime-containing pyridinium ring's position is similar to that observed in the HI-6₂ conformation found in the hAChE-HI-6 structure (Figure 2.3d). The divergence in position of the acetamide-containing pyridinium ring appears to be driven by the conformational changes induced by hAChE's accommodation of the P_R-VX isomer. In detail, the movement of Phe295 to accommodate the ethoxy group of the P_R-VX adduct shifts the acyl loop (positions 287–299) of hAChE. The movement appears to alter not only the position of the acyl loop (positions 280–297) but also the nearby α -helix. The global impact of these movements appears to be 2-fold. Specifically, it moves the backbone amine of Phe295 into a less ideal orientation for hydrogen bonding with HI-6. Additionally, the movement allows the side chain of Tyr337 to adopt an orientation that would be supportive of the HI-6₄ conformation. While there are notable differences between the HI-6₄ and HI-6₂ conformations after the oxime-containing pyridinium rings, the oxime-containing pyridinium rings are positioned in a significantly similar orientation influenced by their π - π stacking interactions with Trp86 (Figure 2.3d). As a result, the oxime-containing arm

of HI-6 in the HI-6₄ conformation is also sequestered into a pocket generated by His447, Trp86, Tyr337, and Tyr449, suggesting that it is unavailable for catalysis.

HI-6 Post-Catalysis Active Site of VX Inhibit hAChE.

With limited understanding of the chemical mechanism by which HI-6 reactivates hAChE, a post-reativation structure of hAChE was sought. By immersing P_{R/S}-VX soaked hAChE crystals in HI-6 solutions substantially longer than the crystals that produced the hAChE-VX-HI-6 structure, a 2.45 Å hAChE structure bound with HI-6 and a reactivation byproduct were captured. In detail, the close inspection of each hAChE active site revealed no additional $F_o - F_c$ simulated annealing omit map density for any VX adduct. This along with the hydroxyl of Ser203 forming the typical hydrogen-bond interaction with His447 underscores that the hAChE active sites are reactivated. Nearby $F_o - F_c$ simulated annealing omit map density is observed for a HI-6 resembling the HI-6₃ conformation and forming similar hydrogen-bond and hydrophobic interactions (S5 Figure). Interestingly, additional density was observed not belonging to HI-6 and disconnected from the Ser203 (Figure 2.4). This density was a perfect fit for ethyl methylphosphonic acid (EMPA), one of the suspected byproducts of VX (Figure 2.4, S2.5).^{45,46} The orientation of EMPA is guided by two entities: the ability to participate in the hydrogen-bond network of Ser203 and His447 and positioning its methyl and ethyl groups along the hydrophobic wall created by Trp86. Additionally, the presence of EMPA was likely linked to the HI-6 molecule blocking the exit of the active site to the bulk solvent by binding at the PAS. This suggests that the HI-6 present is also the end state of HI-6 after the reactivation process.

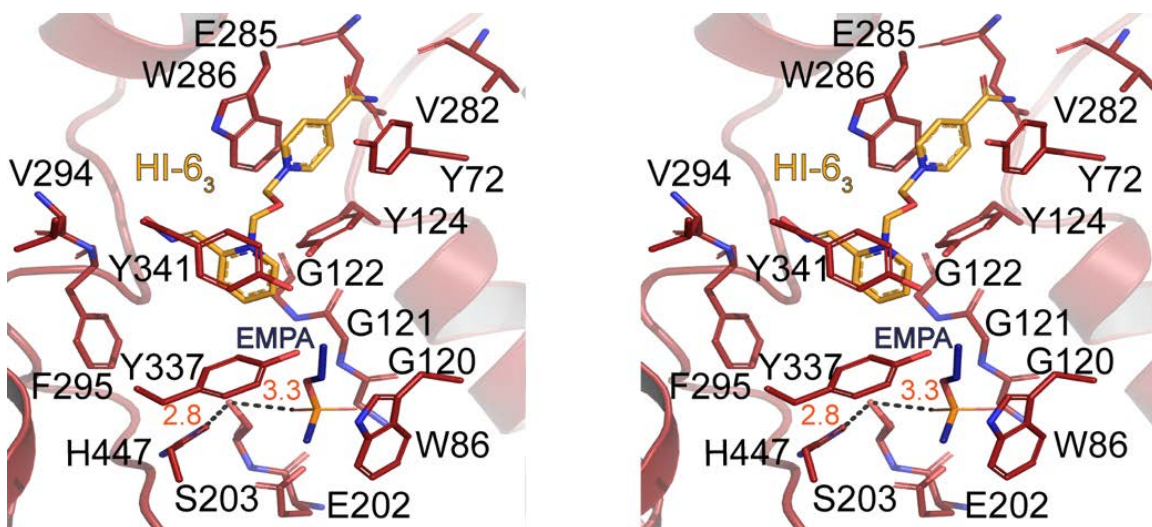


Figure 2.4. The active site of human acetylcholinesterase with post-catalysis HI-6 and a byproduct, EMPA. Wall-eyed stereo view of the active site of hAChE (brick red) with reactivator HI-6 (bright orange) and ethyl methyl phosphonic acid (EMPA) (indigo) (PDB 6CQY).

Discussion

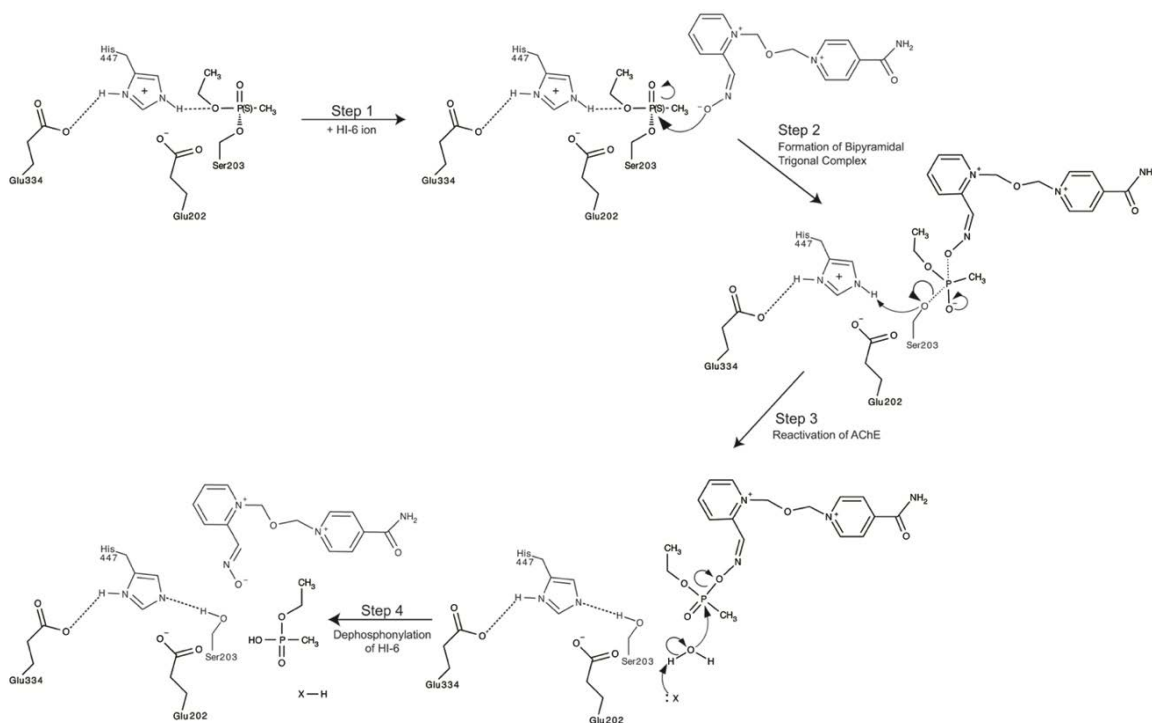
Mechanism of HI-6 Reactivation of VX Inhibited hAChE.

The inability to visualize the products of AChE reactivation previously created uncertainty about a number of mechanistic steps that AChE may undergo when under reactivation. Observing the presence of EMPA and a post-catalysis HI-6 in an uninhibited hAChE active site provided critical clues to this part of the mechanism. Utilizing this new evidence along with other structural observations from the hAChE-VX inhibited structure, a four-step mechanism may be envisioned (Scheme 2.2). Starting with the P_S-VX inhibited hAChE structure, crystallization buffers at pH 7.8, and that oxime groups deprotonate at 7.4,⁴⁷ HI-6 likely enters as a deprotonated oxime. Given the orientation of His447 and its distance to the oxygen of the ethoxy group of the adduct in the hAChE-P_S-VX structure, the hydrogen bond between these two entities increases the susceptibility of VX adduct's phosphorus atom to undergo a nucleophilic attack by HI-6.

The nearby Glu202, which has been previously implicated in the process, appears to interface electrostatically with His447, perhaps assisting in placing His447 in a catalytically relevant position (Figure 2.1 b).^{32,48} In keeping with previous models including the recent DFT computationally derived model, the attack of the oxime likely creates a bipyramidal trigonal intermediate.^{27,28} As the bipyramidal trigonal complex collapses, Ser203 deprotonates His447, restoring the native catalytic triad arrangement with a phosphorylated HI-6 product.

The majority of previous models tend to end at this stage as little previous data is available on the fate of the VX adduct and HI-6. However, with the added X-ray crystallographic information of the post-reactivation state of the hAChE active site, additional steps can now be proposed with greater confidence. Specifically, the observation of EMPA in the active site likely sequestered by a HI-6 blocking its exit appears to add further credence to the previously proposed rapid breakdown of the phosphorylated HI-6.⁴⁹ Given the identity of the breakdown products EMPA and HI-6, the rapid breakdown of the phosphorylated HI-6 likely is triggered by a nucleophilic water attack on the phosphorus atom. This water may be assisted by hydrogen-bond formation with acidic active site residues such as Glu202 or Asp74. Glu202 has been previously suggested through observation of solvent isotope effects to assist in deprotonating the oxime when the pH is not favorable to do so,²⁸ but may also, or instead, assist at this step. If the latter is true, the breakdown of the phosphorylated HI-6 itself may be the rate-limiting step, or the breakdown of the product may be necessary for the product to exit the active site and for hAChE to regain activity. Understandably, additional studies will have to fully settle the role of Glu202, or other residues at this

stage of the mechanism, and if this mechanism broadly occurs in other V-agent and G-agent reactivations. However, the presence of EMPA and HI-6 in the post- reactivation active site of hAChE provides the first insight into this process.



Scheme 2.2. Schematic of nerve agent, VX, in complex with reactivator, HI-6, and potential manner for the removal of VX from AChE S203.

Impact of VX Stereochemistry on hAChE Inhibition and Reactivation.

In addition to fleshing out the reactivation mechanism of hAChE by HI-6, the additional biochemical and structural information highlights the significant impact the stereochemistry of nerve agents plays in toxicity as well as the inhibition and reactivation of hAChE. As expected, the orientations of the VX stereoisomers differ primarily in the positioning of the methyl and ethoxy groups. P_S-VX adduct fit snugly into the active site pocket with little repositioning of active site residues, when compared to the apo state of

hAChE. However, P_R -VX adduct's accommodation is not as straightforward. As the ethoxy group of P_R -VX is oriented into the smaller hydrophobic pocket, Phe295 needs to shift significantly away from the active site in order to accommodate the stereoisomer (Figure 2.1d). The importance of this movement is supported by a previous study that mutated Phe295 to an alanine and saw a relaxation in stereospecificity as the mutant had lower reactivity for P_S -VX and a 3-fold increase in reactivity toward P_R -VX.^{50,51} Phe297 also shifts to accommodate the movement of Phe295, suggesting it may be a necessary component due to its flexibility and ability to help Phe295 shift, allowing the accommodation of bulkier groups. This assertion is supported as the mutation of Phe297 alone reduced stereoselectivity slightly, but mutating both residues resulted in the same reduction as F295A, which suggests that Phe297 may play a role in stereoselectivity, but likely through its influence on Phe295.^{50,51} Without Phe295 to aid in steering P_S -VX into the active site, the stereoisomer likely approaches from different, potentially less favorable, angles, whereas P_R -VX is likely less sterically hindered.⁵⁰⁻⁵² Phe295 sterically blocking the catalytically relevant P_R -VX orientation in the active site and the energy input necessary to move Phe295 likely form significant underlying factors in the slower inhibition by P_R -VX, its preference for P_S -VX, and their differences in toxicity.¹³

Intriguingly, the impact of the stereochemical nature of VX is not only limited to its inhibition but also appears to impact the efficacy of reactivation by HI-6. Reactivation by HI-6 of recombinant hAChE inhibited by P_R -VX is almost unobservable compared to that of its P_S -VX counterpart does. In comparing the structures of hAChE with VX stereoisomers, several of the underlying causes in this divergence in efficacy can be envisioned. Immediately evident is that the stereo-chemistry of P_R -VX results in the

placement of its ethoxy group into the smaller hydrophobic pocket away from His447. This prevents the formation of a hydrogen bond between the two entities as observed when the adduct of P_S-VX is present. This likely deprives hAChE's His447 of the ability to assist in drawing electrons away from the phosphorus atom of the P_R- VX adduct, which makes it less suitable for nucleophilic attack than that of the P_S-VX adduct. Beyond bond formations, placement of the smaller methyl group of the P_R-VX adduct into the larger hydrophobic pocket leaves a substantial opening in the anionic site between the VX adduct and the residues of the pocket. This along with displacement of Trp286 by acyl changes, rooted in the impact of the ethoxy of P_R-VX adduct on Phe295, appears to be enough enticement for HI-6 to move deeper into the hAChE active site compared to the hAChE-P_S- VX-HI-6 structure (Figure 2.3a-c). This influence of the acyl loop on Trp286 and the PAS overall highlights another mechanism explaining how the chemical nature of the nerve agent adduct influences reactivator position and potency. With HI-6₄ position deeper in active site of hAChE-P_R-VX-HI-6, its oxime arm becomes inserted into a void between Tyr449, Tyr337, and the VX adduct (Figure 2.5). A similar ring and oxime pose of 2-pralidoxime (2-PAM) were observed in hAChE inhibited by paraoxon and AChE from *Torpedo californica* (tAChE) were a similar spaced is created by aging of the enzyme by soman.⁵³ Nucleophilic attack from this pose of HI-6 is improbable given the limited range of motion for the oxime-containing pyridinium rings and sequestration of the oxime itself (Figure 2.3).

Apart from providing a rationale on the lack of efficacy HI-6 has for P_R-VX inhibited hAChE, the structures of hAChE inhibited with VX enantiomers further stress the likely need of reactivators to be at an ideal standoff distance from the AChE modified

serine. With HI-6 within the hAChE- P_S -VX-HI-6 structure anchored by its acetamide pyridinium ring to the hAChE's PAS, it is positioned in a manner that would allow HI-6 to strike with greater ease at the P_S -VX adduct. This further supports a recent computational DFT model of mAChE.²⁸ Additionally, the same rationale could also be applied to explain the substantial lower efficacy of 2-PAM and other single ring reactivators with long oxime side chains for VX and similar nerve agents. These reactivators would also lack the benefit of an anchor to the PAS. Given their smaller size, they are likely prone to adopting additional nonproductive poses. Put together, this suggests a possible path forward for the enhancement of HI-6 scaffold such as seeking to prevent HI-6-like reactivators from adopting nonproductive poses as seen with 2-PAM and HI-6 in the AChE- P_R -VX structure. By limiting nonproductive poses, the overall efficacy of these types of compounds may be improved, thus reducing the necessary therapeutic dose and potentially decreasing the risk of adverse effects.

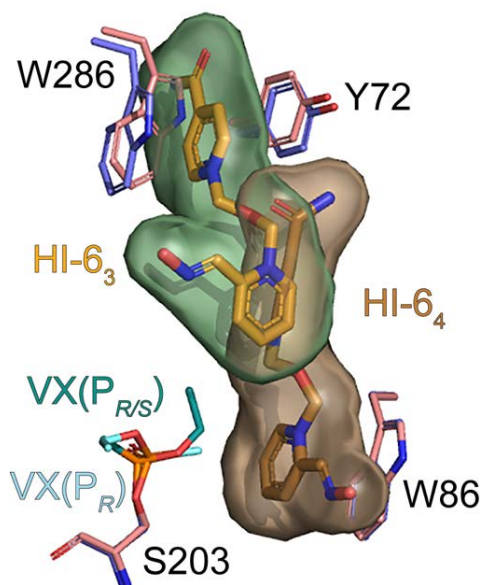


Figure 2.5. Binding modes of HI-6 in human acetylcholinesterase active site. hAChE (indigo) with HI-6 (bright orange) bound in conformation 3 (light green cavity) and $P_{R/S}$ -VX(\pm) (dark teal) and hAChE (salmon pink) with HI-6 (copper-colored) bound in conformation 4 (wheat brown cavity) and P_R -VX (aquamarine).

Accommodation of VX and HI-6 by hAChE versus Those from Other Species.

The well-resolved distinct poses of HI-6 within the active site of hAChE in various states of its interaction with VX stereoisomers along with structures recently reported interacting with paraoxon appear distinct from previous observations with AChE model systems such as mAChE and tAChE.^{8,27,28,33,44,54} In these systems, density for HI-6 has largely been limited to both or just one of the pyridinium rings of HI-6, respectively, implying that the oxime-containing side chain or substantial parts of HI-6 in these systems have a higher degree of flexibility than in hAChE.^{8,27,44,54} Previously, other AChE ligands have also shown such a divergence between these AChEs, suggesting an underlying fundamental difference between their active sites.⁵ This has been perplexing as the active site lining residues between the mAChE and hAChE are nearly perfectly conserved, and there are only a few conserved changes present between the active site of these and that of tAChE.^{5,55} However, conservation around the active site is not as consistent as the active site residues. These second-shell active site residues have in other enzymes been shown to greatly impact their biochemical behavior by influencing the flexibility of the active site.⁵⁶⁻⁵⁹ The stability of certain HI-6 poses within the active site of hAChE compared to that of AChEs of other species appears to suggest a similar phenomenon in AChEs.

Beyond the stability of certain unproductive poses of HI-6 within the active site of hAChE more than other AChEs, the acyl loop appears to provide a different example in which second-shell residues could influence AChE's behavior between species. For the acyl loop of AChEs from human, mouse, and torpedo, all appear to be anchored by Phe299 at one end before diverging. In general, the acyl loop is highly conserved

between species with the exception of hAChE positions 294 and 291. Although these residues are VQ in human, they are IQ and IF in mice and torpedo, respectively. These residues point into substantially differing environments overall suggesting that the loop may be anchored divergently at the end (Figure 2.6). Given that relatively poor hAChE OP inhibitors, paraoxon, P_R -VX, and DFP have been shown to require the movement of Phe295 and by extension the acyl loop in many species, any differences in plasticity of the loop could influence differences in susceptibility of being inhibited by different OPs or their specific stereoisomers. Naturally, closer examination of the acyl loop dynamics will likely need to occur in order to fully reveal differences in flexibility between species acyl loops and how it specifically impacts inhibition by certain OPs and their toxicity. However, hAChE structures inhibited by specific stereoisomers of VX with and without the presence of HI-6 further underscore the need to better understand the dynamic factors beyond those of straightforward steric and electrochemical considerations when it comes to OP toxicity and hAChE reactivation.

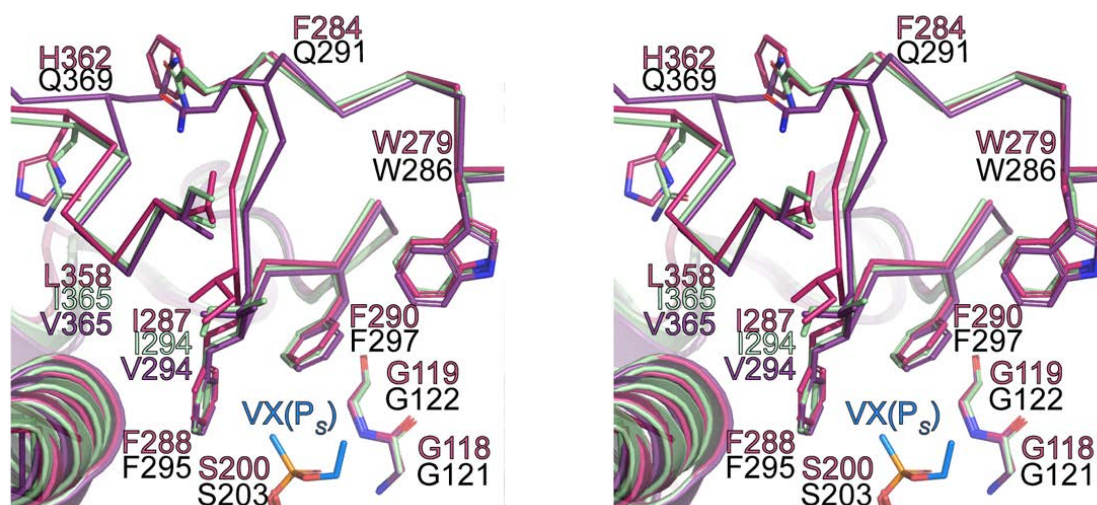


Figure 2.6. Structural Diversity in Specific Residues surrounding the Active Site between Acetylcholinesterase Species. Wall-eyed stereo view of an overlay of the acyl loop of hAChE inhibited by P_S -VX (violet purple), mAChE (mint green) with $P_{R/S}$ -VX (not shown) (PDB 2Y2U), and tAChE (hot pink) with $P_{R/S}$ -VX (not shown) (PDB 1VXR).

References

- (1) Paddock, R., Sang-Hun, C., and Wade, N. (2017) In Kim Jong- nam's Death, North Korea Lets Loose a Weapon of Mass Destruction, *New York Times*, New York Times Company, New York, <https://www.nytimes.com/2017/02/24/world/asia/north-korea-kim-jong-nam-vx-nerve-agent.html> (accessed Mar 7, 2017).
- (2) Kingsley, P., and Barnard, A. (2017) Banned Nerve Agent Sarin Used in Syria Chemical Attack, Turkey Says, *New York Times*, New York Times Company, New York, <https://www.nytimes.com/2017/04/06/world/middleeast/chemical-attack-syria.html> (accessed Apr 10, 2017).
- (3) Barry, E., and Yeginsu, C. (2018) The Nerve Agent Too Deadly to Use, Until Someone Did, *New York Times*, New York Times Company, New York, <https://www.nytimes.com/2018/03/13/world/europe/uk-russia-spy-poisoning.html> (accessed Mar 23, 2018).
- (4) Eddleston, M. (2000) Patterns and problems of deliberate self- poisoning in the developing world. *QJM* 93, 715–731.
- (5) Cheung, J., Rudolph, M. J., Burshteyn, F., Cassidy, M. S., Gary, E. N., Love, J., Franklin, M. C., and Height, J. J. (2012) Structures of human acetylcholinesterase in complex with pharmacologically important ligands. *J. Med. Chem.* 55, 10282–10286.
- (6) Daczkowski, C. M., Pegan, S. D., and Harvey, S. P. (2015) Engineering the Organophosphorus Acid Anhydrolase Enzyme for Increased Catalytic Efficiency and Broadened Stereospecificity on Russian VX. *Biochemistry* 54, 6423–6433.
- (7) Guven, M., Sungur, M., Eser, B., Sari, I., and Altuntas, F. (2004) The effects of fresh frozen plasma on cholinesterase levels and outcomes in patients with organophosphate poisoning. *J. Toxicol., Clin. Toxicol.* 42, 617–623.
- (8) Ekstrom, F., Pang, Y. P., Boman, M., Artursson, E., Akfur, C., and Borjegen, S. (2006) Crystal structures of acetylcholinesterase in complex with HI-6, Ortho-7 and obidoxime: structural basis for differences in the ability to reactivate tabun conjugates. *Biochem. Pharmacol.* 72, 597–607.
- (9) Worek, F., Reiter, G., Eyer, P., and Szinicz, L. (2002) Reactivation kinetics of acetylcholinesterase from different species inhibited by highly toxic organophosphates. *Arch. Toxicol.* 76, 523–529.
- (10) Michel, H. O. (1955) Kinetics of the reactions of cholinesterase chymotrypsin and trypsin with organophosphorus inactivators. *Fed. Proc., Fed. Am. Soc. Exp. Biol.* 14.255
- (11) Hall, C. R., Inch, T. D., Inns, R. H., Muir, A. W., Sellers, D. J., and Smith, A. P. (1977) Differences between some biological properties of enantiomers of alkyl S-alkyl methylphosphonothioates. *J. Pharm. Pharmacol.* 29, 574–576.

- (12) Benschop, H. P., Konings, C. A., Van Genderen, J., and De Jong, L. P. (1984) Isolation, anticholinesterase properties, and acute toxicity in mice of the four stereoisomers of the nerve agent soman. *Toxicol. Appl. Pharmacol.* 72, 61–74.
- (13) Reiter, G., Muller, S., Hill, I., Weatherby, K., Thiermann, H., Worek, F., and Mikler, J. (2015) In vitro and in vivo toxicological studies of V nerve agents: molecular and stereoselective aspects. *Toxicol. Lett.* 232, 438–448.
- (14) Buckley, N. A., Roberts, D., and Eddleston, M. (2004) Overcoming apathy in research on organophosphate poisoning. *BMJ.* 329, 1231–1233.
- (15) Hobbiger, F. (1955) Effect of nicotinhydroxamic acid methiodide on human plasma cholinesterase inhibited by organo-phosphates containing a dialkylphosphato group. *Br. J. Pharmacol. Chemother.* 10, 356–362.
- (16) Hobbiger, F. (1957) Protection against the lethal effects of organophosphates by pyridine-2-aldoxime methiodide. *Br. J. Pharmacol. Chemother.* 12, 438–446.
- (17) Hobbiger, F. (1957) Reactivation of phosphorylated acetylcholinesterase by pyridine-2-aldoxime methiodide. *Biochim. Biophys. Acta* 25, 652–654.
- (18) Simeon, V., Skrinjaric-Spoljar, M., and Wilhelm, K. (1973) Reactivation of phosphorylated cholinesterases in vitro and protecting effects in vivo of some pyridinium and quinolinium oximes. *Arh Hig Rada Toksikol* 24, 11–18.
- (19) Sun, M., Chang, Z., Shau, M., Huang, R., and Chou, T. (1979) The mechanism of ageing of phosphonylated acetylcholinesterase. *Eur. J. Biochem.* 100, 527–530.
- (20) Maxwell, D. M., Koplovitz, I., Worek, F., and Sweeney, R. E. (2008) A structure-activity analysis of the variation in oxime efficacy against nerve agents. *Toxicol. Appl. Pharmacol.* 231, 157–164.
- (21) Worek, F., and Thiermann, H. (2011) Reactivation of organophosphate-inhibited human acetylcholinesterase by isonitro-soacetone (MINA): a kinetic analysis. *Chem.-Biol. Interact.* 194, 91–96.
- (22) Worek, F., Thiermann, H., Szinicz, L., and Eyer, P. (2004) Kinetic analysis of interactions between human acetylcholinesterase, structurally different organophosphorus compounds and oximes. *Biochem. Pharmacol.* 68, 2237–2248.
- (23) Aas, P. (2003) Future considerations for the medical management of nerve-agent intoxication. *Prehosp Disaster Med.* 18, 208–216.
- (24) Bartosova, L., Kuca, K., Kunesova, G., and Jun, D. (2006) The acute toxicity of acetylcholinesterase reactivators in mice in relation to their structure. *Neurotoxic. Res.* 9, 291–296.

- (25) Clement, J. G. (1981) Toxicology and pharmacology of bispyridium oximes—insight into the mechanism of action vs Soman poisoning in vivo. *Fundam. Appl. Toxicol.* *1*, 193–202.
- (26) Jokanovic, M., and Prostran, M. (2009) Pyridinium oximes as cholinesterase reactivators. Structure-activity relationship and efficacy in the treatment of poisoning with organophosphorus compounds. *Curr. Med. Chem.* *16*, 2177–2188.
- (27) Ekstrom, F., Hornberg, A., Artursson, E., Hammarstrom, L. G., Schneider, G., and Pang, Y. P. (2009) Structure of HI-6* sarin- acetylcholinesterase determined by X-ray crystallography and molecular dynamics simulation: reactivator mechanism and design. *PLoS One* *4*, No. e5957.
- (28) Allgardsson, A., Berg, L., Akfur, C., Hornberg, A., Worek, F., Linusson, A., and Ekstrom, F. J. (2016) Structure of a prereaction complex between the nerve agent sarin, its biological target acetylcholinesterase, and the antidote HI-6. *Proc. Natl. Acad. Sci. U. S. A.* *113*, 5514–5519.
- (29) Kronman, C., Velan, B., Gozes, Y., Leitner, M., Flashner, Y., Lazar, A., Marcus, D., Sery, T., Papier, Y., Grosfeld, H., et al. (1992) Production and secretion of high levels of recombinant human acetylcholinesterase in cultured cell lines: microheterogeneity of the catalytic subunit. *Gene* *121*, 295–304.
- (30) Ellman, G. L., Courtney, K. D., Andres, V., Jr., and Feather-Stone, R. M. (1961) A new and rapid colorimetric determination of acetylcholinesterase activity. *Biochem. Pharmacol.* *7*, 88–95.
- (31) Forsberg, A., and Puu, G. (1984) Kinetics for the inhibition of acetylcholinesterase from the electric eel by some organophosphates and carbamates. *Eur. J. Biochem.* *140*, 153–156.
- (32) Luo, C., Tong, M., Chilukuri, N., Brecht, K., Maxwell, D. M., and Saxena, A. (2007) An in vitro comparative study on the reactivation of nerve agent-inhibited guinea pig and human acetylcholinesterases by oximes. *Biochemistry* *46*, 11771–11779.
- (33) Franklin, M. C., Rudolph, M. J., Ginter, C., Cassidy, M. S., and Cheung, J. (2016) Structures of paraoxon-inhibited human acetylcholinesterase reveal perturbations of the acyl loop and the dimer interface. *Proteins: Struct., Funct., Genet.* *84*, 1246–1256.
- (34) Otwinowski, Z., and Minor, W. (1997) Processing of X-ray Diffraction Data Collected in Oscillation Mode, *Macromolecular Crystallography, Part A*, Vol. 276, Academic Press, New York.
- (35) Winn, M. D., Ballard, C. C., Cowtan, K. D., Dodson, E. J., Emsley, P., Evans, P. R., Keegan, R. M., Krissinel, E. B., Leslie, A. G., McCoy, A., McNicholas, S. J., Murshudov, G. N., Pannu, N. S., Potterton, E. A., Powell, H. R., Read, R. J., Vagin, A., and Wilson, K. S. (2011) Overview of the CCP4 suite and current developments. *Acta Crystallogr., Sect. D: Biol. Crystallogr.* *67*, 235–242.

- (36) McCoy, A. J., Grosse-Kunstleve, R. W., Adams, P. D., Winn, M. D., Storoni, L. C., and Read, R. J. (2007) Phaser crystallographic software. *J. Appl. Crystallogr.* *40*, 658–674.
- (37) Adams, P. D., Afonine, P. V., Bunkoczi, G., Chen, V. B., Davis, I. W., Echols, N., Headd, J. J., Hung, L. W., Kapral, G. J., Grosse-Kunstleve, R. W., McCoy, A. J., Moriarty, N. W., Oeffner, R., Read, R. J., Richardson, D. C., Richardson, J. S., Terwilliger, T. C., and Zwart, P. H. (2010) PHENIX: a comprehensive Python-based system for macromolecular structure solution. *Acta Crystallogr., Sect. D: Biol. Crystallogr.* *66*, 213–221.
- (38) Emsley, P., and Cowtan, K. (2004) Coot: model-building tools for molecular graphics. *Acta Crystallogr., Sect. D: Biol. Crystallogr.* *60*, 2126–2132.
- (39) Worek, F., Aurbek, N., and Thiermann, H. (2007) Reactivation of organophosphate-inhibited human AChE by combinations of obidoxime and HI 6 in vitro. *J. Appl. Toxicol.* *27*, 582–588.
- (40) Pohanka, M., Hrabínová, M., Kuca, K., and Simonato, J. P. (2011) Assessment of acetylcholinesterase activity using indoxylacetate and comparison with the standard Ellman's method. *Int. J. Mol. Sci.* *12*, 2631–2640.
- (41) Hornberg, A., Tunemalm, A. K., and Ekström, F. (2007) Crystal structures of acetylcholinesterase in complex with organo-phosphorus compounds suggest that the acyl pocket modulates the aging reaction by precluding the formation of the trigonal bipyramidal transition state. *Biochemistry* *46*, 4815–4825.
- (42) Millard, C. B., Kryger, G., Ordentlich, A., Greenblatt, H. M., Harel, M., Raves, M. L., Segall, Y., Barak, D., Shafferman, A., Silman, I., and Sussman, J. L. (1999) Crystal structures of aged phosphonylated acetylcholinesterase: nerve agent reaction products at the atomic level. *Biochemistry* *38*, 7032–7039.
- (43) Phillips, M. R., Li, X., and Zhang, Y. (2002) Suicide rates in China, 1995–99. *Lancet* *359*, 835–840.
- (44) Artursson, E., Andersson, P. O., Akfur, C., Linusson, A., Borjegen, S., and Ekström, F. (2013) Catalytic-site conformational equilibrium in nerve-agent adducts of acetylcholinesterase: possible implications for the HI-6 antidote substrate specificity. *Biochem. Pharmacol.* *85*, 1389–1397.
- (45) Gravett, M. R., Hopkins, F. B., Self, A. J., Webb, A. J., Timperley, C. M., and Baker, M. J. (2014) Evidence of VX nerve agent use from contaminated white mustard plants. *Proc. R. Soc. London, Ser. A* *470*, 20140076.
- (46) Hamelin, E. I., Schulze, N. D., Shaner, R. L., Coleman, R. M., Lawrence, R. J., Crow, B. S., Jakubowski, E. M., and Johnson, R. C. (2014) Quantitation of five organophosphorus nerve agent metabolites in serum using hydrophilic interaction liquid chromatography and tandem mass spectrometry. *Anal. Bioanal. Chem.* *406*, 5195–5202.

- (47) Radic, Z., Kalisiak, J., Fokin, V. V., Sharpless, K. B., and Taylor, P. (2010) Interaction kinetics of oximes with native, phosphorylated and aged human acetylcholinesterase. *Chem.-Biol. Interact.* 187, 163–166.
- (48) Chambers, C., Luo, C., Tong, M., Yang, Y., and Saxena, A. (2015) Probing the role of amino acids in oxime-mediated reactivation of nerve agent-inhibited human acetylcholinesterase. *Toxicol. In Vitro* 29, 408–414.
- (49) Berman, H. A. (1998) In *Structure and Function of Cholinesterases and Related Proteins*. Springer Science + Business, New York.
- (50) Ordentlich, A., Barak, D., Sod-Moriah, G., Kaplan, D., Mizrahi, D., Segall, Y., Kronman, C., Karton, Y., Lazar, A., Marcus, D., Velan, B., and Shafferman, A. (2005) The role of AChE active site gorge in determining stereoselectivity of charged and noncharged VX enantiomers. *Chem.-Biol. Interact.* 157–158, 191–198.
- (51) Ordentlich, A., Barak, D., Sod-Moriah, G., Kaplan, D., Mizrahi, D., Segall, Y., Kronman, C., Karton, Y., Lazar, A., Marcus, D., Velan, B., and Shafferman, A. (2004) Stereoselectivity toward VX is determined by interactions with residues of the acyl pocket as well as of the peripheral anionic site of AChE. *Biochemistry* 43, 11255–11265.
- (52) Mesecar, A. D., Stoddard, B. L., and Koshland, D. E., Jr. (1997) Orbital steering in the catalytic power of enzymes: small structural changes with large catalytic consequences. *Science* 277, 202–206.
- (53) Sanson, B., Nachon, F., Colletier, J. P., Froment, M. T., Toker, L., Greenblatt, H. M., Sussman, J. L., Ashani, Y., Masson, P., Silman, I., and Weik, M. (2009) Crystallographic snapshots of nonaged and aged conjugates of soman with acetylcholinesterase, and of a ternary complex of the aged conjugate with pralidoxime. *J. Med. Chem.* 52, 7593–7603.
- (54) Hornberg, A., Artursson, E., Warne, R., Pang, Y. P., and Ekstrom, F. (2010) Crystal structures of oxime-bound fenamiphos- acetylcholinesterases: reactivation involving flipping of the His447 ring to form a reactive Glu334-His447-oxime triad. *Biochem. Pharmacol.* 79, 507–515.
- (55) Wiesner, J., Kriz, Z., Kuca, K., Jun, D., and Koca, J. (2007) Acetylcholinesterases—the structural similarities and differences. *J. Enzyme Inhib. Med. Chem.* 22, 417–424.
- (56) Lopez, C. J., Yang, Z., Altenbach, C., and Hubbell, W. L. (2013) Conformational selection and adaptation to ligand binding in T4 lysozyme cavity mutants. *Proc. Natl. Acad. Sci. U. S. A.* 110, E4306–4315.
- (57) Miller, P. S., Topf, M., and Smart, T. G. (2008) Mapping a molecular link between allosteric inhibition and activation of the glycine receptor. *Nat. Struct. Mol. Biol.* 15, 1084–1093.

(58)Rajasekaran, N., Suresh, S., Gopi, S., Raman, K., and Naganathan, A. N. (2017) A General Mechanism for the Propagation of Mutational Effects in Proteins. *Biochemistry* 56, 294–305.

(59)Tanwar, A. S., Goyal, V. D., Choudhary, D., Panjekar, S., and Anand, R. (2013) Importance of hydrophobic cavities in allosteric regulation of formylglycinamide synthetase: insight from xenon trapping and statistical coupling analysis. *PLoS One* 8, No. e77781.

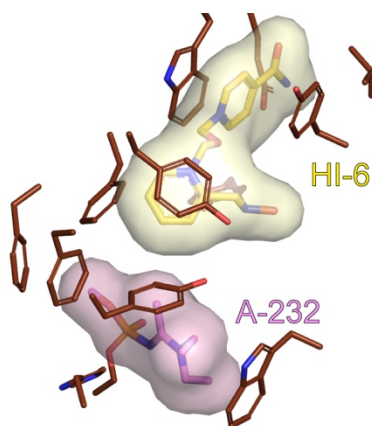
CHAPTER 3

INSIGHTS INTO INHIBITION OF HUMAN ACETYLCHOLINESTERASE BY NOVICHOK, A-SERIES NERVE AGENTS²

²Height, J.J.*, S.M. Bester*, M.A. Guelta, S.Y. Bae, J. Cheung, and S.D. Pegan. To be submitted to *Journal of the American Chemical Society*.

Abstract

The intentional use of organophosphate based nerve agents poses a significant health threat through their inhibition of human acetylcholinesterase (hAChE). This has been exacerbated by the potential threat to the public by advanced nerve agents known as Novichok, A-series agents. Currently, no information exists pertaining to the potency of A-series agents towards hAChE, or pure enantiomers of these agents. Here, X-ray crystallographic structures of hAChE inhibited by three A-series agents were determined to provide insights into their different influences on the active site and potentially their ability to inhibit. Furthermore, X-ray crystallographic structures of hAChE inhibited by these agents in complex with the reactivator HI-6, were determined to help illuminate their structural differences related to their influence on the active site.. This provides not only the first look at inhibition by A-series agents, but also a substantial basis for the rational design of potential reactivators for these unique threat agents.



Introduction

Events in Salisbury, United Kingdom on March 4, 2018 ushered in a new chapter in the public conscience related to the use of advanced chemical warfare agents¹. A former Russian military intelligence officer, Sergei Skripal and his daughter Yulia Skripal were found incapacitated at a park bench after having dined at a local restaurant. Shortly afterwards, one of the responding police officers developed symptoms indicative of nerve agent poisoning¹. Months later, two more UK citizens became incapacitated resulting in a fatality by exposure to the same substance found in a perfume bottle². Unlike the use of VX to assassinate Kim Jong-nam, the half-brother of the leader of North Korea Kim Jong-un, in a Malaysian airport nearly a year earlier³, investigations in the subsequent days and weeks after the Salisbury attack revealed the use of a Novichok agent. Novichok, meaning newcomer in Russian, agents were first mentioned publicly in an article in the Baltimore Sun newspaper⁴. Subsequently, characteristics of Novichok agents were more fully revealed in the book "State Secrets: an Insider's chronicle of the Russian chemical weapons program"⁵. Born out of the Soviet's FOLIANT program in the mid-1970s, these agents fall into the Fourth Generation (FGA) class of nerve agents also called A-series agents. To date, this series is reported to include at least three variants, A-230, A-232, and A-234 (Figure 3.1)⁵.

Similar to V- and G-series agents as well as other closely related pesticides, A-series agents employ an organophosphorus core to inhibit acetylcholinesterase (AChE) activity. For instance, pesticide mipafox (*N,N'*-Diisopropyldiamidofluorophosphate; DDFP) and G-series nerve agents such as soman (o-pinacolyl methylphosphonofluoridate; GD) possess a fluorophosphate moiety. The leaving group

differs for members of the V-series agents where the fluoride on the organophosphate core is swapped with a thiol leaving group in order to imbue greater stability and toxicity into the nerve agent⁶⁻⁸. For A-series agents, they share the G-series agents' fluoride leaving group on their organophosphorus core but differ by possessing a large *N,N*-diethylmethanimidamide moiety non-leaving group (S_{Large}) along with either a methyl, O-methyl or O-ethyl substituent group on the phosphorous (S_{Small} ; Figure 3.1). The presence of this non-leaving group is rather unique to the A-series agents and likely lends to their nontraditional agent status. Like other nerve agents, A-series agents are proposed to covalently modify the active site serine of AChEs. Interestingly, unlike other nerve agents, A-series agents' large moieties are not connected to the organophosphorus through a phosphoester bond suggesting that these agents may not readily undergo further alkylation or aging in the conventional sense (Scheme 3.1). Overall, the chemical configuration of A-series agents is believed to be an effort to overcome weaknesses with G- and V-type agents and avoid detection while not falling into the scope of molecules covered by the Chemical Weapons Convention. These efforts included providing a better balance between physical-chemical properties to include volatility, density, and stability towards light and moisture⁹.

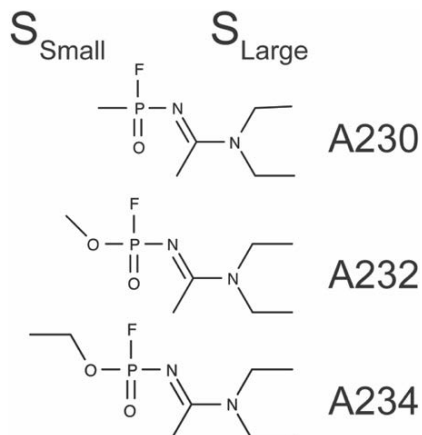
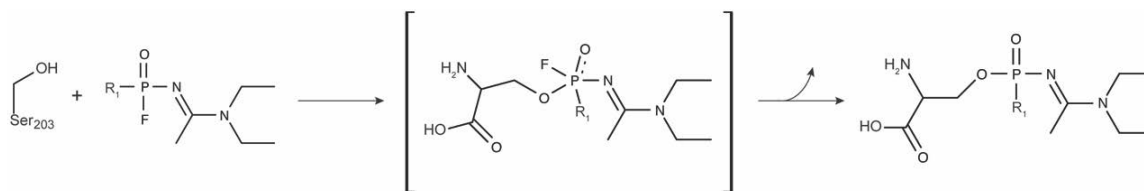


Figure 3.1. The chemical structures of nerve agents.



$R_1 = \text{CH}_3$ or $\text{CH}_3\text{-O-}$ or $\text{CH}_3\text{-CH}_2\text{-O-}$

Scheme 3.1. Inhibition of hAChE by A-series with transition state of S_2N concerted substitution.

Since their emergence into the public conscience, sporadic unconfirmed reports have been made pertaining to their ability to inhibit hAChE related to other organophosphorus based nerve agents⁹. Adding to the complexity, hAChE has been shown to be stereo selective in terms of their OP inhibitors¹⁰⁻¹². Not surprisingly, reports have indicated that the toxicity of chemical nerve agents is dependent on the particular agent and its chirality at the phosphorous core. For example, VX (O-ethyl S-[2-(diisopropylamino)ethyl] methylphosphonothioate) has about up to a 13-fold difference in toxicity between its enantiomers, with the P_S enantiomer being the more toxic of the two^{10, 11}. Other reports have shown similar trends with soman, where most toxic ScSP enantiomer is more than 100 times as toxic as the least toxic RcrP enantiomer¹³. Currently, there is no publicly available knowledge on if hAChE is stereoselective towards A-series agents. This has spurred numerous questions pertaining to which enantiomer is preferred by hAChE and the structural basis for that preference.

Currently, the recommended treatment for organophosphate agent poisoning involves an amalgamation of benzodiazepines to control seizures, atropine (a muscarinic antagonist), and pralidoxime, [(2-PAM) (2-[(hydroxyimino) methyl]-1-methylpyridin-1-ium chloride)], a reactivator of inhibited acetylcholinesterase enzymes¹⁴. 2-PAM seeks to reverse the phosphoryl inhibitor moiety from the catalytic serine, Ser203 in the AChE active site. The efficacy of 2-PAM and other preclinical oxime and non-oxime based

reactivator candidates have been found to vary widely based on exposure to different nerve agents^{15, 16}. For instance, another oxime based reactivator, HI-6 (1,1'-[oxybis(methylene)]bis{4-[(hydroxyamino)methyl]pyridin-1-ium}) demonstrates a 3-4 times greater potency towards human AChE (hAChE) inhibited by VX versus inhibited GB, also known as sarin¹⁷. The potency of HI-6 for VX and a number of other agents has elevated its potential for widespread use¹⁷. However, no data exists on how HI-6 may fit into the hAChE active site.

To provide an initial step towards understanding A-series agents in their molecular role as a nerve agent, the X-ray crystal structures of hAChE inhibited by racemic mixtures (P_{R/S}) of A-230, A-232, and A-234 were determined. Furthermore, the X-ray crystal structures of hAChE inhibited by pure P_S enantiomer of A-232 was determined to highlight the influence of stereochemistry on inhibition of hAChE by A-series agents. Subsequently, the X-ray crystal structures of hAChE inhibited by racemic A-series agents in the presence of HI-6 were obtained. Leveraging this information, a molecular rationale for A-series stereospecific preference is discussed. Additionally, a path toward the development of reactivators specialized to reverse A-series agent inhibition of hAChE is illuminated.

Results

A-232 stereo specifically inhibited hAChE structures

With the significantly larger non-leaving group side chain of *N,N*-diethylmethanimidamide of A-series compounds over those of V- and G-series nerve agents and no public data available on the ability of A-series agents to inhibit hAChE, the molecular basis of hAChE inhibition by A-series compounds and their stereoisomers was

investigated. Hence, hAChE crystals were soaked in a solution containing a racemic mixture of the A-series agent, A-232, for 5 minutes before freezing. These crystals produced a 2.41 Å dataset in the space group $P3_121$. A structural solution was elucidated by molecular replacement using apo hAChE, PDB 4EY4, as a search model.¹⁸ The asymmetric unit contained two hAChE subunits. Initial investigation of the active site revealed significant $F_o - F_c$ simulated annealing omit map density was observed proximal to the OG atom of Ser203 in the active sites of both chains (Figure S3.1a). Different stereoisomer adducts were assessed for their ability to fully account for the density. The A-232 adduct could be produced through an S_N1 reaction of the A-232 P_R enantiomer, however an S_N2 reaction of the A-232 P_S enantiomer was found to account for the density observed. The nature of the adduct was confirmed through the structure of a dataset at 2.42 Å of crystals soaked in the A-232 P_S enantiomer. Density within the active site of hAChE-A-232 P_S was similar to that observed in the hAChE-A-232 $P_{R/S}$ structure (Figure 3.2, S3.1a,b) identifying it as the product of a S_N2 inversion reaction.

The P_S A-232 adduct seems to assume an orientation that exemplifies the capitalization of the cavities present in the apo hAChE structure and other AChE¹⁹. More comprehensively, the methoxy group of A-232 P_S adduct points into a small hydrophobic pocket which consists of Trp236, Phe297, and Phe295. While the large N,N -diethylmethanimidamide extends out in the opposite direction into a considerably larger hydrophobic pocket formed by Trp86, Tyr133, Tyr337, and Phe338 (Figure 3.2). The N,N -diethylmethanimidamide takes up a considerable portion of the large pocket and seems positioned to form the best van der Waals interactions within the hydrophobic pocket. This includes flattening of the ethyl branches of the N,N -diethylmethanimidamide

against Trp86. Moreover, the Ser203 OG oxygen forms a hydrogen bond with nitrogen on His447, which forms the catalytic triad of the active site along with Ser203 and Glu334. Additional hydrogen bond interactions between hAChE and the A-232 P_S adduct are formed in the oxyanion pocket. Specifically, hydrogen bonds are formed between the backbone amines of Gly121, Gly122, Ala204 and the double bonded oxygen present within A-232 P_S adducts phosphonate core. The hydrogen bonds made by A-232 P_S adduct predominantly mirror the bonds expected to form between hAChE and its natural substrate, acetylcholine (ACh). The similarity of A-232 with the acetylcholine appears to provide a basis for the improved fit of P_S A-series agents in the hAChE active site. In other words, hAChE likely prefers the P_S A-series enantiomers because the larger pocket (S_{Large}) of the active site provides a more reasonable steric volume and charge environment for both the transition state and final configuration of the large *N,N*-diethylmethanimidamide into the larger pocket of the active site.

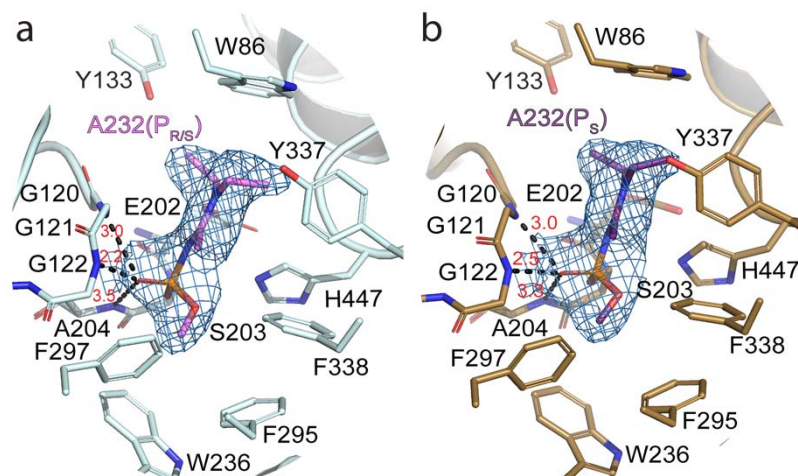


Figure 3.2. Crystal Structures of Human Acetylcholinesterase in complex with Stereoisomers of Nerve Agent, A232. (a) View of A232 P_{R/S} adduct (violet pink) bound to the active site of hAChE (light cyan) with 2F_o - F_c density scaled to 1σ (light blue mesh) (PDB 6NTK). (b) View of A232 P_S adduct (dark purple) bound to the active site of hAChE (sand) with 2F_o - F_c density scaled to 1σ (light blue mesh). (PDB 6NTH). The black lines represent hydrogen bonds. The AChE residues are represented by black letters, while the red letters are the distances.

The active sites of hAChE inhibition by A-230 or A-234

The A-series small side chain (S_{Small}), methyl, O-methyl, or O-ethyl, are quite small compared to the S_{Large} side chain, *N,N*-diethylmethanimidamide, and reversal of the occupied pockets to accommodate each enantiomer causes considerable limits of the fit in the respective pockets. To ascertain how these modifications may influence accommodation within the hAChE active site, apo hAChE crystals were soaked in either A-230 for 1 minute, or A-234 for 2 minutes. All crystals immediately underwent flash cooling. Using molecular replacement, structures of hAChE-A-230 and hAChE-A-234 were resolved to 2.05 Å and 2.25 Å respectively. An examination of the active sites of these structures revealed the presence of significant $F_o - F_c$ simulated annealing omit map density at the OG atom of Ser203 in both active sites (Figure S3.1c,d). Globally, the map density of these three structures resembled one another and hAChE-A-232. Naturally upon closer inspection of their respective active sites, differences between their $2F_o - F_c$ density became apparent (Figure 3.3a,b).

All three of the A-series nerve agent adducts fit well into the active site despite their large size and occupy similar orientations (Figure 3.3c). The large side chains of the agent adducts, *N,N*-diethylmethanimidamide, orient into the larger hydrophobic pocket formed by Trp86, Tyr133, Phe338, and Tyr337. Notably, the two tertiary amines of the A-series agents face Glu202. However, all of the tertiary amines are greater than 4 Å apart from Glu202. As a result, they are well outside hydrogen bonding distance suggesting that they do not play a role in the accommodation of the adducts, but their proximity and influence in facilitating the nerve agent binding and catalysis cannot be fully discounted.

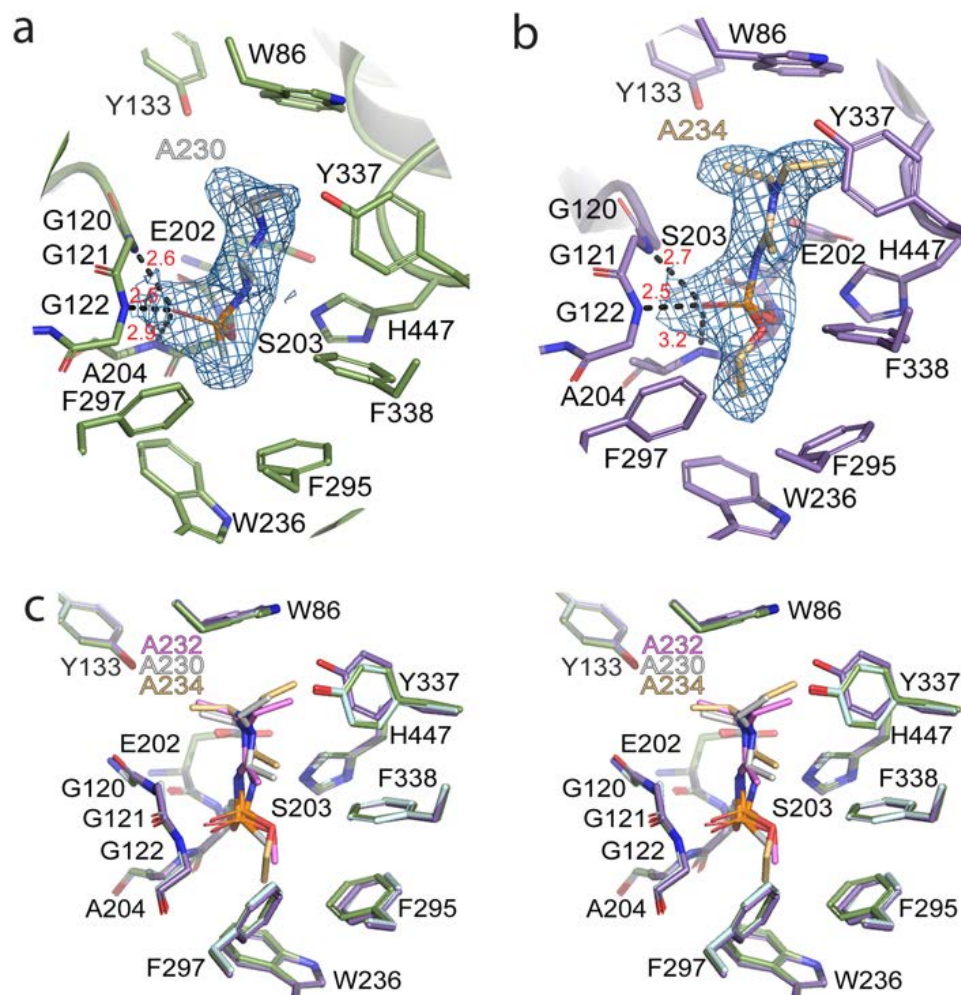


Figure 3.3. Comparison of Crystal Structures of Human Acetylcholinesterase in complex with A-series agents. (a) View of A230 P_{R/S} adduct (light grey) bound to the active site of hAChE (fern green) with 2F_o - F_c density scaled to 1σ (light blue mesh) (PDB 6NTO). (b) View of A234 P_{R/S} adduct (light orange) bound to the active site of hAChE (light purple) with 2F_o - F_c density scaled to 1σ (light blue mesh). (PDB 6NNTL). (c) An active site overlay of hAChE (fern green) with bound A230 P_{R/S} adduct (light grey), hAChE (light cyan) with bound A232 P_{R/S} adduct (violet pink), and hAChE (light purple) with bound A234 P_{R/S} adduct (light orange). The black lines represent hydrogen bonds. The AChE residues are represented by black letters, while the red letters are the distances.

Although all the A-series agents are generally oriented in the same manner within the active site, minor differences do exist. These differences appear to be driven by two interactions. One is the interplay between Tyr337 and the A-series adducts seeking to optimize the Van der Waal interactions. The other is more substantial and rooted in the differences in size of the A-series S_{Small} moieties that point into the smaller active

hydrophobic pocket within the hAChE active site and distinguishes the A-series members from each other. This pocket is formed by Trp236, Phe295, and Phe297. The differences in steric volume between the A-series S_{Small} moieties appear to influence rotation around nitrogen phosphorous single bond. Among the A-series agents, the larger the small side chain, the greater the degree that the agent is moved up with a slight clockwise rotation of the S_{Large} moiety into large pocket (Figure 3.3c). For instance, the rotation of the A-234 S_{Large} adduct moiety positions it closer to His447 and Phe338 than the others, which is directly related to the accommodation of its S_{Small} ethoxy group in the second pocket. Positions of the residues lining the small pocket also appear to be affected by the size of the small side chains found in these agents' adducts. For instance, a shift in Phe295 was observed in A-232 and A-234 inhibited hAChE with a difference of about 0.5 Å at CZ of Phe295 as compared to A-230 inhibited hAChE, which is likely due to the accommodation of their slightly larger small side chain groups into this small pocket. An additional minor shift was noted of Trp236 in A-234 inhibited hAChE compared to Trp236 in the other A-series agents inhibited hAChE. Shifting of one Phe295 has been previously observed to cause changes to other amino acids on the acyl loop^{11, 20}, which can influence inhibition as well as reactivation overall¹⁹.

Accommodation of HI-6 within hAChE inhibited by A-Series nerve agents

As the ability of HI-6 to reactivate hAChE inhibited by these A-series agents is still unknown, atomic level insights into how their inhibition of hAChE impacts the ability of hAChE to be reactivated by HI-6 were sought. To this end, apo hAChE crystals were soaked in a solution containing racemic A-230, A-232, A-234, and were then placed in a solution containing HI-6 prior to mounting and flash cooling. Subsequently, data sets

of 2.70 Å, 2.55 Å, and 2.65 Å were collected. Structural solutions were then obtained by molecular replacement using the inhibited counterparts without inhibitor present as the search models. Upon examination of the active sites, $F_o - F_c$ simulated annealing omit map density was immediately apparent not only for their respective adduct, but also for HI-6 (Figure S3.2a,b). For the HI-6 bound to hAChE inhibited by A-230 and A-232 only one pose of HI-6 was observed within the active site. This pose was highly conserved between these two complexes and is held in place by numerous electrostatic and hydrophobic interactions (Figure 3.4). Immediately apparent is HI-6's close proximity to the PAS (peripheral anionic site) rather than near the catalytic triad (Figure 3.3c, 3.4). Tyr341 is aligned with the oxime containing pyridinium ring and interacts with the reactivator through π - π stacking. The oxime containing pyridinium ring is also influenced by hydrophobic interactions with Tyr337. The acetamide containing pyridinium ring is stabilized by a π - π stacking interaction with Trp286 and Tyr72 at the PAS. The acetamide containing pyridinium ring is further stabilized by strong interactions between the HI-6 acetamide group, Val282, and Glu285. The oxime-containing arm is stabilized by an interaction between the nitrogen on the oxime arm and the hydroxide of Tyr124. Tyr124 also forms a hydrophobic interaction with the tail-end pyridinium ring of HI-6. Within hAChE-A-230-HI-6, the position of the oxime arm is additionally supported in its position by a water mediated hydrogen bond network connected to Asn87. However, the lack of a comparable water in the hAChE-A-232-HI-6 complex may suggest this interaction is not essential for the observed orientation of the oxime arm. In this orientation, the oxime arm is ~ 10 Å away from the phosphonate of the A-230 and A-232 adducts in an up and away position.

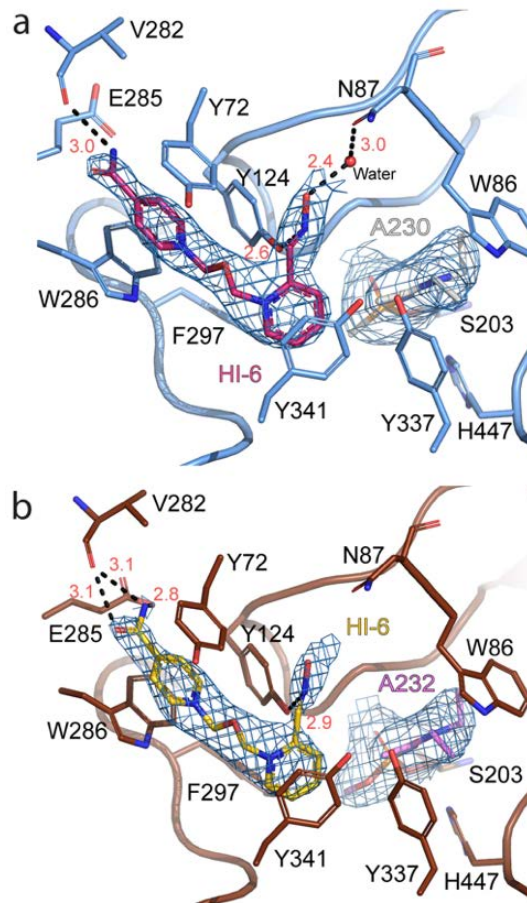


Figure 3.4. Accommodation of HI-6 in A230 and A232 bound hAChE active sites. (a) View of HI-6 (hot pink) bound to the active site of hAChE-A230 (baby blue; light grey) with 2F_o - F_c density scaled to 1σ (light blue mesh) (PDB 6NTN). (b) View of HI-6 (golden yellow) bound to the active site of hAChE-A232 (chocolate; violet pink) with 2F_o - F_c density scaled to 1σ (light blue mesh) (PDB 6NTM). The black lines represent hydrogen bonds and the red spheres denote waters. The AChE residues are represented by black letters, while the red letters are the distances.

Unlike the other two hAChE inhibited active sites, F_o - F_c simulated annealing omit map density within the hAChE-A-234-HI-6 supports two poses of HI-6 with one appearing to be more dominant (Figure 3.5a, S3.2c). Between the two alternative conformations, the orientation of the acetamide containing pyridinium ring is the most striking difference. The acetamide containing pyridinium ring of one conformation, pose 1, is stabilized by a π - π stacking interaction with Tyr124 and Trp286 at the PAS and the other pose, pose 2, is similar to the other HI-6 bound A-series inhibited hAChE

complexes (Figure 3.5b). Although initial $F_o - F_c$ simulated annealing omit map density appears to suggest pose 2 is less favorable, upon occupancy refinement of the two poses this conformation is slightly favored. Specifically, it has an occupancy of 0.52 and the other conformation has an occupancy of 0.48. The acetamide containing pyridinium ring of the first conformation is stabilized by a π - π stacking interaction with Tyr124 and a second conformation of Trp286 at the PAS (Figure 3.5c). The hydroxyl group of Tyr124 also forms a hydrogen bond with one conformation of HI-6 at the oxygen between the two pyridinium rings. The nitrogen of the acetamide on the pyridinium ring of the first conformation interacts with Val282 and Glu285. The acetamide on the pyridinium ring interacts with Ser298 with the nitrogen interacting with the hydroxyl group and both the oxygen and nitrogen potentially interacting with the main chain amine. Although the two poses have divergent orientations of their acetamide containing pyridinium rings, their oxime containing pyridinium rings are oriented in the same position. Specifically, their oxime arm points towards the carbonyl of Ser293, forming a hydrogen bond network with it and a nearby water molecule. Additionally, the oxime arm is stabilized by Tyr341 hydroxyl forming a hydrogen bond with the nitrogen of the oxime (Figure 3.5c). The position of the arm is further stabilized by the oxime containing pyridinium ring forming π - π stacking interactions with Tyr341. In this conformation, HI-6 is pointed away and ~ 11 Å from the phosphonate of the A-234 adduct. Alignment of the three complexes, reveals the likely reason for divergent conformation of the HI-6 oxime containing arm and flipped pyridinium ring in the hAChE-A-234-HI-6 active site (Figure 3.6a). Specifically, there is a small shift in the 292-295 acyl loop in the A-234 bound active site versus the hAChE active sites inhibited by A-230 and A-232 (Figure 3.6b). This shift

appears to result from hAChE seeking to accommodate the larger ethoxy in the S_{Small} position of A-234 appearing to push Phe295 slightly away. This has the effect of slightly torquing the backbone and presenting the carbonyl of Ser293 in a more favorable orientation for interactions with HI-6. These poses highlight the tenuous nature of HI-6 orientations within the inhibited hAChE sites and reinforces the flexible nature of HI-6.

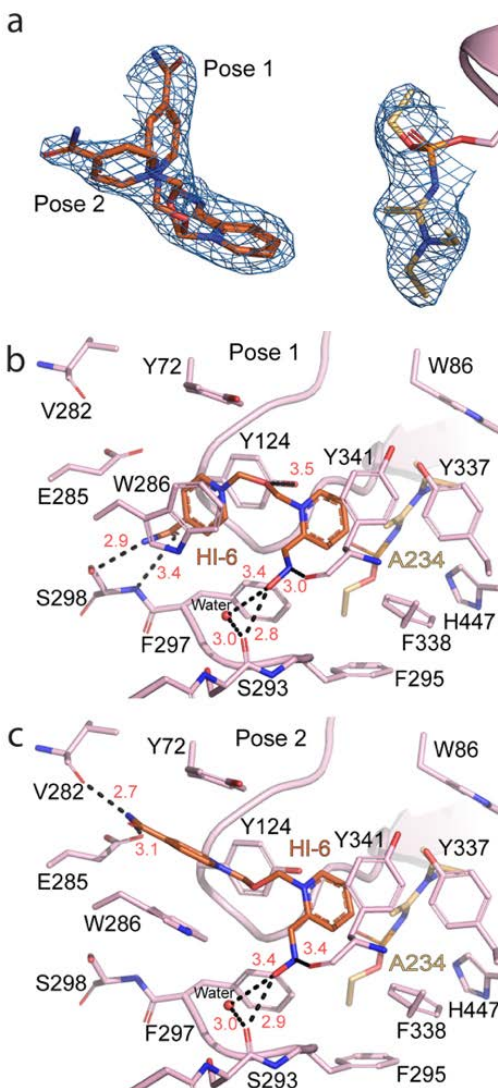


Figure 3.5. Multiple Orientations of HI-6 in A234 bound hAChE active site. (a) View of $2F_o - F_c$ density scaled to 1σ (light blue mesh) for HI-6 (dark orange) and A234 (light orange) bound to hAChE (light pink) (PDB 6NTG). (b) hAChE-A234 (light pink; light orange) active site with position 1 of HI-6. (c) hAChE-A234 (light pink; light orange) active site with position 2 of HI-6. The black lines represent hydrogen bonds and red spheres denote waters. The AChE residues are represented by black letters, while the red letters are the distances.

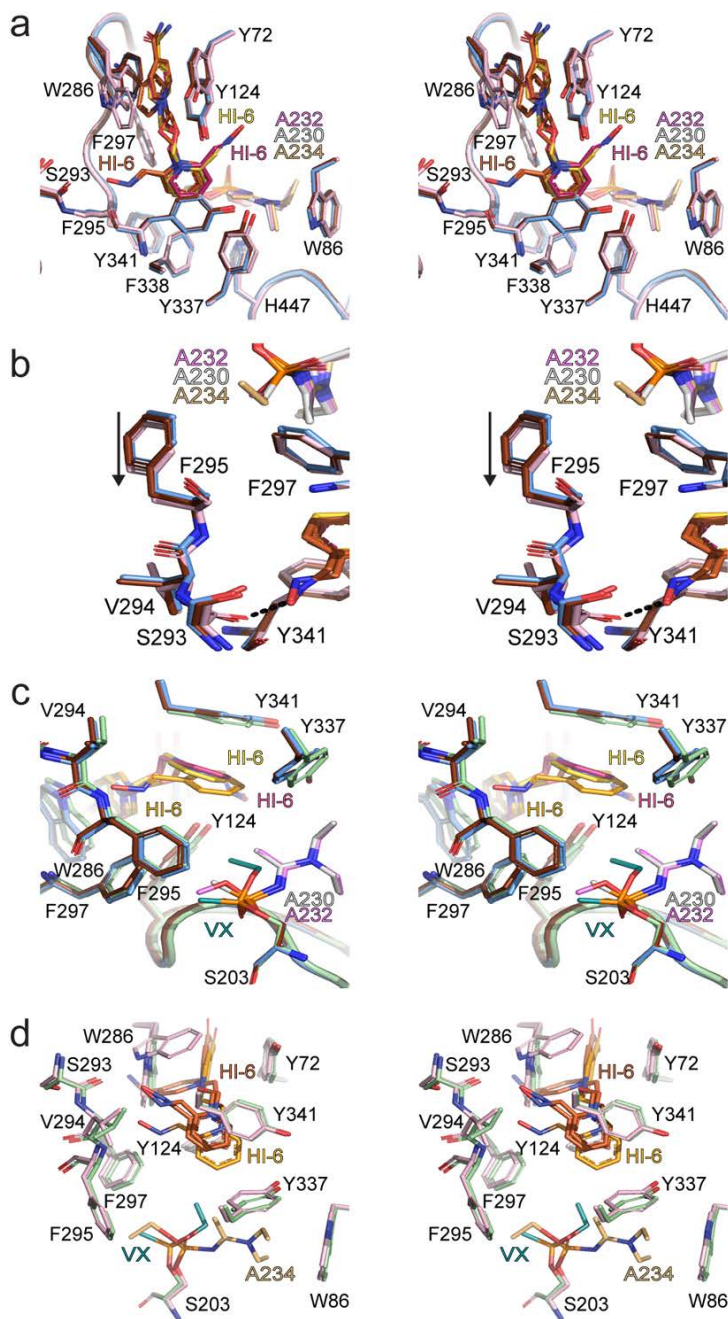


Figure 3.6. Comparison of HI-6 accommodation with the A-series inhibited hAChE active site. (a) Wall-eyed stereo view of an overlay of hAChE-A230-HI-6 (baby blue; light grey; hot pink), hAChE-A232-HI-6 (chocolate; violet pink; golden yellow), and hAChE-A234-HI-6 (light pink; light orange; dark orange). (b) A wall-eyed stereo view of a close up overlay of hAChE active sites in complex with HI-6 and inhibited by A230, A232, and A234. (c) A wall-eyed stereo view of a close up overlay of hAChE-A230-HI-6, (baby blue; light grey; hot pink), hAChE-A232-HI-6 (chocolate; violet pink; golden yellow), and hAChE-VX-HI-6 (pale green; dark teal; bright orange) (PDB 6CQW). (d) A wall-eyed stereo view of an overlay of hAChE-A234-HI-6 (light pink; light orange; dark orange) and hAChE-VX-HI-6 (pale green; dark teal; bright orange). The black dashed line represents hydrogen bonds and the AChE residues are represented by black letters.

Discussion & Conclusions

Potential influence of A-series structural properties upon their potency

Based on visualizing the P_S A-232 when the hAChE in its crystal form is inhibited by a racemic mixture of A-232 hAChE appears to possess a stereoselective preference for the P_S enantiomer of A-232. Recently, this trend was also observed in the manner by which VX and its stereoisomers inhibited hAChE¹¹. This result further supports the recent assertion¹¹ that inhibition of hAChE by racemic mixtures of nerve agents can be used to reveal the preferred stereoisomers of a nerve agent without having to synthesize each separately. Hence, this structural approach with well-characterized hAChE crystals offers a relatively more rapid approach in identifying those stereoisomers, particularly ones dealing with nerve agents that possess more than one chiral center, that are preferred by hAChE. The visualization of the hAChE active site altered by racemic A-232 and P_S A-232 also highlights that this type of nerve agent also undergoes a S_N2 inversion and provides insight into the underlying reason for hAChE's P_S stereoisomer preference. Due to the location of the oxyanion hole, the P_R stereoisomer of A-232 as well as other A-series agents would only differ from its counterpart by the reversal of the S_{Small} and S_{Large} group locations. The conformation of the P_R enantiomers would involve positioning the smaller methyl, methoxy, or ethoxy groups of A-series agents into the larger pocket and the *N,N*-diethylmethanimidamide into the smaller hydrophobic pocket. However, the available steric volume of the smaller hydrophobic pocket is relatively small. When put together, this highlights that a much larger moiety such as *N,N*-diethylmethanimidamide, of P_R A-232 or the other A-series agents would not be accommodated well in the small pocket of hAChE. As a result, the P_S stereoisomer is probably more potent because it

more closely resembles the placement of acetylcholine in terms of placing certain sized groups into enzyme pockets that can reasonably accommodate them.

Beyond playing a role in the preference of hAChE by the P_s enantiomers of A-232 and likely similar agents, the small pocket size and nature could also be a factor in the potency of the A-series agents. Comparing the structures of hAChE inhibited by A-234, A-232, and A-230, small shifts within the small pocket of hAChE do occur to accommodate their small side chains. This falls within a larger trend among nerve agents in regard to the small pocket. Recently, Phe295, Phe297, and other members of the acyl loop comprising hAChE amino acids 287-299 illustrated their role in shaping the potency of hAChE for stereoisomers of VX as well as between nerve agents themselves^{11, 20}. Although within these and other studies^{19, 20, 22}, the acyl loop appears to have some flexibility, they also highlight that nerve agents needing movement typically come with a loss of potency towards hAChE. Due to these assertions, a prediction can be made that A-232 likely has a higher potency than A-234 for hAChE as a shift in Phe295 was observed in both A-234 and A-232 inhibited hAChE, but an additional shift in Trp236 was observed in only A-234-inhibited hAChE (Figure 3.3c). This would also assume that the additional binding energy gained through a greater number of Van der Waal interactions of the ethoxy over that of the methoxy would not offset the energy required to displace both hAChE residues, Phe295 and Trp 236. Unlike A-232 and A-234 inhibited hAChE, no noticeable shifts of small pocket residues of A-230 inhibited hAChE occur, which suggests that A-230 could have the highest potency of the three A-series agents. Nonetheless, A-232 could have greater potency than A-230 as well despite the shifting of Phe295 due to stronger van der Waals interactions which would be supported by the

closer proximately of A-232's methoxy to the small pocket residues than A-230's methyl. Based on the structural data, predictions can be made of the A-series agents' potency towards hAChE compared to one another due to the shifting of the small pocket residues. This aforementioned trend can be used to help predict the potency of other yet unknown or untested nerve agents.

Structural properties of A-series and nerve agents that may influence HI-6 reactivation potency

While the exact reactivation potency of reactivators for the A-series agents are not known, the presence of a nitrogen group on the *N,N*-diethylmethanimidamide side chain as well as its size could influence the ability of HI-6 to reactivate hAChE. The hydrogen bond interactions made by nerve agent adducts including those forming the oxyanion hole draw electrons away from the phosphorus atom which likely makes it more electropositive and more suitable for nucleophilic attack by a reactivator. However, the presence of two nitrogen atoms on the *N,N*-diethylmethanimidamide side chain and other nerve agents could reduce the electropositivity of the phosphorus, making the atom less suitable for nucleophilic attack by an oxime reactivator. The nitrogen atoms could also draw the nucleophilic oxime away from the phosphorus acting as a trap. Additionally the size of the *N,N*-diethylmethanimidamide side chain may play a role in reactivation as access to the phosphorylated serine is key to its removal.

The hAChE-A-230-HI-6, hAChE-A-232-HI-6, and hAChE-A-234-HI-6 complex structures provide insight into the task faced by HI-6 and other reactivators. Intriguingly as the structure's highlight, HI-6 can be accommodated in the active site of hAChE

(Figure 3.4, 3.5). Accommodation of HI-6 by hAChE inhibited by A-series and follows a number of similarities to other hAChE structures from other species bound to HI-6. Specifically, the acetamide containing pyridinium ring of their bound HI-6 interact extensively with their respective PAS binding sites, which is similar to other known HI-6 structures to include the recently reported hAChE-VX-HI-6 complex completed by this group (PDB 6CQW; Figure 3.6)¹¹.

The comparison between hAChE-VX-HI-6 complex and hAChE inhibited by A-series agents in complex with HI-6 allows for a comparison between a HI-6 conformation in an active site inhibited by an agent that is readily susceptible to reactivation and an HI-6 conformation in an active site where the efficacy of the reactivator towards that inhibiting agent is not yet known. This comparison could provide evidence towards the efficacy of the reactivator with A-series agents. Overlaying, the hAChE-VX-HI-6 structure with some of those of hAChE inhibited by A-series with HI-6 present, a small shift away from the inhibited Ser203 is immediately apparent for the A-series structures (Figure 3.6c,d). This movement appears to be linked to the A-series *N,N*-diethylmethanimidamide sidechain optimizing its placement within the larger pocket of hAChE. This results in this S_{Large} side chain taking up more volume in the large pocket of hAChE then seen with other nerve agent adducts (Figure 3.7)^{11, 23}. The presence of this larger hydrophobic entity actually pulls Tyr337 closer to the S_{Large} side chain of A-series agents likely to optimize van der Waals interactions. Intriguingly, this movement of Tyr337 appears to also block HI-6 from moving deeper into the hAChE active site, which is necessary to occupy the orientation seen in the hAChE-VX-HI-6 structure. Additionally, this movement may also considerably restrict the oxime containing

pyrimidine ring in HI-6 compared to other nerve agent hAChE active sites. For the hAChE active sites inhibited by A-230 and A-232, this feature appears to be the main structural driving force for HI-6 to seek out what is likely the next lowest energy confirmation available. The S_{Small} group does not appear to influence the orientation of the HI-6 in these active sites as A-230 and A-232 have smaller S_{Small} groups. However, the influence of A-234's ethoxy does appear to bring back into play hAChE small pocket into the orientation of HI-6 within the active site. The resulting orientation of the oxime arm of HI-6 bound to A-234 inhibited hAChE is in the same direction as that of HI-6 bound to hAChE-VX. However, the HI-6 in this A-series hAChE inhibited structure is farther from the active site than as observed in the hAChE-VX-HI-6 structure. This suggests that unlike the HI-6 in the hAChE-VX-HI-6 structure, where a simple rotation around the linker between HI-6's two pyridinium rings could orient it in a catalytically relevant position, the HI-6 in the A-series structures would likely have difficulty in adopting a similar catalytically relevant orientation.

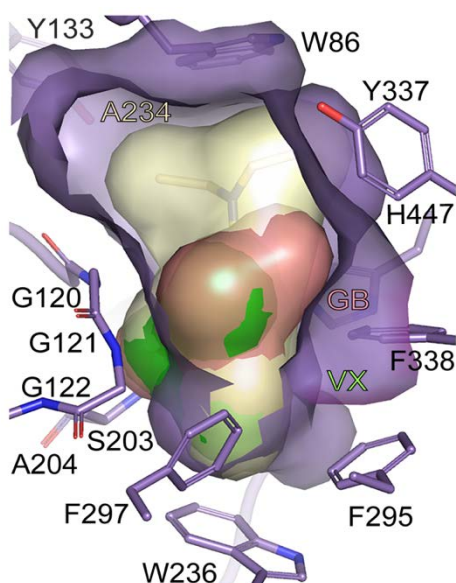


Figure 3.7. Comparison of nerve agent accommodation in hAChE active site. hAChE active site cavity view of hAChE-234 (light purple) with surface renders of A234 (pale yellow-orange), GB (salmon pink) (PDB 5FPP), and VX (green) (PDB 6CQW).

Beyond simply pushing the HI-6 farther out of the active site as well as likely restricting its movement, an A-series nerve agent inhibited active site of hAChE presents reactivators with additional unique structural features. Specifically, their larger *N,N*-diethylmethanimidamide side chain takes up considerably more volume of the hAChE active site. For instance, A-series agent's *N,N*-diethylmethanimidamide molar volume is $\sim 134 \text{ \AA}^3$, which dwarfs the 59 \AA^3 of the ethoxy on VX's hAChE adduct. The ability of HI-6 to strike at the phosphonate core have been suggested to rely in part on the ability to access the core. The presence of the larger *N,N*-diethylmethanimidamide in the orientation observed in the hAChE structures appears to make this more problematic. Additionally, the adduct's nitrogen may even further influence HI-6 by eliciting interactions with the oxime and acting as a trap. This larger steric volume also poses potential problems for reactivators such as 2-PAM that has been observed to bind directly above the inhibitors in the large pocket of AChEs. Naturally with the A-series agents now occupying this space, this suggests that if this orientation of 2-PAM is necessary for reactivation, reactivation may no longer occur.

The hAChE structures inhibited by A-series agents with HI-6 present offer a number of silver linings for targeted A-series reactivator development. For instance, inhibition of A-series agents does not impede HI-6 from binding within the active site. This includes the ability of HI-6's acetamide containing pyridinium ring to be stabilized by π - π stacking interactions at the PAS. This interaction has been suggested to hold HI-6 and likely other reactivators with dual ring systems at a standoff distance. Naturally, this suggests that using such an approach is still plausible to include in reactivators optimized for A-series agents. Along the same lines, illuminating the HI-6 bound poses overall can

provide a first step on a path towards HI-6 analogues optimized to combat A-series agent poisoning. Efforts such as modification of the linker distance between rings, size of the oxime containing ring, or length of the oxime containing arm all appear to be still viable approaches to further improve the HI-6. This along with the revelation that A-series agents behave from a biochemical standpoint the same as other V- and G-agents^{10, 11, 13} including their stereospecificity further demystifies A-series agents.

Experimental section

Chemicals and reagents

Acetylthiocholine, 5,5'-bis-dithio-2-nitrobenzene (DTNB), HI-6, sodium carbonate, monosodium phosphate and disodium phosphate were purchased from Sigma-Aldrich (St. Louis, MO USA). HEPES, KN03, PEG-3350 solutions purchased from Hampton Research, Aliso Viejo, CA; Laboratory deionized water > 17 MO was used for all assays. Hexane and isopropyl alcohol were purchased from Fisher Scientific (Waltham, MA), Lux Cellulose-1 Axia and Lux Cellulose-1 HPLC columns from Phenomenex, Torrance, CA; PCR primers, promoters, vectors and reagents for cloning from Invitrogen, Ni-NTA agarose, from Qiagen, CA, HEK-293H cells from NYSBC, DMEM GlutaMAX from Sigma-Aldrich, fetal bovine serum (FBS) Sigma-Aldrich; Lipofectamine 2000 Invitrogen, Hygromycin B from Invitrogen, CA; Quantichrom Acetylcholinesterase Assay Kit

Agent enantiomers

All chemical agents (purity > 95%), were synthesized by the Agent Chemistry Branch of the Research and Technology Directorate of the U.S. Army Edgewood Chemical Biological Center (Aberdeen Proving Ground, MD). A-series compounds were

prepared as racemic mixtures. Enantiomers were prepared, and the purity characterized by HPLC methods. Briefly, preparative samples were prepared at 100 $\mu\text{g/ml}$ and preparative samples were prepared at 22 mg/ml , all reagents and solvents were high-performance LC grade. The enantioselective preparative-scale separation of agents was achieved using an Agilent 1100 series preparative-scale LC system equipped with a diode array detector. Injections were monitored at 210 nm. Separation was through a Phenomenex Lux Cellulose-1 Axia packed column (250 x 30 mm) at an isocratic condition of 96/4 (v/v %) A/B, n-hexane (A) and isopropyl alcohol (B), a flow rate of 20 mL/min, and a sample volume of 1000 μL . Both enantiomers were baseline separated within 23 min. The Agilent 1200 Infinity series fraction collector was configured using the peak-time-based collection protocol, and the separated enantiomers were combined into 500 ml round-bottom flasks for solvent removal by rotary evaporation. Individual enantiomers were confirmed by polarimetry using an Autopol I (Rudolph Research Analytical, U.S.) and a 100 mm optical cell. The analytical separations of the enantiomers were characterized using an Agilent 1200 Infinity series LC system (Agilent Technologies; Santa Clara, CA), with an Agilent TOF- MS and APCI source using TIC, 5-500 m/z with the molecular ion at 268.1505 was performed on a Lux Cellulose-1 column, 250 x 4.6 mm, 5 μm ; Phenomenex; Torrance, CA. The mobile phase consisted of n-hexane (A) and isopropyl alcohol (B) and the sample volume was 10 μL . Separation was achieved using isocratic conditions of 96/4 (v/v %) A/B for all agents with a flow rate of 0.6 mL/min. Agent inhibition constants (k_i) for hAChE was obtained in triplicate using a modified Ellman assay²⁴ approach previously described^{17, 25, 26}.

Cloning, Expression and Purification of hAChE

All procedures for cloning, expression and purification were adapted from previous studies^{18, 20}. Briefly, a PCR fragment, which corresponds to amino acids 1 to 574 of human acetylcholinesterase, was amplified using suitable primers and sub-cloned into pcDNA 3.3-TOPO (Invitrogen) by adhering to the manufacturer's protocol. Using PCR and the corresponding primers, an octahistidine tag followed by the amino acid sequence ENLYFQ was inserted after residue 32 to form an ENLYFQ TEV protease site. Employing the Multisite Gateway Pro (Invitrogen) and Jump-In Fast Gateway Targeted Integration System (Invitrogen) with manufacturer procedures, the region of the pcDNA 3.3-TOPO rhAChE construct from the start of the promoter to the end of the polyadenylation signal was cloned into pJTI Fast DEST by a two-step recombination, forming pJTI Fast DEST rhAChE.

Expression and Purification of hAChE

HEK-293H cells were grown in DMEM GlutaMAX (Dulbecco's Modified Eagle Medium) supplemented with 10 % pre-warmed fetal bovine serum (FBS) in an adherent layer and then co-transfected with pJTI Fast DEST rhAChE and pJTI PhiC31 Int using Lipofectamine 2000 at the 24-well scale and treated with Hygromycin B (150 µg/L) for selective growth of the transfectants. The clones were individually isolated and further expanded by diluting from the 24-well into 96-well plates and then onto the 6-well level. QuatiChrom Acetylcholinesterase Assay Kit was then used to determine relative expression levels across the 6-well plates. Clones with high expression levels of hAChE were expanded onto the HYPERFlask cell culture vessels (Corning). Media containing the secreted His-tagged rhAChE was collected, concentrated and buffer-exchanged into a

binding buffer containing 20 mM HEPES, pH 7.6, 500 mM NaCl 40 mM imidazole using Vivaflow 200 (Sartorius Stedim Biotech) cross-flow diafiltration cells. The purification method involved two-columns on an AKTExpress system (GE Healthcare) which consisted of a nickel affinity column followed by a Superdex 200. gel filtration column. The elution buffer contained 0.5M imidazole in the binding buffer and the buffer for the gel filtration column consisted of 20 mM HEPES, pH 7.6, 150 mM NaCl and 20 mM imidazole. The fractions containing rhAChE were combined and the His-tag cleaved using a HIS-TEV protease at room temperature for 4 hours. The cleaved hAChE, corresponding to hAChE residues 33-574, was passed over a Ni-NTA agarose (Qiagen) gravity column to remove the HIS-TEV protease, cleaved tag residues, and residual uncleaved hAChE. The purified protein was then dialyzed into storage buffer (10 mM HEPES pH 7.0, and 10 mM NaCl) over night and concentrated to between 16-20 mg/ml for subsequent crystallization experiments.

Human acetylcholinesterase crystallization and inhibitor soaking

hAChE crystals were prepared and conjugated with OP chemical agent inhibitors with and without reactivator compounds present in the solution by soaking methods as described previously^{18, 20}. hAChE crystals were grown by sitting drop vapor diffusion at 22°C against 5 µL crystallization buffer. The crystallization buffer contained a gradient of 15-21% polyethylene glycol 3350 (PEG) and 0.17- 0.21M potassium nitrate (KNO₃). The crystals were hexagonal rod-shaped and usually nucleated within 5 days and finished their growth after an additional 3 days. Crystals of a ligand in complex with rhAChE were obtained by soaking apo crystals at 22°C in crystallization buffer accompanied by either 20-25% ethylene glycol or DMSO, glycerol, and ethylene glycol in a 1:1:1 ratio

and specific concentrations of each ligand for individually designated periods of time to ensure the ligand is present. In order to obtain AChE- P_{RS}-A-232 inhibited hAChE, the apo AChE crystals were soaked in crystallization buffer with a concentration of 19.0 mM of A-232 for five minutes. For AChE-A-234 complex the apo AChE crystal was soaked in a 26.8 mM A-234 mixture for two minutes, while to achieve AChE-P_S-A-232, the apo crystals were soaked in buffer with 9.52 mM P_S-A-232 for two minutes. For AChE-A-230 complex, the crystals were soaked in buffer with 30.9 mM A-230 for one minute. To obtain the AChE-P_{RS}-A-232-HI-6 complex, the crystal was soaked in a 28.5 mM P_{RS}-A-232 solution for one minute and a 111.4 mM HI-6 solution for two minutes. For the AChE-A-234-HI-6 complex, the apo crystals were soaked in crystallization buffer with a concentration of 4.46 mM A-234 for five minutes and then buffer with 11.1 mM concentration of HI-6 for five minutes. The AChE-A-230-HI-6 complex was achieved via soaking the crystals in buffer with a A-230 mixture concentration of 30.9 mM for two minutes and in 111.4 mM HI-6 buffer for two minutes. The crystals were then mounted onto liquid nitrogen flash-cooled nylon loops.

Data sets were collected for hAChE binary conjugates with A-232 and A-234 and ternary conjugate with A-230-HI-6 with a resolution of 2.40 Å, 2.25 Å, and 2.70 Å respectively on beamline 19-ID of SBCCAT at the Argonne National Laboratory (ANL), Advanced Photon Source (APS) using a monochromic X-ray beam with an ADSC Quantum 315r CCD detector. Data sets were collected for hAChE binary conjugates with A-230 and P_S A-232 enantiomer and ternary conjugate with A-232-HI-6 with a resolution of 2.05 Å, 2.42 Å and 2.55 Å respectively on beamline 22ID of SERCAT. This beam line is also located at Argonne National Laboratory, Advanced Photon Source using a

monochromic X-ray beam with a Rayonix (Mar) 300HS high speed CCD detector. Data sets were collected for the hAChE-A-234-HI-6 complex with a resolution of 2.65 Å respectively on the 22BM beamline of SERCAT using a monochromic X-ray beam with a Mar225 CCD detector.

Data collection, reduction, and refinement.

Using HKL2000 the X-ray images were indexed, strategized, integrated, scaled, and processed²⁹. The CCP4 software suite was utilized to generate a cross-validation set from a random 5% of the reflections which was throughout the structural refinement³⁰. The initial phase solutions for the structures were formed using molecular replacement via Phaser with 4EY4 as an initial model³¹. The structures were refined using repetitive cycles of model building and refinement via COOT and phenix.refine respectively³². To analyze the structures for flexibility, TLS Motion Determination (TLSMD) was utilized. This analysis was employed for TLS parameters in phenix.refine to assist in refining the structures for anisotropic displacements³². The original addition of water molecules was to the $2F_o - F_c$ density peaks of greater than 1σ using the Find Water COOT program function and then each water was evaluated individually³³. Carbohydrates, PEGs, and other ligands were individually positioned into structures based on the $F_o - F_c$ omit map density at 3σ and refined with phenix.refine afterwards to ensure these ligands fit the $2F_o - F_c$ density at 1σ ³². The final model of each structure was assessed via Molprobit to verify the quality of the structures. The data collection and refinement statistics for each structure are listed in Table 3.1.

Table 3.1. Data collection and refinement statistics

	AChE-A232 (PDB 6NTK)	hAChE-A232(P _s) (PDB 6NTH)	AChE-A230 (PDB 6NTO)	AChE-A234 (PDB 6NTL)
Data collection				
Space group	P 31 2 1	P 31 2 1	P 31 2 1	P 31 2 1
Cell dimensions				
<i>a</i> , <i>b</i> , <i>c</i> (Å)	105.1, 105.1, 324.4	105.6, 105.6, 324.2	104.4, 104.4, 323.6	105.0, 105.0, 323.8
α , β , γ (°)	90, 90, 120	90.0, 90.0, 120.0	90, 90, 120	90.0, 90.0, 120.0
Resolution (Å)	50.0 - 2.4 (2.44-2.40) ^a	50.0 - 2.42 (2.46-2.42) ^a	50.0 - 2.05 (2.2-2.1) ^a	50.0 - 2.25 (2.29-2.25) ^a
Completeness (%)	99.1 (99.6) ^a	99.6 (97.1) ^a	100 (99.9) ^a	99.7 (99.4) ^a
<i>R</i> _{merge} ^b (%)	9.6 (50.9) ^a	7.7 (47.5) ^a	7.2 (62.9) ^a	9.6 (74.4) ^a
<i>R</i> _{pim} (%)	6.0 (32.1) ^a	3.5 (24.5) ^a	3.2 (29.4) ^a	4.5 (35.8) ^a
CC1/2	(0.855) ^a	(0.954) ^a	(0.864) ^a	(0.846) ^a
<i>I</i> / σ <i>I</i>	10.9 (2.2) ^a	17.5 (3.5) ^a	21.2 (2.0) ^a	16.8 (2.4) ^a
Redundancy	3.5 (3.5) ^a	6.0 (4.7) ^a	6.1 (5.4) ^a	5.5 (5.2) ^a
Refinement				
Resolution (Å)	46.5 - 2.41 (2.49-2.41)	41.3 - 2.42 (2.51-2.42)	47.0 - 2.05 (2.12-2.05)	46.4 - 2.25 (2.33-2.25)
No. reflections	75891	80750	128617	89710
<i>R</i> _{work} ^c (%) / <i>R</i> _{free} ^c (%)	17.7/19.9	16.2/18.1	17.1/19.6	16.8/19.2
No. atoms				
Protein	8234	8319	8351	8295
Ligand/ion	156	166	192	161
Water	885	606	1233	1039
B-factors				
Protein	39.1	55.8	34.0	32.8
Ligands	81.3	114.3	79.46	80.5
Water	50.4	61.6	49.1	47.2
R.m.s deviations				
Bond lengths (Å)	0.008	0.009	0.007	0.006
Bond angles (°)	0.79	1.12	1.15	1.10
<hr/>				
	AChE-A230-HI6 (PDB 6NTN)	AChE-A232-HI6 (PDB 6NTM)	AChE-A234-HI6 (PDB 6NTG)	
Data collection				
Space group	P 31 2 1	P 31 2 1	P 31 2 1	
Cell dimensions				
<i>a</i> , <i>b</i> , <i>c</i> (Å)	104.4, 104.4, 323.7	105.3, 105.3, 324.6	104.7, 104.7, 325.0	
α , β , γ (°)	90.0, 90.0, 120.0	90, 90, 120	90, 90, 120	
Resolution (Å)	50.0 - 2.70 (2.75-2.70) ^a	50.0 - 2.54 (2.58-2.54) ^a	50.0 - 2.65 (2.7-2.65) ^a	
Completeness (%)	99.6 (99.9) ^a	99.4 (94.6) ^a	99.7(98.1) ^a	
<i>R</i> _{merge} ^b (%)	13.0 (83.2) ^a	10.2 (49.3) ^a	14.7 (68.2) ^a	
<i>R</i> _{pim} (%)	6.1 (38.0) ^a	4.2 (22.2) ^a	7.2 (37.4) ^a	
CC1/2	(0.906) ^a	(0.921) ^a	(0.690) ^a	
<i>I</i> / σ <i>I</i>	13.1 (2.2) ^a	15.2 (2.2) ^a	8.62 (2.82) ^a	
Redundancy	5.5 (5.7) ^a	5.4 (4.6) ^a	4.9(4.1) ^a	
Refinement				
Resolution (Å)	45.2 - 2.70 (2.79-2.70)	39.7 - 2.55 (2.64-2.55)	43.7 - 2.65 (2.75-2.65)	
No. reflections	57077	58546	60706	
<i>R</i> _{work} ^c (%) / <i>R</i> _{free} ^c (%)	16.9/21.2	19.0/23.0	19.0/23.2	
No. atoms				
Protein	8249	8359	8310	
Ligand/ion	192	229	231	
Water	461	345	495	
B-factors				
Protein	61.2	69.3	51.4	
Ligand/ion	98.2	118.2	90.3	
Water	58.0	65.7	57.0	
R.m.s deviations				
Bond lengths (Å)	0.008	0.012	0.004	
Bond angles (°)	0.93	1.394	0.72	

References

1. Dodd, V.; Harding, L.; MacAskill, E. Sergei Skripal: former Russian spy poisoned with nerve agent, say police. *The Guardian* 2018.
2. Amesbury poisoning: Experts confirm substance was Novichok. *British Broadcasting Company* September 4, 2018, 2018.
3. Paddock, R.; Sang-Hun, C.; Wade, N. In Kim Jong-nam's Death, North Korea Lets Loose a Weapon of Mass Destruction. *The New York Times* 2017.
4. Englund, W. Russia still doing secret work on chemical arms Research goes on as government seeks U.N. ban. *The Baltimore Sun* 1992.
5. Mirzayanov, V. S. *State secrets : an insider's chronicle of the Russian chemical weapons program*. Outskirts Press, Inc: Denver, Colorado, 2009.
6. Guven, M.; Sungur, M.; Eser, B.; Sari, I.; Altuntas, F. The effects of fresh frozen plasma on cholinesterase levels and outcomes in patients with organophosphate poisoning. *J Toxicol Clin Toxicol* 2004, 42, 617-23.
7. Mirfazaelian, H.; Nikfar, S.; Rezvanfar, M. A.; Abdollahi, M. Efficacy of Plasma Transfusion in Acute Human Organophosphorus Poisoning: A Systematic Review and Meta-analysis. *International Journal of Pharmacology* 2014, 10, 299-306.
8. Pazooki, S.; Solhi, H.; Vishteh, H. R.; Shadnia, S.; Beigi, M. J. Effectiveness of fresh frozen plasma as supplementary treatment in organophosphate poisoning. *Med J Malaysia* 2011, 66, 342-5.
9. Nepovimova, E.; Kuca, K. Chemical warfare agent NOVICHOK - mini-review of available data. *Food Chem Toxicol* 2018, 121, 343-350.
10. Hall, C. R.; Inch, T. D.; Inns, R. H.; Muir, A. W.; Sellers, D. J.; Smith, A. P. Differences between some biological properties of enantiomers of alkyl S-alkyl methylphosphonothioates. *J Pharm Pharmacol* 1977, 29, 574-6.
11. Bester, S. M.; Guelta, M. A.; Cheung, J.; Winemiller, M. D.; Bae, S. Y.; Myslinski, J.; Pegan, S. D.; Height, J. J. Structural insights of stereospecific inhibition of human acetylcholinesterase by VX and subsequent reactivation by HI-6. *Chem Res Toxicol* 2018.
12. Michel, H. O. Kinetics of the reactions of cholinesterase chymotrypsin and trypsin with organophosphorus inactivators. *Fed. Proc, Fed. Am. Soc. Exp. Biol* 1955, 14.
13. Benschop, H. P.; Konings, C. A.; Van Genderen, J.; De Jong, L. P. Isolation, anticholinesterase properties, and acute toxicity in mice of the four stereoisomers of the nerve agent soman. *Toxicol Appl Pharmacol* 1984, 72, 61-74.

14. Buckley, N. A.; Roberts, D.; Eddleston, M. Overcoming apathy in research on organophosphate poisoning. *BMJ* 2004, 329, 1231-3.
15. Ekstrom, F.; Hornberg, A.; Artursson, E.; Hammarstrom, L. G.; Schneider, G.; Pang, Y. P. Structure of HI-6*sarin-acetylcholinesterase determined by X-ray crystallography and molecular dynamics simulation: reactivator mechanism and design. *PLoS One* 2009, 4, e5957.
16. Ekstrom, F.; Pang, Y. P.; Boman, M.; Artursson, E.; Akfur, C.; Borjegen, S. Crystal structures of acetylcholinesterase in complex with HI-6, Ortho-7 and obidoxime: structural basis for differences in the ability to reactivate tabun conjugates. *Biochem Pharmacol* 2006, 72, 597-607.
17. Worek, F.; Thiermann, H.; Szinicz, L.; Eyer, P. Kinetic analysis of interactions between human acetylcholinesterase, structurally different organophosphorus compounds and oximes. *Biochem Pharmacol* 2004, 68, 2237-48.
18. Cheung, J.; Rudolph, M. J.; Burshteyn, F.; Cassidy, M. S.; Gary, E. N.; Love, J.; Franklin, M. C.; Height, J. J. Structures of human acetylcholinesterase in complex with pharmacologically important ligands. *J Med Chem* 2012, 55, 10282-6.
19. Hornberg, A.; Tunemalm, A. K.; Ekstrom, F. Crystal structures of acetylcholinesterase in complex with organophosphorus compounds suggest that the acyl pocket modulates the aging reaction by precluding the formation of the trigonal bipyramidal transition state. *Biochemistry* 2007, 46, 4815-25.
20. Franklin, M. C.; Rudolph, M. J.; Ginter, C.; Cassidy, M. S.; Cheung, J. Structures of paraoxon-inhibited human acetylcholinesterase reveal perturbations of the acyl loop and the dimer interface. *Proteins* 2016, 84, 1246-56.
21. Reiter, G.; Muller, S.; Hill, I.; Weatherby, K.; Thiermann, H.; Worek, F.; Mikler, J. In vitro and in vivo toxicological studies of V nerve agents: molecular and stereoselective aspects. *Toxicol Lett* 2015, 232, 438-48.
22. Millard, C. B.; Kryger, G.; Ordentlich, A.; Greenblatt, H. M.; Harel, M.; Raves, M. L.; Segall, Y.; Barak, D.; Shafferman, A.; Silman, I.; Sussman, J. L. Crystal structures of aged phosphonylated acetylcholinesterase: nerve agent reaction products at the atomic level. *Biochemistry* 1999, 38, 7032-9.
23. Allgardsson, A.; Berg, L.; Akfur, C.; Hornberg, A.; Worek, F.; Linusson, A.; Ekstrom, F. J. Structure of a prereaction complex between the nerve agent sarin, its biological target acetylcholinesterase, and the antidote HI-6. *Proc Natl Acad Sci U S A* 2016, 113, 5514-9.
24. Ellman, G. L.; Courtney, K. D.; Andres, V., Jr.; Feather-Stone, R. M. A new and rapid colorimetric determination of acetylcholinesterase activity. *Biochem Pharmacol* 1961, 7, 88-95.

25. Worek, F.; Reiter, G.; Eyer, P.; Szinicz, L. Reactivation kinetics of acetylcholinesterase from different species inhibited by highly toxic organophosphates. *Arch Toxicol* 2002, 76, 523-9.
26. Worek, F.; Thiermann, H. Reactivation of organophosphate-inhibited human acetylcholinesterase by isonitrosoacetone (MINA): a kinetic analysis. *Chem Biol Interact* 2011, 194, 91-6.
27. Forsberg, A.; Puu, G. Kinetics for the inhibition of acetylcholinesterase from the electric eel by some organophosphates and carbamates. *Eur J Biochem* 1984, 140, 153-6.
28. Luo, C.; Tong, M.; Chilukuri, N.; Brecht, K.; Maxwell, D. M.; Saxena, A. An in vitro comparative study on the reactivation of nerve agent-inhibited guinea pig and human acetylcholinesterases by oximes. *Biochemistry* 2007, 46, 11771-9.
29. Otwinowski, Z.; Minor, W. *Processing of X-ray Diffraction Data Collected in Oscillation Mode*. Academic Press: New York, 1997; Vol. 276: Macromolecular Crystallography, Part A, p 307-326.
30. Winn, M. D.; Ballard, C. C.; Cowtan, K. D.; Dodson, E. J.; Emsley, P.; Evans, P. R.; Keegan, R. M.; Krissinel, E. B.; Leslie, A. G.; McCoy, A.; McNicholas, S. J.; Murshudov, G. N.; Pannu, N. S.; Potterton, E. A.; Powell, H. R.; Read, R. J.; Vagin, A.; Wilson, K. S. Overview of the CCP4 suite and current developments. *Acta Crystallogr D Biol Crystallogr* 2011, 67, 235-42.
31. McCoy, A. J.; Grosse-Kunstleve, R. W.; Adams, P. D.; Winn, M. D.; Storoni, L. C.; Read, R. J. Phaser crystallographic software. *J Appl Crystallogr* 2007, 40, 658-674.
32. Adams, P. D.; Afonine, P. V.; Bunkoczi, G.; Chen, V. B.; Davis, I. W.; Echols, N.; Headd, J. J.; Hung, L. W.; Kapral, G. J.; Grosse-Kunstleve, R. W.; McCoy, A. J.; Moriarty, N. W.; Oeffner, R.; Read, R. J.; Richardson, D. C.; Richardson, J. S.; Terwilliger, T. C.; Zwart, P. H. PHENIX: a comprehensive Python-based system for macromolecular structure solution. *Acta Crystallogr D Biol Crystallogr* 2010, 66, 213-21.
33. Emsley, P.; Cowtan, K. Coot: model-building tools for molecular graphics. *Acta Crystallogr D Biol Crystallogr* 2004, 60, 2126-32.

CHAPTER 4
THE STRUCTURAL AND BIOCHEMICAL IMPACT OF MONOMERIZING
HUMAN ACETYLCHOLINESTERASE³

³Bester, S.M., K.A. Adipietro, V.L. Funk, J. Myslinski, N.D. Keul, J. Cheung, P.T. Wilder, Z.A. Wood, D.J. Weber, J.J. Height, and S.D. Pegan. Accepted by *Protein Science*. Reprinted here with permission of the publisher.

Abstract

Serving a critical role in neurotransmission, human acetylcholinesterase (hAChE) is the target of organophosphate (OP) nerve agents. Hence, there is an active interest in studying the mechanism of inhibition and recovery of enzymatic activity, which could lead to better countermeasures against nerve agents. Because hAChE is found in different oligomeric assemblies, certain approaches to studying it have been problematic. Herein, we examine the biochemical and structural impact that occurs when monomerizing hAChE by using two mutations: L380R/F535K. The activity of monomeric hAChE L380R/F535K and dimeric hAChE were determined to be comparable utilizing a modified Ellman Assay. To investigate the influence of subunit-subunit interactions on the structure of hAChE, a 2.1 Å X-ray crystallographic structure was determined. Apart from minor shifts along the dimer interface, the overall structure of hAChE L380R/F535K mutant mirrors that of hAChE. To probe whether the plasticity of the active site was overtly impacted by monomerizing hAChE, the kinetics of inhibition with (*P_{R/S}*)-VX and subsequent rescue of hAChE L380R/F535K activity with HI-6 were determined and found to be comparable to dimeric hAChE. Thus, hAChE L380R/F535K could be used as a substitute for the dimer when experimentally probing the ability of the hAChE active site to accommodate future nerve agent threats or judge the ability of new therapeutics to access the active site.

Introduction

Acetylcholinesterase (E.C. 3.1.1.7, AChE) catalyzes the hydrolysis of the neurotransmitter acetylcholine into acetate and choline, terminating its signal. AChE is located in the neuromuscular junction (NMJ) of all innervated organs, the autonomic ganglia, as well as the cholinergic synapses in the brain and spinal cord (1). AChE exists in multiple forms including monomers, dimers, and tetramers (2-6). These forms are distinguishable by their oligomeric assembly and attachment mode to cell membranes (6).

As a result of its role in the nervous system, AChE is the biological target of organophosphate (OP) nerve agents. Recent examples of the nerve agent threat include uses by Syria (7), the VX-facilitated assassination of the half-brother of the North Korean leader(8), as well as the use of a Novichok nerve agent in the United Kingdom (9). Currently, the preferred treatment for OP poisoning is a combination of benzodiazepine, atropine, and the hAChE reactivator pralidoxime (2-PAM) (10). Reactivators seek to reverse the covalent modification of hAChE's catalytic serine by OPs, which must occur prior to ageing of the nerve agent-AChE complex (11-13). The efficacy of reactivators was shown to vary based on the OP, the stereochemistry of the OP, and the species of the AChE (14-18). The flexibility of the active site, in particular the acyl loop, was recently been shown to play a role in the ability of nerve agents to inhibit hAChE and subsequent reactivation (19; 18). Although known to play a role in the inhibition and reactivation of hAChE, probing the exact influence of hAChE active site plasticity has on these events has been problematic. The oligomeric size of the hAChE dimer exceeds 120 KD limiting the effectiveness of employment of methods such as Molecular Dynamics (MD) and NMR.

Herein, we describe the influence of monomerization upon hAChE functionality and its ability to accommodate the nerve agent VX as well as be salvaged by a reactivator known as HI-6. To this end, two hydrophilic mutations L380R/F535K were introduced into the hAChE dimer interface to prevent dimer formation. The enzymatic activity of monomeric and dimeric forms hAChE were compared. Using X-ray crystallography, a structure of hAChE L380R/F535K was obtained and compared to wild-type hAChE. Inhibition of monomeric and dimeric forms of hAChE with VX and subsequent reactivation with HI-6 was evaluated. Through these comparisons, monomeric L380R/F535K hAChE was found to have similar structural and biochemical behavior to that of the wild-type enzyme. Hence, this opens the door to utilizing the monomeric hAChE L380R/F535K in place of the hAChE dimeric form for size sensitive studies such as modeling or molecular dynamic techniques.

Results

Biochemical Characterization of monomer hAChE

To investigate the influence of subunit-subunit interactions on the functionality the hAChE active site, two mutations, L380R and F535K, were engineered in order to disrupt the interface of between the two hAChE subunits (PDB 4EY4). To confirm the mutations were effective in preventing dimerization, the oligomeric state of hAChE and the hAChE L380R/F535K variant was validated through sedimentation velocity analysis (Figure S4.1). The sedimentation coefficient for hAChE L380R/F535K was 4.03 S, which was slightly slower than the predicted value of 4.36 S. This was substantially different from the 6.35 S of the hAChE, which was largely in line with the predicted value of 6.4 S. This confirmed the monomeric nature of hAChE L380R/F535K and

reinforced the dimeric oligomeric state of wild type hAChE. To investigate the impact dimerization has on the functionality of hAChE, the K_m and k_{cat} for both this mutant and the dimeric hAChE were obtained side-by-side using a modified Ellman's assay (Table 4.1). The K_m of the monomer and dimer hAChE were consistent with one another at $8.6 \pm 1.3 \times 10^{-5}$ M and $7.7 \pm 1.0 \times 10^{-5}$ M, respectively. Whereas k_{cat} of the dimer, 93 ± 3 s⁻¹ was slightly higher than that of the monomer, 70 ± 3 s⁻¹ these values fall within a range of percent deviation that is less than two fold different and as such are comparable (3; 20; 21). The k_{cat} values were determined using purified enzyme (>99%) with the enzyme concentration determined quantitatively via amino acid analyses, which is about 100-fold lower than previous reports (22; 23). This discrepancy likely results as these studies were completed in cell culture media with enzyme concentrations calculated via antibody-based methods. This could also be due to AChE binding other components in the cell culture media (I.e. membrane), which provides the enzyme with a higher specific activity. Nonetheless, the monomerization of hAChE does not appear to affect activity as compared to dimer hAChE.

Table 4.1. Enzymatic activity of dimer hAChE and hAChE L380R/F535K.

	Monomer	Dimer
E_t (M)	1.0×10^{-9}	9.26×10^{-10}
k_{cat} (sec ⁻¹)	70 ± 3	93 ± 3
K_m (M)	$8.6 \pm 1.3 \times 10^{-5}$	$7.7 \pm 1.0 \times 10^{-5}$
V_{max} (M/sec)	$6.9 \pm 0.3 \times 10^{-8}$	$8.6 \pm 0.3 \times 10^{-8}$

Structural Characterization of monomer hAChE

With the catalytic activity of monomeric and dimeric forms of hAChE being similar, insight into the structural impact of monomerizing mutations L380R/F535K on

hAChE was sought. To obtain structural information on hAChE L380R/F535K, purified protein was screened against 768 crystallization conditions. Final crystal conditions were obtained by screening pH and sodium citrate concentrations. Using crystals generated under these conditions, a 2.09 Å dataset was obtained in the space group P6₅22, which differs from previous hAChE space groups (24; 25; 19; 18). Using molecular replacement with one subunit of hAChE (PDB 4EY4) (24) a solution was readily found (Table 4.2). Unlike previous hAChE structures (24; 25; 19; 18) that had a dimer in the asymmetric unit, hAChE L380R/F535K was a monomer. Inspection of the hAChE L380R/F535K lattice mate contacts revealed no interaction between hAChE L380R/F535K and its symmetry mates at the traditional hAChE dimer interface located at $\alpha F'3$ and $\alpha H(26)$ (Figure 4.1). Naturally, this contributed to hAChE L380R/F535K having a strikingly different lattice packing than previously solved structures. Hence, these findings reinforce the monomeric nature of hAChE L380R/F535K.

Globally, the monomeric hAChE L380R/F535K structure closely resembles its dimer counterpart with only a few exceptions (Figure 4.2). These exceptions are largely confined to the two alpha helices that comprise the dimer interface in hAChE and contain the L380R/F535K mutations. Upon closer inspection of the region, the mutations themselves do not appear to overtly cause a disruption to the secondary structure of either helix or the interaction between αH and $\alpha F'$ helices themselves. Instead, the slight divergence of this region with that of the dimer hAChE appears to be linked to a lack of constraints on the αH helix due to the absence of its dimeric mate. Moreover, the αH helix lacks any other crystal contacts with other monomers in the crystal lattice likely allowing it to move freely than when part of the dimer interface. Also, the $\alpha F'3$ helix is

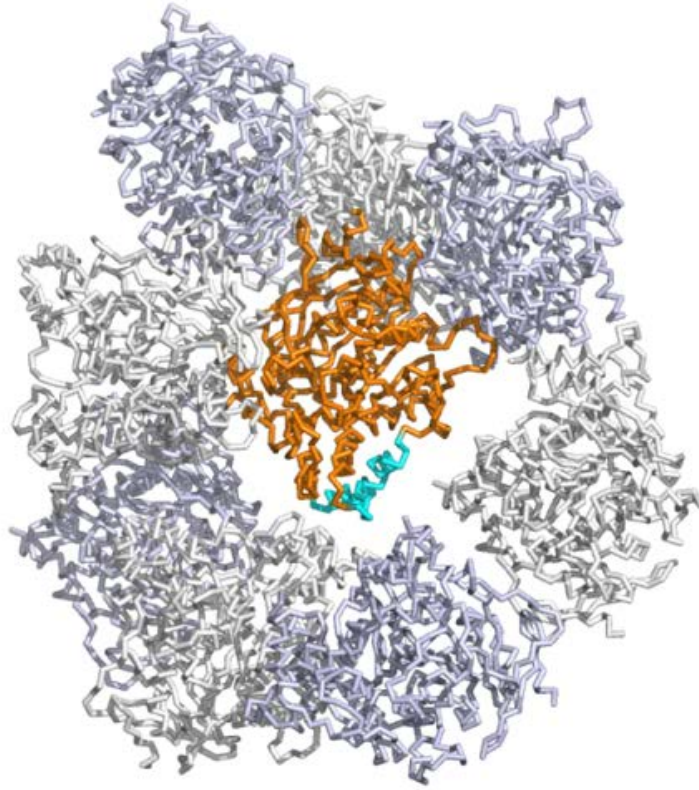
positioned closer to the core of the subunit with the lack of involvement in a dimeric interface (Figure 4.2). The mutations L380R/F535K themselves appear to work as designed by turning a hydrophobic patch into one with a positive charge that is no longer sterically compatible with another subunit (Figure 4.2B, 4.2C). Beyond monomerizing hAChE, this also highlights the importance of the L380/F535 hydrophobic interaction on the dimer interface.

Table 4.2. Data collection and refinement statistics (PDB 6O69)

Data collection	
Space group	P 65 2 2
Cell dimensions	
<i>a</i> , <i>b</i> , <i>c</i> (Å)	115.8, 115.8, 191.9
α , β , γ (°)	90.0, 90.0, 120.0
Resolution (Å)	50.0-2.09 (2.13-2.09) ^a
Completeness (%)	99.6 (100) ^a
CC1/2	0.977 (0.814) ^a
R _{pim} (%)	5.4 (32.6) ^a
<i>I</i> / σ <i>I</i>	11.1 (2.4) ^a
Redundancy	12.7 (12.7) ^a
Refinement	
Resolution (Å)	43.3-2.08
No. reflections	45,954
R _{work} /R _{free} (%) ^b	18.5/22.0
No. atoms	
Protein	4,138
Ligand/ion	38
Water	259
B-factors	
Protein	49.4
Ligand/ion	97.7
Water	52.2
R.m.s deviations	
Bond lengths (Å)	0.015
Bond angles (°)	1.07

^aData for the last resolution shell are provided in parentheses. ^bR_{work} and R_{free} = $h[|F(h)_{obs}| - |F(h)_{calc}|]/h|F(h)_{obs}|$ for reflections corresponding to the working and test sets.

A



B

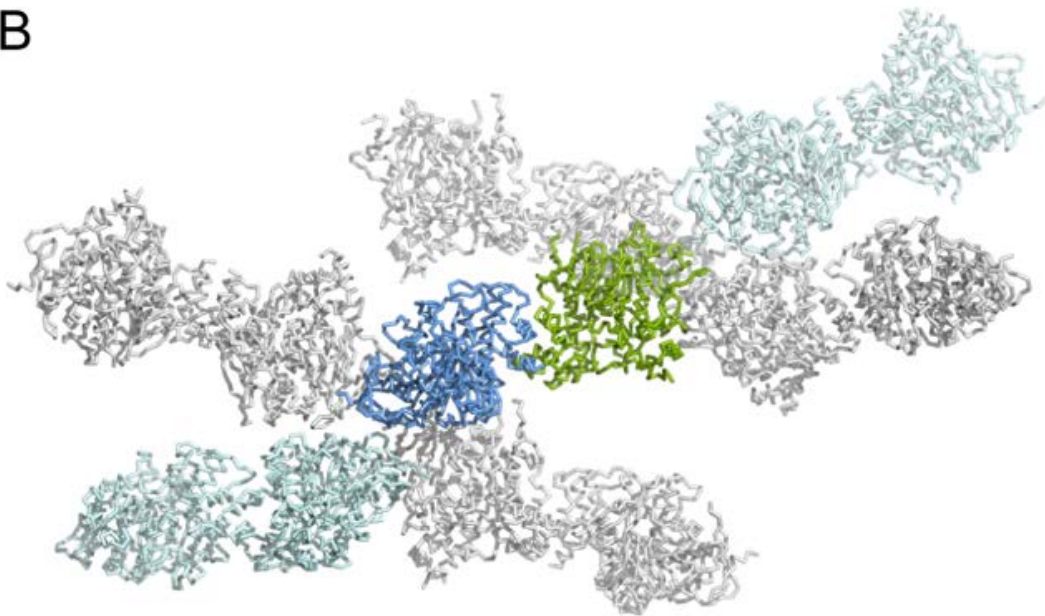


Figure 4.1. Comparison of the crystal lattice of hAChE L380R/F535K and dimeric hAChE. The asymmetric unit of the A) monomeric (orange) and B) dimeric hAChE (2 subunits: baby blue, green) surrounded by symmetry mates (white/blue-white and light blue/light grey). The dimer interface of hAChE is depicted in aqua.

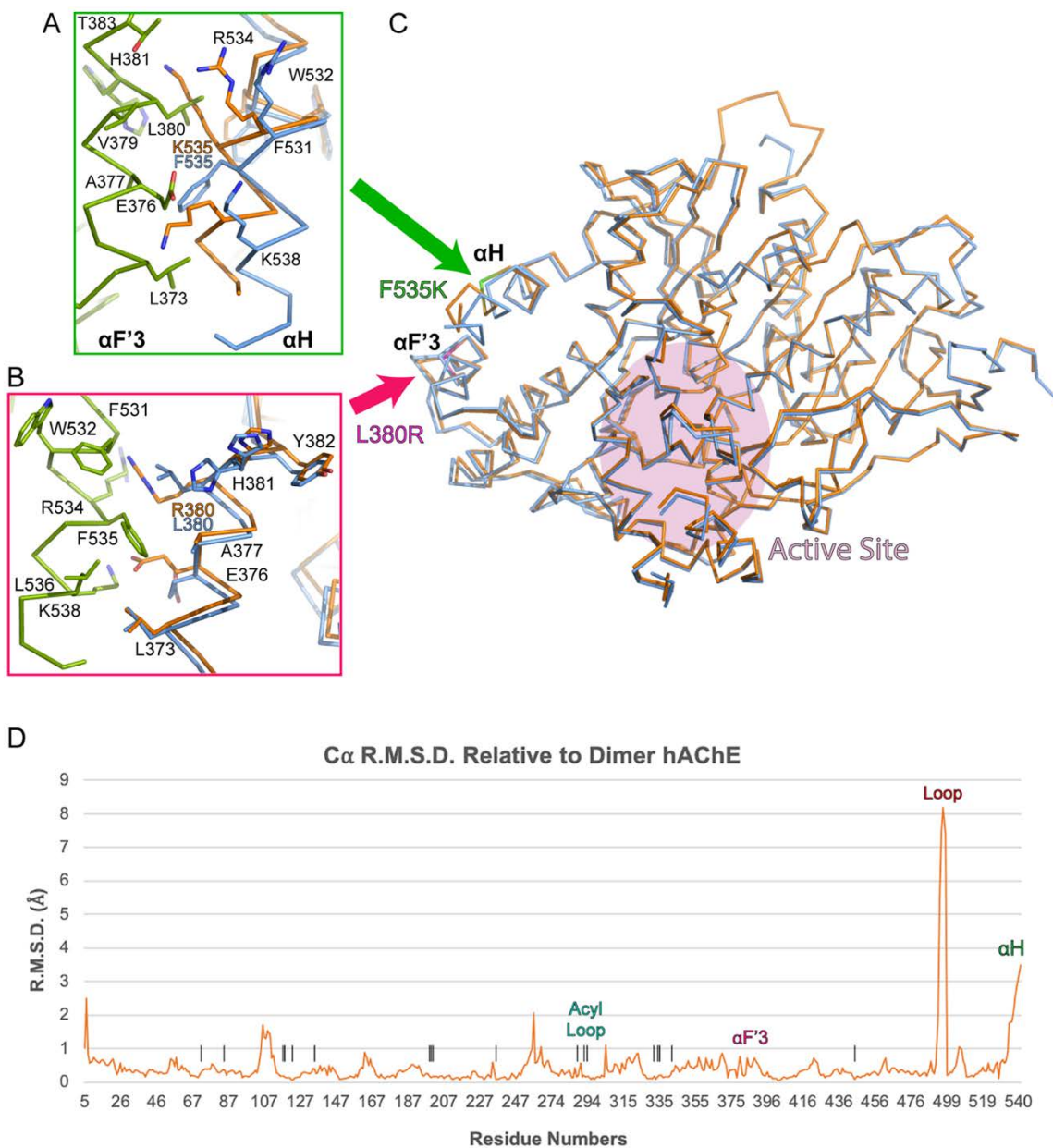


Figure 4.2. Global structural comparison of monomeric hAChE L380R/F535K and dimeric hAChE. A) Structural overlay of monomeric (orange) (PDB 6O69) and dimeric hAChE (PDB 4EY4) (2 subunits: baby blue, green). B/C) Close-up overlays of the two mutation sites on hAChE L380R/F535K compared to the dimer. The colored arrows denote the mutation sites and the rose-colored circle indicates the active site. D) A line graph of the root mean square deviation of monomeric hAChE alpha carbons when measured against dimer hAChE. $\alpha F'3$ denotes the L380R mutated $\alpha F'3$ helix, while αH highlights the F535K mutated αH helix. Loop and Acyl Loop label the 491-499 loop and acyl loop residues, respectively. The black lines emphasize the active site residues.

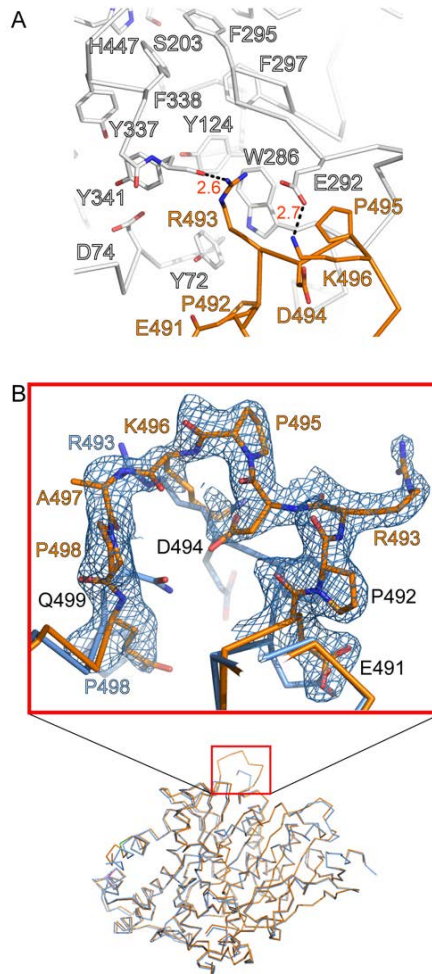


Figure 4.3. Comparison of the 491-499 loop of monomeric hAChE L380R/F535K and dimeric hAChE. View of $2F_o - F_c$ density scaled to 1σ (light blue mesh) for the 491-499 loop of the monomeric (orange) (PDB 6O69), compared to the same loop in dimeric hAChE (baby blue) (PDB 4EY4). The structures are superimposed using least-squares fit of residues 176-232 of each subunit. The black, orange, and blue letters are for labeling both, monomeric, and dimeric residues, respectively.

Outside dimer interface, the presence of a loop at residues 491–499 is the most noticeable structural difference between the structures of the dimer and monomer. This loop in structures of the dimer is rarely complete and usually lacks electron density, implicating structural flexibility (24; 25; 19; 18). As a result, modeling of this region has been sparse. However, in the L380R/F535K structure, residues 492–496, in particular Arg493 and Lys496, form hydrogen bonds via crystal contacts with the acyl loop and peripheral anionic site (PAS) of a neighboring symmetry mate (Figure 4.3A). This

contact appears to have a stabilizing effect on the 491-499 loop reflected in the loop having well-defined electron density throughout revealing at least one confirmation that the loop could adopt (Figure 4.3B).

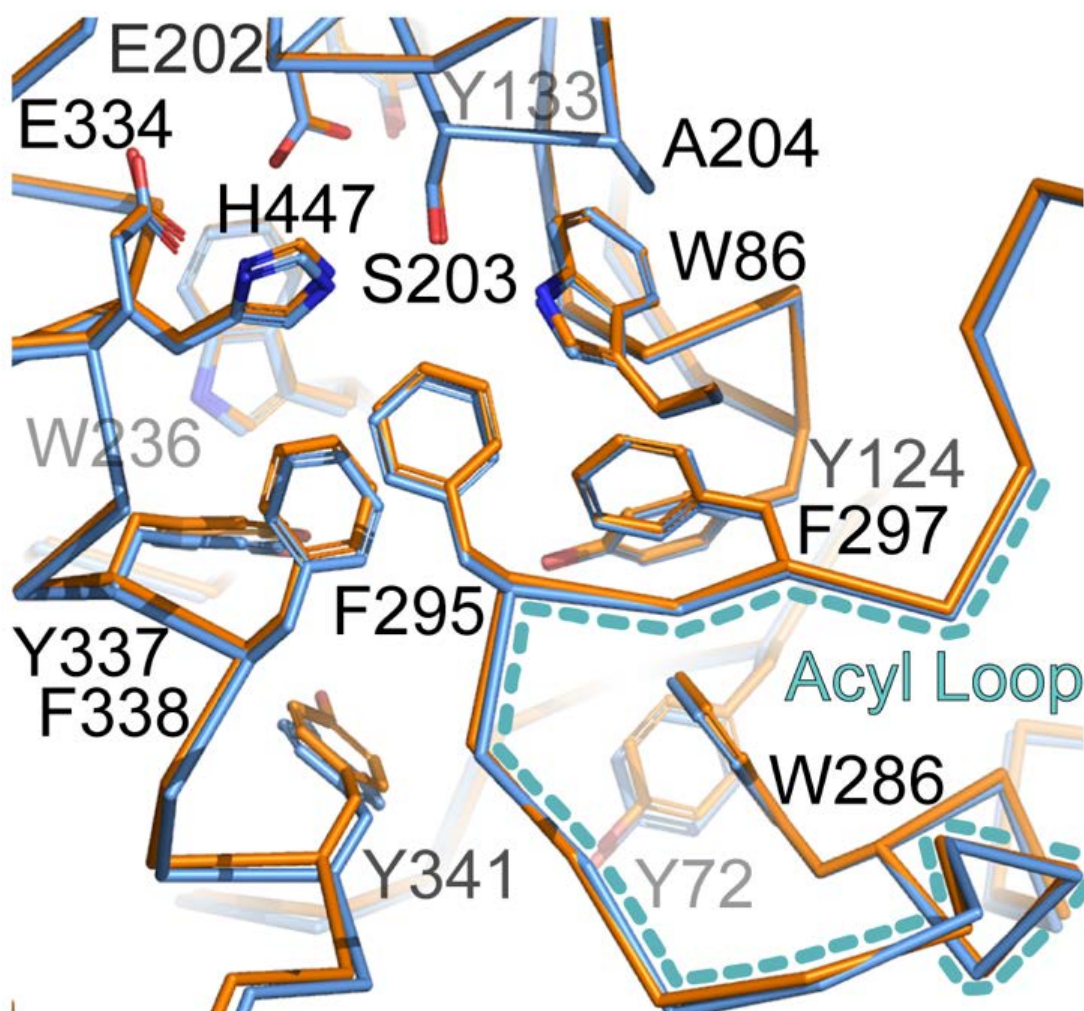


Figure 4.4. Comparison of the active sites and acyl loop of monomeric hAChE L380R/F535K and dimeric hAChE. The structures of monomeric (orange) (PDB 6O69) and dimeric hAChE (baby blue) (PDB 4EY4) are superimposed using least-squares fit of residues 176-232 of each subunit. The hAChE residues are indicated by black letters. The acyl loop is outlined with a teal dashed line and labeled in teal letters.

In contrast to the structural differences located in peripheral regions of the subunit between hAChE and its hAChE L380R/F535K monomer, the core of the enzyme is

highly conserved (Figure 4.2A). This is reflected quantitatively by the root mean square alpha carbon deviation of the monomeric hAChE L380R/F535K relative to hAChE (Figure 4.2D). Closer inspection of the hAChE active sites also supports this assertion (Figure 4.4). Even the position of the highly flexible acyl loop (287–299) within the monomeric hAChE L380R/F535K structure is indistinguishable from that of the wild-type dimer.

Reactivation and Inhibition of monomer hAChE

Recently the plasticity within the active site of hAChE has been implicated in the ability of the enzyme to be inhibited by the nerve agents as well as their rescue by reactivating agents (19; 18). To explore if the flexibility of the active site was overtly impacted by the monomerization of hAChE by the mutations L380R/F535K, the kinetic constants of (P_{R/S})-VX inhibition and subsequent rescue by HI-6 were obtained. The determined dissociation constant, K_d, and unimolecular bonding rate constant, k₂, of hAChE L380R/F535K are slightly different from the values previously recorded for dimeric hAChE, however the yielded bimolecular rate constant, k_i, of 7.9 x 10⁷ M⁻¹ min⁻¹ for (P_{R/S})-VX inhibited hAChE L380R/F535K is consistent with the k_i of dimer hAChE from previous studies (Table 4.3) (18). As the potency of (P_{R/S})-VX appeared consistent for both enzymes, a modified Ellman's assay was utilized to assess the ability of HI-6 to reactivate P_{R/S}-VX inhibited monomeric hAChE L380R/F535K. The k_r of HI-6 for monomer hAChE inhibited by P_{R/S}-VX was revealed to be 0.02 ± 0.01 μM⁻¹ min⁻¹. When compared to previous studies, this fits the general trend observed for HI-6 reactivation of (P_{R/S})-VX inhibited dimer hAChE (15; 17; 18).

Table 4.3. A) Inhibition of hAChE, B) Reactivation of inhibited hAChE by HI-6

A	hAChE	OP	k_2 (min ⁻¹)	K_d (M)	k_i (M ⁻¹ min ⁻¹)	
	Monomer	(P _R /P _S)-VX	2.2×10^{-1}	2.9×10^{-9}	7.9×10^7	
	Dimer ^a	(P _R /P _S)-VX	4.5×10^{-2}	5.9×10^{-10}	7.7×10^7	
B			k_2 (min ⁻¹)	K_{OX} (μM)	k_r (μM ⁻¹ min ⁻¹)	max%
	Monomer	(P _R /P _S)-VX	0.30 ± 0.08	19.9 ± 7.0	0.02 ± 0.01	>100
	Dimer ^a	(P _R /P _S)-VX	0.63 ± 0.04	7.50 ± 2.1	0.08 ± 0.02	>100
	Dimer ^a	(P _S)-VX	0.71 ± 0.06	23.3 ± 8.0	0.03 ± 0.01	92

^a is from (18).

Discussion

Role of Dimerization for hAChE

In nature, AChE has been found in various oligomeric states among animals (6; 27). Given AChE various oligomeric forms, there has been an interest in whether cooperativity exists for this class of enzymes. Binding of AChE ligands, such as fasciculin-2 at peripheral sites has been suggested to induce allosteric intrasubunit effects on the independent catalytic sites (28-30). However, in general there is no evidence for subunit cooperativity in hAChE based on its substrates (30). Although the lack of communication between subunits of hAChE is well documented, information on whether the dimeric interface itself influences the behavior of the enzyme has largely been limited to *in silico* modeling of the molecular dynamics of hAChE related to oligomerization. For example, Gorfe et al. determined that despite steric effects arising from oligomerization of hAChE, enzymatic efficiency between different oligomeric states was maintained, due to favorable electrostatic interactions (31). In our work, the monomerization of hAChE through dimer interface disrupting mutations L380R/F535K allowed an initial glance into biochemical and structural experimentation into this question. As demonstrated, the monomeric hAChE L380R/F535K behaves biochemically similar to that of its dimeric

wild-type form. The similar kinetics, along with the structural similarities of the active site of hAChE L380R/F535K and wild-type hAChE, reinforces the notion that interactions along the dimer interface do not impact the functionality of hAChE appreciably. Thus, the oligomerization of hAChE is likely driven by other biological factors, such as the spatial and temporal demands of specific synapses (27).

Monomer hAChE as a tool in for development of nerve agent therapeutics

As several nations have rushed to develop nerve agents that target hAChE, acetylcholine has not been the only ligand of scientific interest when it comes to this enzyme (32). The hAChE active site did not evolve to process these organophosphate agents that at times appear to be ill-fitting to the active site. Not surprisingly, recent reports have tied the plasticity of the active site, particularly that of the acyl loop, as playing a role in the ability of nerve agents to inhibit the enzyme as well as therapeutic agents salvaging it (19; 18). Although X-ray crystal structures of hAChE have provided insight into the role plasticity can play regarding nerve agents and current therapeutics, the ability to measure the actual flexibility of the active site has been limited. Additionally, the ability to simulate or model the behavior of these compounds including their exit and entry into the active site would be immensely beneficial for the development of new reactivators and other therapeutics. Molecular Dynamic techniques as well as nuclear magnetic resonance (NMR) are potential methods to resolve some of these lingering questions. However, the size of the studied protein can be a major complication with utilizing many of these techniques to the point of being impossible (33). For instance, NMR is an excellent technique for obtaining dynamic information for different regions and domains of a protein including protein flexibility. However, it is

generally extremely challenging for proteins exceeding 70 kDa unless the system being studied has unique properties (34; 35). Additionally, larger macromolecules can affect root-mean-square deviation (RMSD) of structures or atomic coordinates, a measure of similarity that is often used to analyze MD trajectories, modeling, and docking (36-39). MD simulations run on larger macromolecules can result in the RMSD losing the ability to discriminate conformation differences between structures and dynamics (33).

As the subunit molecular weight of this recombinant hAChE is ~60 kDa, dimeric and tetrameric forms of hAChE pose problems for these NMR or MD simulation approaches. The monomerizing of hAChE through selective mutagenesis at L380R/F535K appears to offer a new way around these size constraints. Not only is the hAChE L380R/F535K active site structurally indistinguishable from that of wild-type, but it mirrors the wild-type hAChE performance in regard to acetylcholine. Even for large nerve agents such as VX and reactivating agents like HI-6 that require additional plasticity of the active site, hAChE L380R/F535K reacts similarly to wild-type hAChE. Thus, the monomer hAChE L380R/F535K could be used as a stand in for the dimer, or even a hAChE tetramer in NMR and MD studies. This would facilitate experimentally probing the ability of the hAChE active site to accommodate future nerve agent threats like those of A-series agents or judge the ability of new therapeutics *in silico* to access the active site to counter them.

Material and Methods

Materials

BSA was purchased from VWR International (Radnor, PA), while acetylthiocholine iodide (ATCI), sodium citrate, sodium chloride, potassium chloride,

sodium carbonate, monosodium phosphate, and disodium phosphate were purchased from Sigma-Aldrich (St. Louis, MO). Hexanes, 5,5'-dithio-bis-[2-nitrobenzoic acid] (DTNB), and isopropyl alcohol were purchased from Thermo Fisher Scientific (Waltham, MA). Laboratory deionized water $> 17 \text{ M}\Omega$ was used for all assays.

Cloning, Expression, and Purification of hAChE

GeneArt Site-Directed Mutagenesis System (ThermoFisher Scientific) was used to introduce site-directed amino acid substitutions of L380R/F535K into the hAChE sequence of the pJTI Fast Dest hAChE vector using PCR-based methods (24). Cloning, expression, and purification of mutant and dimer hAChE were adapted from a previous study (24) by inserting the octahistidine (His8)-tag followed by ENLYFQ after residue 32 at the N-terminus to form a complete ENLYFQG TEV protease site with G33 of the native hAChE sequence and transfecting the recombinant hAChE mutant amino acid sequence 1-574 (pre-processed protein numbering which includes the native secretion signal) encoded construct into Freestyle 293-F Cells (ThermoFisher Scientific). Purified protein was dialyzed into storage buffer (10 mM HEPES, pH 7.0, and 10 mM NaCl) overnight and then concentrated to desired concentrations.

Sedimentation Velocity

Monomer hAChE (11 μM) was dialyzed into 50 mM HEPES pH 7.5 and 150 mM KCl) and loaded into an equilibrated cell equipped with 12 mm double-sector Epon centerpieces and quartz windows. Sedimentation velocity data were collected in an Optima XLA analytical ultracentrifuge at 50,000 rpm for 8 hrs. SEDNTERP (40) was used to estimate the partial specific volume of monomer AChE (0.73248 mL/g), and the density (1.00726 g/mL) and viscosity (0.01018 P) of the buffer. Data were modeled as a

continuous sedimentation coefficient ($c(s)$) distribution using SEDFIT (41). The following parameters were fit during data modeling: baseline, meniscus, frictional coefficient, and systematic time-invariant and radial-invariant noise (42). The fit data had a root-mean-square deviation (rmsd) of 0.006579 AU. Dimeric hAChE (10 μ M) was diluted with 10mM HEPES, 10mM NaCl at pH 7.4 to 1 μ M. The sedimentation velocity experiment was run at 20°C in a Beckman XL-I Analytical Ultracentrifuge using an An60Ti rotor. HYDROPRO(43) was used to predict the s -values of both monomeric and dimeric hAChE based on atomic coordinates (PDB: 6O69; PDB 4EY4).

Enzymatic Characterization of Monomer & Dimer hAChE

Equivalent concentrations of purified dimer and monomer AChE subunits were added to a 96-well plate and used in a modified Ellman's assay (final volume: 250 μ l) at 25°C. Each well contained a final concentration of 0.1M phosphate buffer (PB) pH 8.0 with 0.1 mg/mL BSA pH 8.0, 0.3mM DTNB and increasing amounts of acetylthiocholine iodide (0 – 1.5 mM) that was added immediately before analysis. The assay plate was read in a PHERAstar FS (BMG Labtech) at absorbance 412 nm with path length correction on, every 20 secs for 20 mins. K_m , V_{max} , and k_{cat} values were determined using the equation $V_{max} = k_{cat} * [E_t]$, where E_t is the total enzyme concentration (M), as determined using quantitative amino acid analyses (QAAA; Bio-Synthesis, Inc.). Data was plotted using GraphPad Prism.

X-ray structure determination of human acetylcholinesterase mutant L380R/F535K

The hAChE L380R/F535K (16 mg/ml) was screened against eight Qiagen NeXtal suites in hanging drop format with a TTP LabTech Mosquito (TTP Labtech, Herfordshire, UK). The final crystals were obtained by hanging drop vapor diffusion at

22 °C against 500 μ L of crystallization buffer. Crystals were subsequently placed in crystallization buffer with 20% of a 1:1:1 solution of ethylene glycol, dimethyl sulfoxide, and glycerol (EDG) (44) as a cryoprotectant before being mounted onto liquid nitrogen flash-cooled nylon loops. A data set was collected for monomer AChE with a resolution of 2.09 Å on the 22ID beamline of SERCAT at a wavelength of 1 Å at the Advanced Photon Source, Argonne National Laboratory using a monochromic X-ray beam with a Dectris Eiger 16M detector PIXEL detector. The data collection, reduction, and refinement occurred as previously described (18). To verify the structure's quality, the final model was analyzed via Molprobit. The data collection and refinement statistics for the structure is in Table 4.2.

Measurement of inhibition and reactivation rate constants

All procedures in regard to measurement of inhibition and reactivation rate constants of L380R/F535K (monomer) hAChE were adapted from a previous study (18). To determine the inhibition rate constants, modified Ellman's assays were run with a quantity of hAChE, equivalent to 3–4 U/mL of activity, varying concentrations of (P_{RS})-VX (0.38, 0.34, 0.25, 0.17, 0.12, and 0 μ M), DTNB (0.3 mM), and ATC (acetylthiocholine) (1 mM) (final volume: 250 μ L). The method used to calculate inhibition rate constants was a continuous method (45). The procedures and calculations utilized to determine the reactivation rate constants of hAChE L380R/F535K were modified from a previous study where k_2 is the intrinsic reaction constant; K_{OX} is the apparent equilibrium constant; and k_r is the second-order reactivation rate constant (18). Reactivation of inhibited hAChE was established by adding the reactivator, HI-6, (1250,

312.5, 187.5, 18.75, 1.875 μ M, final concentration) to inhibited hAChE followed by DTNB and ATC. The activity was measured at 30 s, 1, 2, 3, 4, 5, and 30 min.

References

1. Eddleston M (2000) Patterns and problems of deliberate self-poisoning in the developing world. *QJM* 93:715-731.
2. Bon S, Massoulie J (1976) An active monomeric form of *Electrophorus electricus* acetylcholinesterase. *FEBS Lett* 67:99-103.
3. Gordon MA, Carpenter DE, Wilson IB (1978) The turnover numbers of acetylcholinesterase forms. *Mol Pharmacol* 14:266-270.
4. Vigny M, Bon S, Massoulie J, Leterrier F (1978) Active-site catalytic efficiency of acetylcholinesterase molecular forms in *Electrophorus*, torpedo, rat and chicken. *Eur J Biochem* 85:317-323.
5. Barnett P, Rosenberry TL (1979) Functional identity of catalytic subunits of acetylcholinesterase. *Biochim Biophys Acta* 567:154-160.
6. Massoulie J, Bon S (1982) The Molecular-Forms of Cholinesterase and Acetylcholinesterase in Vertebrates. *Annu Rev Neurosci* 5:57-106.
7. Kingsley P, Barnard A. Banned Nerve Agent Sarin Used in Syria Chemical Attack, Turkey Says. (2017) *The New York Times*.
8. Paddock R, Sang-Hun C, Wade N. In Kim Jong-nam's Death, North Korea Lets Loose a Weapon of Mass Destruction. (2017) *The New York Times*.
9. Barry E, Yeginsu C. The Nerve Agent Too Deadly to Use, Until Someone Did. (2018) *The New York Times*.
10. Buckley NA, Roberts D, Eddleston M (2004) Overcoming apathy in research on organophosphate poisoning. *BMJ* 329:1231-1233.
11. Hobbiger F (1957) Reactivation of phosphorylated acetylcholinesterase by pyridine-2-aldoxime methiodide. *Biochim Biophys Acta* 25:652-654.
12. Simeon V, Skrinjaric-Spoljar M, Wilhelm K (1973) Reactivation of phosphorylated cholinesterases in vitro and protecting effects in vivo of some pyridinium and quinolinium oximes. *Arh Hig Rada Toksikol* 24:11-18.
13. Sun M, Chang Z, Shau M, Huang R, Chou T (1979) The mechanism of ageing of phosphonylated acetylcholinesterase. *Eur J Biochem* 100:527-530.

14. Worek F, Reiter G, Eyer P, Szinicz L (2002) Reactivation kinetics of acetylcholinesterase from different species inhibited by highly toxic organophosphates. *Arch Toxicol* 76:523-529.
15. Worek F, Thiermann H, Szinicz L, Eyer P (2004) Kinetic analysis of interactions between human acetylcholinesterase, structurally different organophosphorus compounds and oximes. *Biochem Pharmacol* 68:2237-2248.
16. Maxwell DM, Koplovitz I, Worek F, Sweeney RE (2008) A structure-activity analysis of the variation in oxime efficacy against nerve agents. *Toxicol Appl Pharmacol* 231:157-164.
17. Reiter G, Muller S, Hill I, Weatherby K, Thiermann H, Worek F, Mikler J (2015) In vitro and in vivo toxicological studies of V nerve agents: molecular and stereoselective aspects. *Toxicol Lett* 232:438-448.
18. Bester SM, Guelta MA, Cheung J, Winemiller MD, Bae SY, Myslinski J, Pegan SD, Height JJ (2018) Structural insights of stereospecific inhibition of human acetylcholinesterase by VX and subsequent reactivation by HI-6. *Chem Res Toxicol*.
19. Franklin MC, Rudolph MJ, Ginter C, Cassidy MS, Cheung J (2016) Structures of paraoxon-inhibited human acetylcholinesterase reveal perturbations of the acyl loop and the dimer interface. *Proteins* 84:1246-1256.
20. Quinn DM (1987) Acetylcholinesterase - Enzyme Structure, Reaction Dynamics, and Virtual Transition-States. *Chem Rev* 87:955-979.
21. Hsieh JY, Chen SH, Hung HC (2009) Functional roles of the tetramer organization of malic enzyme. *J Biol Chem* 284:18096-18105.
22. Shafferman A, Velan B, Ordentlich A, Kronman C, Grosfeld H, Leitner M, Flashner Y, Cohen S, Barak D, Ariel N (1992) Substrate inhibition of acetylcholinesterase: residues affecting signal transduction from the surface to the catalytic center. *EMBO J* 11:3561-3568.
23. Masson P, Schopfer LM, Bartels CF, Froment MT, Ribes F, Nachon F, Lockridge O (2002) Substrate activation in acetylcholinesterase induced by low pH or mutation in the pi-cation subsite. *Biochim Biophys Acta* 1594:313-324.
24. Cheung J, Rudolph MJ, Burshteyn F, Cassidy MS, Gary EN, Love J, Franklin MC, Height JJ (2012) Structures of human acetylcholinesterase in complex with pharmacologically important ligands. *J Med Chem* 55:10282-10286.
25. Allgardsson A, Berg L, Akfur C, Hornberg A, Worek F, Linusson A, Ekstrom FJ (2016) Structure of a prereaction complex between the nerve agent sarin, its biological target acetylcholinesterase, and the antidote HI-6. *Proc Natl Acad Sci U S A* 113:5514-5519.

26. Sussman JL, Harel M, Frolow F, Oefner C, Goldman A, Toker L, Silman I (1991) Atomic structure of acetylcholinesterase from *Torpedo californica*: a prototypic acetylcholine-binding protein. *Science* 253:872-879.
27. Massoulié J, Pezzementi L, Bon S, Krejci E, Vallette FM (1993) Molecular and cellular biology of cholinesterases. *Prog Neurobiol* 41:31-91.
28. Radic Z, Quinn DM, Vellom DC, Camp S, Taylor P (1995) Allosteric control of acetylcholinesterase catalysis by fasciculin. *J Biol Chem* 270:20391-20399.
29. Johnson G, Moore SW (2006) The Peripheral Anionic Site of Acetylcholinesterase: Structure, Functions and Potential Role in Rational Drug Design. *Current Pharmaceutical Design* 12:217-225.
30. Meister A. 2009. *Advances in Enzymology and Related Areas of Molecular Biology*, Wiley.
31. Gorfe AA, Lu B, Yu Z, McCammon JA (2009) Enzymatic activity versus structural dynamics: the case of acetylcholinesterase tetramer. *Biophys J* 97:897-905.
32. Newmark J. CHAPTER 56 - Nerve Agents. In: Dobbs MR, Ed. (2009) *Clinical Neurotoxicology*. W.B. Saunders, Philadelphia, pp. 646-659.
33. Sargsyan K, Grauffel C, Lim C (2017) How Molecular Size Impacts RMSD Applications in Molecular Dynamics Simulations. *J Chem Theory Comput* 13:1518-1524.
34. Berjanskii M, Wishart DS (2006) NMR: prediction of protein flexibility. *Nat Protoc* 1:683-688.
35. Kristensen SM, Kasimova MR, Led JJ. The Use of NMR in the Studies of Highly Flexible States of Proteins: Relation to Protein Function and Stability. In: Webb GA, Ed. (2006) *Modern Magnetic Resonance*. Springer Netherlands, Dordrecht, pp. 1369-1376.
36. Shoichet BK, Kuntz ID (1991) Protein docking and complementarity. *J Mol Biol* 221:327-346.
37. Kozakov D, Clodfelter KH, Vajda S, Camacho CJ (2005) Optimal clustering for detecting near-native conformations in protein docking. *Biophys J* 89:867-875.
38. Mukherjee S, Balius TE, Rizzo RC (2010) Docking validation resources: protein family and ligand flexibility experiments. *J Chem Inf Model* 50:1986-2000.
39. Schuetz DA, Bernetti M, Bertazzo M, Musil D, Eggenweiler HM, Recanatini M, Masetti M, Ecker GF, Cavalli A (2019) Predicting Residence Time and Drug Unbinding Pathway through Scaled Molecular Dynamics. *J Chem Inf Model* 59:535-549.

40. Laue TM, Shah BD, Ridgeway TM, Pelletier SL. 1992. Analytical Ultracentrifugation, The Royal Society of Chemistry, Cambridge.
41. Schuck P (2000) Size-distribution analysis of macromolecules by sedimentation velocity ultracentrifugation and lamm equation modeling. *Biophys J* 78:1606-1619.
42. - (2003) On the analysis of protein self-association by sedimentation velocity analytical ultracentrifugation. *Anal Biochem* 320:104-124.
43. Ortega A, Amoros D, Garcia de la Torre J (2011) Prediction of hydrodynamic and other solution properties of rigid proteins from atomic- and residue-level models. *Biophys J* 101:892-898.
44. Sanchez JE, Gross PG, Goetze RW, Walsh RM, Peeples WB, Wood ZA (2015) Evidence of Kinetic Cooperativity in Dimeric Ketopantoate Reductase from *Staphylococcus aureus*. *Biochemistry* 54:3360-3369.
45. Forsberg A, Puu G (1984) Kinetics for the inhibition of acetylcholinesterase from the electric eel by some organophosphates and carbamates. *Eur J Biochem* 140:153-156.

CHAPTER 5

DISCUSSION

AChE's stereoselectivity for OP nerve agents

Despite the more commonplace usage of racemic nerve agents mixtures in kinetic assessments, hAChE's stereoselectivity for OP nerve agents has been demonstrated through the measured toxicity of enantiomers of both G- and V-series agents^{99, 122, 123}. A kinetic assessment run in a previous study with human erythrocyte ghosts found that the ScSP enantiomer of GD, which has two chiral centers, is the most toxic of its enantiomers¹²². The toxicity of P_{R/S}-VX (racemic mixture), P_S-VX (P_S enantiomer), and P_R-VX (P_R enantiomer) towards purified hAChE was calculated and the relationship between P_{R/S}-VX and the two enantiomers was consistent with previous studies^{99, 123}. Expectedly, the P_S enantiomer of VX exhibited the highest toxicity with a similar inhibition rate demonstrated by the racemic mixture (2-fold difference) and the P_R enantiomer had significantly lower potency. Crystal structures of hAChE inhibited with either a racemic mixture of VX or A-232 displayed strong electron density fitting the same conformation as their P_S enantiomers, suggesting the enzyme has a strong preference for the P_S enantiomer over the P_R enantiomer. While VX has small side chains, methyl and ethoxy groups, extending off the organophosphonate core, Novichok agents are known for having one significantly larger side chain, *N,N*-diethylmethanimidamide, as compared to those of other OP nerve agents¹⁴. When examining the hAChE active site inhibited by racemic A-232 and P_S A-232, the larger side chain was fit into the larger

hydrophobic pocket quite snugly, which provides some insight into the underlying reason for hAChE's P_S stereoisomer preference. Based on the positioning of the oxyanion hole, the P_R enantiomer of A-232 as well as other A-series agents, would only differ from the P_S enantiomer by the reversal of the S_{Small} and S_{Large} group positions. This conformation would involve the P_R stereoisomer enantiomers positioning their smaller side chains into the larger hydrophobic pocket and the *N,N*-diethylmethanimidamide side chain into the smaller hydrophobic pocket. The smaller hydrophobic pocket also has a more limited steric volume than the large hydrophobic pocket. Taken together, this emphasizes that a larger moiety, such as the A-series agents' *N,N*-diethylmethanimidamide group, would not be accommodated well into the smaller hydrophobic pocket. hAChE's preference for the P_S enantiomer of VX, A-232, and likely other A-series agents could be in part due to their similarity to ACh's placement within the active site and the formation of similar bonds and interactions.

Additionally, the P_S enantiomer for VX had the highest toxicity of those assessed, which indicates that there is a potential link between the toxicity of an agent and hAChE's preference towards it. The recognition of this potential association could aid in identifying the most toxic enantiomer of every OP nerve agent and pesticide currently developed. This would be especially beneficial for nerve agents with more than one chiral center such as GD. In order to test the inhibitory ability of every enantiomer of every nerve agent being tested, each compound's enantiomers would first have to be individually synthesized and separated from any other enantiomers formed in the process, which is an immensely difficult and laborious process. Therefore rather than synthesize and calculate the inhibitory ability of each enantiomer individually, one could simply

soak hAChE crystals in a racemic mixture and then identify which of the enantiomers best fits the subsequent electron density. In general, if this assertion is true, then the preferred enantiomer can be treated as the most toxic without running activity assays on every enantiomer.

Most importantly, identifying the most toxic enantiomer of each nerve agent would allow for more preparedness with available treatments. Frequently nerve agent exposure is to a racemic mixture rather than a pure enantiomer, which can be problematic if the enantiomer hAChE is stereoselective for is uncertain. Oxime reactivators are known to be influenced by the stereochemistry of bound OP nerve agents. Thus, being able to predict in advance which nerve agent enantiomer will be the most prevalent allows for the selection of the oxime reactivator with the greatest potency towards it.

Influence of the small hydrophobic pocket upon potency

In addition to playing a role in the preference of hAChE for the P_S enantiomers of VX and A-232, the small hydrophobic pocket also referred to as the acyl binding pocket could influence potency differences between OP nerve agents, including the A-series agents and VX. When examining the A-series agents, the major difference between the three A-series agents is their smaller side chain which is either a methyl (A-230), methoxy (A-232), or ethoxy (A-234) group. Upon examining the structures of hAChE-inhibited by A-232, A-234, and A-230, small shifts within the smaller hydrophobic pocket of hAChE occur to accommodate their different small side chains. A similar trend was noticed when comparing the structures of P_S-VX and P_R-VX inhibited hAChE, there was a noticeable shift in Phe295, Arg296, and Phe297 and other members of the acyl loop in order to accommodate the ethoxy group of P_R-VX into the smaller hydrophobic

pocket. The energy cost of this shift seemed to be reflected in the significantly lower potency of P_R-VX compared to P_{R/S}-VX and P_S-VX. A recent study noticed an even more dramatic acyl loop shift when accommodating a side chain group into the smaller hydrophobic pocket ¹¹⁵, suggesting that this hydrophobic pocket might routinely influence potency through Van der Waals interactions or shifting to fit less easily accommodated groups. Based on these observations as well as previous studies the acyl loop seems to have some flexibility, however the extent of this flexibility has yet to truly be investigated ^{45, 115, 120}. Moreover, it seems that the larger the shift necessary for accommodation, the greater the loss of potency towards hAChE. Based on these assertions, a prediction can be made that A-232 likely has a higher potency for hAChE than A-234. The structure of A-232-inhibited hAChE only has a shift in Phe295, while a shift in Phe295 and Trp236 was observed in the structure of A-234-inhibited hAChE (Figure 3.3c). This does assume that the additional binding energy gained through A-234's ethoxy group's increased Van der Waal interactions would not offset the energy required to displace both hAChE residues, Phe295 and Trp236. On the other hand, no noticeable shifts of small pocket residues of A-230-inhibited hAChE occur, which suggests that A-230 could have the highest potency of the three A-series agents. Nonetheless, A-232 could have greater potency than A-230 as well despite the shifting of Phe295 due to stronger van der Waals interactions which would be supported by the closer proximity of A-232's methoxy to the small pocket residues than A-230's methyl. Based on the structural data, predictions can be made about the A-series agents' potency towards hAChE due to the shifting of the small pocket residues. Additionally, shifts in acyl loop residues or perturbations in the acyl loop observed within a structure would

immediately be suggestive of a reduced potency towards hAChE for that inhibitor. Overall, recognition of this relationship between potency and the smaller hydrophobic pocket could be useful in the future for predicting the potency of unknown and experimental nerve agents.

Recognition of structural features involved in reactivation

The efficacy of reactivators is known to vary based on the OP nerve agent or pesticide bound to the catalytic serine as well as other factors. Based on the pre- and post-activation structures of VX-inhibited hAChE, a scheme for OP nerve agent and pesticide reactivation by HI-6 and other reactivators was theorized. In this mechanism, the hydrogen bond interactions made by the nerve agent moiety including the oxyanion hole draw electrons away from the phosphorus atom, which likely makes it more electropositive and more suitable for nucleophilic attack by the reactivator. The additional hydrogen bond formed by P_S-VX with His447 that P_R-VX is improperly oriented to form likely contributes to the electropositivity of its phosphorus atom and might play a minor role in the greater potency of HI-6 towards P_S-VX. While the exact reactivation potency of reactivators for the A-series agents are not known, there is enough structural evidence and similarity to other inhibitors to suggest that current reactivators would have limited effectiveness towards them. However, the presence of two nitrogen atoms on the N,N-diethylmethanimidamide side chain of the A-series agents could reduce the electropositivity of the phosphorus, making the atom less suitable for nucleophilic attack by an oxime reactivator. The nitrogen atoms could also draw the nucleophilic oxime away from the phosphorus acting as a trap. An example of this is potentially seen in GA, which also has a nitrogen atom on its side chain. As most current reactivators

have little to no success in reactivating this nerve agent, it is possible that the nitrogen atom might in part interfere with reactivation.

Despite the large size of the N,N-diethylmethanimidamide sidechain, HI-6 was accommodated into the active site. HI-6 is accommodated by the A-series-inhibited hAChE in a manner comparable to reactivators in other inhibited hAChE structures. In particular, the acetamide containing pyridinium ring of HI-6 interacts with the PAS binding site, which is similar to other HI-6 structures including P_{R/S}-VX-inhibited hAChE in complex with HI-6 (PDB 6CQW).

Overlaying hAChE-VX-HI-6 complex with hAChE inhibited by A-series agents in complex with HI-6, provided insight into how different bound nerve agents are able to influence the conformation of HI-6, and thus reactivation. The structures of hAChE-A-232-HI-6 and hAChE-A-230-HI-6 structures had HI-6 in virtually the same conformation, suggesting that their smaller side chains do not have a strong influence on the reactivator. A comparison of hAChE-A-234-HI-6 and hAChE-VX-HI-6 complex revealed that the larger alkyl side chain of A-234 causes Tyr337 to shift for better Van der Waals interactions, however this shift also blocks HI-6 from entering further into the active site. This shift prevents the HI-6 of hAChE-A-234-HI-6 complex from adopting the same conformation as seen in the hAChE-VX-HI-6 complex as well. Additionally, the ethoxy group on A-234 does cause a minor shift in Phe295, which did not occur in the other two structures of A-series agents inhibited-hAChE in complex with HI-6. This suggests Phe295 and the rest of the small hydrophobic pocket might play a role in the differences between their conformations of HI-6 as well as OP nerve agent and pesticide potency. Overall, HI-6 has been shown to form many non-productive poses, which are

often influenced by the bound ligand or the stereochemistry of the bound ligand. These non-productive poses can reduce the efficacy of the reactivator, thus designing reactivators that form fewer non-productive poses would increase effectiveness and lower therapeutic doses no matter the bound nerve agent.

These A-series-inhibited hAChE structures in complex with HI-6 highlighted some obstacles for HI-6 and potentially other reactivators. However, HI-6 was not precluded from entering the active site gorge and was able to form bonds with the PAS despite the bulky alkyl side chain of A-series agents. HI-6's acetamide containing pyridinium ring was stabilized by π - π stacking interactions at the PAS in all three A-series-inhibited hAChE structures as well as P_{R/S}-VX-inhibited hAChE in complex with HI-6. These interactions have been suggested to hold HI-6 and other dual ringed reactivators within a certain distance of the inhibited serine^{92, 94, 115, 119}. This suggests that utilizing a similar approach is still a viable option to include in the development of agents optimized for A-series agents. The A-series agents have a chemical structure that is unique compared to the other two classes of agents, thus this class might warrant specialized reactivators. By visualizing HI-6 in complex with these and other agents, this elucidates the non-productive poses HI-6 and other dual-ringed reactivators can take, and provides a first step towards optimizing HI-6 analogues for A-series agent exposure. Modification to lengthen the middle linker region between the rings, changing the size of the pyridinium rings, lengthening the oxime arm, or adding additional oxime arms are all possible tactics for reactivator improvement. However, the realization that A-series agents behave biochemically very similarly to G- and V-series agents including their

stereospecificity^{122, 123} serves to bring these agents out in the open and remove the smoke and mirrors obscuring them.

Future Directions

Due to some of the limitations of oxime reactivators, novel and improved therapeutic agents are still highly sought. The development of novel reactivators including those specialized for A-series agents would benefit from molecular dynamics (MD) studies including modeling and ligand docking. As most MD simulations and NMR (nuclear magnetic resonance) becomes more complex the larger the macromolecule, the molecular weight of hAChE (60 kDa per monomer subunit) would have until recently prevented using these techniques¹²⁴⁻¹²⁷. The monomerization of hAChE through selective mutagenesis at L380R/F535K appears to create a way around these size constraints. hAChE L380R/F535K was determined to have comparable activity to the dimeric form as well as structural similarity. hAChE L380R/F535K was also found to react similarly to wild-type hAChE with the nerve agents like VX and reactivating agents like HI-6 that need additional plasticity of the active site. Therefore, hAChE L380R/F535K could be utilized as a stand-in for the dimeric form of hAChE in NMR and MD studies.

Utilizing MD studies to simulate and model the behavior of current reactivators could further elucidate the mechanism of reactivation. Additionally, the ability to simulate or model the behavior of these compounds including their exit and entry into the active site would be immensely beneficial for the development of new reactivators and other therapeutics. In particular, specialized therapeutic agents designed to combat A-series agents could be developed by modifying the scaffold of HI-6 and then assessed *in*

in silico for their ability to access the active site and remove phosphonyl moieties. This would allow a large array of compounds to have an initial assessment before time and resources are wasted evaluating them. Overall, this would facilitate experimentally probing the ability of the hAChE active site to accommodate future nerve agent threats like those of A-series agents or judge the ability of new therapeutics *in silico* to access the active site to counter them.

The active site of hAChE tends to have to accommodate different ill-fitting OP nerve agents and pesticides as well as other inhibitors that are not its intended substrate¹²⁸. A recent report suggest that the plasticity of hAChE's active site, in particular the acyl loop, plays a major role in the accommodation of nerve agents and therapeutic compounds in the active site¹¹⁵. Crystal structures of hAChE inhibited by the enantiomers of VXs supported the previous report and helped to further elucidate the role of plasticity regarding inhibition by nerve agents and their removal with current therapeutics. However, the ability to measure the actual flexibility of the active site has been limited. To further elucidate the flexibility of the acyl loop as well as the active site, NMR can be utilized. The monomerized hAChE L380R/F535K would be a prime candidate for NMR to obtain active site dynamic information. However even monomerized the size of hAChE could still be challenging for NMR, thus dual-amino acid selective labeling could also be utilized to examine the flexibility of key active site and acyl loop residues. This technique is especially favorable for higher molecular weight macromolecules as it allows for the selective detection of NMR resonances of specific amino acid residue(s), which significantly reduces spectral complexity^{129, 130}. The level of flexibility of the active site and acyl loop directly influence inhibition of hAChE as well

as subsequent reactivation and this invaluable information could be used in designing new inhibitors and novel therapeutic agents.

Although AChE appears in a wide range of species and the active site residues of AChE tend to remain fairly conserved across species ^{42, 105}, different species of AChE are known to have great variation in inhibitory rates and reactivator potency ¹⁰⁵. As the second shell residues are less conserved and just outside the active site, they could influence the flexibility of the active site residues in AChE. By performing site-directed mutagenesis on hAChE, tAChE, and mAChE to mirror specific non-conserved second shell residues within the other two species, the impact of these residues on the active site and acyl loop including their flexibility can be evaluated through structural and biochemical determination. To investigate the influence of these residues on the accommodation of OP nerve agents in the active site, a structural comparison of the mutated AChE species inhibited by an OP nerve agent, such as VX can be performed. Additionally, modified Ellman's assay can be utilized to examine these residues influence on inhibitor binding and reactivator potency by comparing the inhibitory rate and reactivation rate of all three wild-type hAChE species with each mutated species of hAChE. Exploring these species-species differences may illuminate key residues in the second shell for active site flexibility, provide insight into the species specific active site flexibilities, and potentially explain the differences in OP nerve agent toxicity and reactivator potency between AChE species ^{100, 101}.

When comparing overlays of VX-inhibited mAChE (PDB 2Y2U), tAChE (PDB 1VXR), and hAChE (PDB 6CQT), four residues in particular stood out as potential mutation sites. As the only non-conserved acyl loop residues between the three species,

residues at hAChE position 294 and 291 stood out as potential mutation sites (Figure 2.6). Residue 294 is Phe in tAChE and Gln in both mAChE and hAChE, while residue 291 is Val in hAChE and Ile in the other two species. Due to their interaction with the acyl loop, particularly residues 291 and 294, two additional non-conserved residues at (hAChE) position 369 and 365 stood out in the structural comparison as potential key second shell residues. Residue 369 is His in tAChE and Gln in the other two species, while residue 365 is a different hydrophobic residue in all three species: Val – hAChE, Ile – mAChE, and Leu – tAChE. To garner additional information on the influence of the acyl loop and second shell residues on active site flexibility, double mutations of the interacting pairs of residues at positions 291/369 and 294/365, could be assessed. However, other mutations could be performed based on further comparisons and analyses of the flexibility of each species.

To further elucidate the flexibility of the active site and acyl loop through MD simulations and NMR, hAChE was successfully monomerized through dimer interface mutations. Due to this prior success, it is conceivable that other species of AChE could be monomerized as well, such as mAChE or tAChE. This could be accomplished by introducing specific mutations that will disrupt their dimer interfaces. After a thorough structural and biochemical assessment to ensure monomerized AChE and wild-type are comparable, NMR and MD simulations could be employed to assess the active site flexibility of each species of hAChE individually as well as study the differences between the species. With this additional information, more residues vital to the flexibility of the active site and acyl loop can be discerned and further studied. The flexibility of the active site and acyl loop of AChE appears vital for not only the accommodation of OP nerve

agents, but also for the reactivators salvaging it. Thus, an increased understanding of active site flexibility among many species of AChE can only benefit the development of better therapeutic agents and fill gaps in knowledge on nerve agent accommodation.

REFERENCES

1. Taylor, P., Anticholinesterase Agents. In *Goodman & Gilman's: The Pharmacological Basis of Therapeutics, 12e*, Brunton, L. L.; Chabner, B. A.; Knollmann, B. C., Eds. McGraw-Hill Education: New York, NY, 2015.
2. Holmstedt, B., Structure-Activity Relationships of the Organophosphorus Anticholinesterase Agents. In *Cholinesterases and Anticholinesterase Agents*, Koelle, G. B., Ed. Springer Berlin Heidelberg: Berlin, Heidelberg, 1963; pp 428-485.
3. Brabin, B. J. J. M. J., Malaria's contribution to World War One – the unexpected adversary. **2014**, *13* (1), 497.
4. Anstead, G. M., The centenary of the discovery of trench fever, an emerging infectious disease of World War 1. *The Lancet Infectious Diseases* **2016**, *16* (8), e164-e172.
5. Robinson, J., The Rise of CB Weapons. In *The problem of Chemical and Biological Warfare*, Humanities Press: New York, 1971; Vol. 1, pp 72-87.
6. Schrader, G., Insecticide Phosphoric Esters. *Angew Chem Int Edit* **1957**, *69* (3), 86-90.
7. Antonijevic, B.; Stojiljkovic, M. P., Unequal Efficacy of Pyridinium Oximes in Acute Organophosphate Poisoning. *Clin Med Res* **2007**, *5* (1), 71-82.
8. Gunderson, C. H.; Lehmann, C. R.; Sidell, F. R.; Jabbari, B., Nerve agents: a review. *Neurology* **1992**, *42* (5), 946-50.
9. Vašafhelyi, G.; Földi, L., History of Russia's chemical weapons. *Academic and Applied Research in Military Science* **2007**, (6), 135-146.
10. Karczmar, A. G., History of the research with anticholinesterase agents. In *Anticholinesterase Agents*, Pergamon Press: Oxford, 1970; pp 1-44.
11. Ghosh, R.; Newman, J. E., A new group of organophosphorus pesticides. *Chemistry and Industry* **1955**, (118).
12. Baldit, G. M., Amiton - a New Acaricide and Scalicide. *Chem Ind-London* **1958**, (4), 89-89.
13. Tammelin, L. E., Organophosphorylcholines and Cholinesterases. *Ark Kemi* **1958**, *12* (3), 287-298.
14. Kloske, M.; Witkiewicz, Z., Novichoks - The A group of organophosphorus chemical warfare agents. *Chemosphere* **2019**, *221*, 672-682.
15. Ekstrom, F.; Pang, Y. P.; Boman, M.; Artursson, E.; Akfur, C.; Borjegen, S., Crystal structures of acetylcholinesterase in complex with HI-6, Ortho-7 and obidoxime: structural basis for differences in the ability to reactivate tabun conjugates. *Biochem Pharmacol* **2006**, *72* (5), 597-607.
16. Macilwain, C., Study Proves Iraq Used Nerve-Gas. *Nature* **1993**, *363* (6424), 3-3.
17. Pita, R.; Domingo, J., The Use of Chemical Weapons in the Syrian Conflict. *Toxics* **2014**, *2* (3), 391-402.
18. Sidell, F. R.; Borak, J., Chemical warfare agents: II. nerve agents. *Annals of Emergency Medicine* **1992**, *21* (7), 865-871.

19. Medical Management of Chemical Casualties Handbook. United States Army Medical Research Institute of Chemical Defense, 1998.
20. Shea, D. A., CRS Report for Congress: Chemical Weapons: A Summary Report of Characteristics and Effects. 2013.
21. Office of Surgeon General and U.S. Army Program Manager for Chemical Demilitarization. Prehospital and Hospital Provider Course Syllabus–Chemical Stockpile Emergency Preparedness Program. 1998.
22. Nepovimova, E.; Kuca, K., Chemical warfare agent NOVICHOK - mini-review of available data. *Food Chem Toxicol* **2018**, *121*, 343-350.
23. Mirzayanov, V. S., *State Secrets: an insider's chronicle of the Russian chemical weapons program*. Outskirts Press, Inc.: Denver, Colorado, 2009.
24. Weimaster, J. F.; Beaudry, W. T.; Bossle, P. C.; Ellzy, M. W.; Janes, L. G.; Johnson, D. W.; Lochner, J. M.; Pleva, S. G.; Reeder, J. H.; Rohrbaugh, D. K.; Rosso, T. E.; Szafraniec, L. J.; Szafraniec, L. L.; Albro, T. G.; Creasy, W. R.; Stuff, J. R.; Smith, P. B.; Stewart, I. R., Chemical-Analysis of Environmental-Samples Collected in Iraq - Analysis for the Presence of Chemical Warfare Agents. *J Chem Technol Biot* **1995**, *64* (2), 115-128.
25. Black, R. M.; Clarke, R. J.; Read, R. W.; Reid, M. T. J., Application of Gas-Chromatography Mass-Spectrometry and Gas-Chromatography Tandem Mass-Spectrometry to the Analysis of Chemical Warfare Samples, Found to Contain Residues of the Nerve Agent Sarin, Sulfur Mustard and Their Degradation Products. *J Chromatogr A* **1994**, *662* (2), 301-321.
26. Kadivar, H.; Adams, S. C., Treatment of Chemical and Biological Warfare Injuries - Insights Derived from the 1984 Iraqi Attack on Majnoon Island. *Mil Med* **1991**, *156* (4), 171-177.
27. Nozaki, H.; Aikawa, N.; Shinozawa, Y.; Hori, S.; Fujishima, S.; Takuma, K.; Sagoh, M., Sarin poisoning in Tokyo subway. *Lancet* **1995**, *345* (8955), 980-1.
28. Morita, H.; Yanagisawa, N.; Nakajima, T.; Shimizu, M.; Hirabayashi, H.; Okudera, H.; Nohara, M.; Midorikawa, Y.; Mimura, S., Sarin Poisoning in Matsumoto, Japan. *Lancet* **1995**, *346* (8970), 290-293.
29. Nozaki, H.; Hori, S.; Shinozawa, Y.; Fujishima, S.; Takuma, K.; Sagoh, M.; Kimura, H.; Ohki, T.; Suzuki, M.; Aikawa, N., Secondary exposure of medical staff to sarin vapor in the emergency room. *Intensive Care Med* **1995**, *21* (12), 1032-5.
30. Okumura, T.; Takasu, N.; Ishimatsu, S.; Miyanoki, S.; Mitsunashi, A.; Kumada, K.; Tanaka, K.; Hinohara, S., Report on 640 victims of the Tokyo subway sarin attack. *Ann Emerg Med* **1996**, *28* (2), 129-35.
31. John, H.; van der Schans, M. J.; Koller, M.; Spruit, H. E. T.; Worek, F.; Thiermann, H.; Noort, D., Fatal sarin poisoning in Syria 2013: forensic verification within an international laboratory network. *Forensic toxicology* **2018**, *36* (1), 61-71.
32. Kingsley, P.; Barnard, A. Banned Nerve Agent Sarin Used in Syria Chemical Attack, Turkey Says *The New York Times* [Online], 2017.
33. Paddock, R.; Sang-Hun, C.; Wade, N., In Kim Jong-nam's Death, North Korea Lets Loose a Weapon of Mass Destruction. *The New York Times* 2017.
34. Dodd, V.; Harding, L.; MacAskill, E., Sergei Skripal: former Russian spy poisoned with nerve agent, say police. *The Guardian* 2018.

35. Amesbury poisoning: Experts confirm substance was Novichok. *British Broadcasting Company* September 4, 2018, 2018.
36. Eddleston, M., Patterns and problems of deliberate self-poisoning in the developing world. *QJM* **2000**, *93* (11), 715-31.
37. Barnett, P.; Rosenberry, T. L., Functional identity of catalytic subunits of acetylcholinesterase. *Biochim Biophys Acta* **1979**, *567* (1), 154-60.
38. Massoulie, J.; Bon, S., The Molecular-Forms of Cholinesterase and Acetylcholinesterase in Vertebrates. *Annu Rev Neurosci* **1982**, *5*, 57-106.
39. Vigny, M.; Bon, S.; Massoulie, J.; Leterrier, F., Active-site catalytic efficiency of acetylcholinesterase molecular forms in Electrophorus, torpedo, rat and chicken. *Eur J Biochem* **1978**, *85* (2), 317-23.
40. Quinn, D. M., Acetylcholinesterase - Enzyme Structure, Reaction Dynamics, and Virtual Transition-States. *Chem Rev* **1987**, *87* (5), 955-979.
41. Colovic, M. B.; Krstic, D. Z.; Lazarevic-Pasti, T. D.; Bondzic, A. M.; Vasic, V. M., Acetylcholinesterase inhibitors: pharmacology and toxicology. *Curr Neuropharmacol* **2013**, *11* (3), 315-35.
42. Cheung, J.; Rudolph, M. J.; Burshteyn, F.; Cassidy, M. S.; Gary, E. N.; Love, J.; Franklin, M. C.; Height, J. J., Structures of human acetylcholinesterase in complex with pharmacologically important ligands. *J Med Chem* **2012**, *55* (22), 10282-6.
43. Shafferman, A.; Ordentlich, A.; Barak, D.; Stein, D.; Ariel, N.; Velan, B., Aging of phosphorylated human acetylcholinesterase: catalytic processes mediated by aromatic and polar residues of the active centre. *Biochem J* **1996**, *318* (Pt 3), 833-40.
44. Sun, M.; Chang, Z.; Shau, M.; Huang, R.; Chou, T., The mechanism of ageing of phosphonylated acetylcholinesterase. *Eur J Biochem* **1979**, *100* (2), 527-30.
45. Millard, C. B.; Kryger, G.; Ordentlich, A.; Greenblatt, H. M.; Harel, M.; Raves, M. L.; Segall, Y.; Barak, D.; Shafferman, A.; Silman, I.; Sussman, J. L., Crystal structures of aged phosphonylated acetylcholinesterase: nerve agent reaction products at the atomic level. *Biochemistry* **1999**, *38* (22), 7032-9.
46. Aldridge, W. N.; Reiner, E., *Enzyme inhibitors as substrates: Interactions of esterases with esters of organophosphorus and carbamic acids*. North-Holland Pub. Co.: 1972.
47. Worek, F.; Thiermann, H.; Szinicz, L.; Eyer, P., Kinetic analysis of interactions between human acetylcholinesterase, structurally different organophosphorus compounds and oximes. *Biochem Pharmacol* **2004**, *68* (11), 2237-48.
48. Berry, W. K.; Davies, D. R., Factors influencing the rate of "aging" of a series of alkyl methylphosphonyl-acetylcholinesterases. *Biochem J* **1966**, *100* (2), 572-6.
49. Aurbek, N.; Thiermann, H.; Szinicz, L.; Eyer, P.; Worek, F., Analysis of inhibition, reactivation and aging kinetics of highly toxic organophosphorus compounds with human and pig acetylcholinesterase. *Toxicology* **2006**, *224* (1-2), 91-9.
50. Ellman, G. L.; Courtney, K. D.; Andres, V., Jr.; Feather-Stone, R. M., A new and rapid colorimetric determination of acetylcholinesterase activity. *Biochem Pharmacol* **1961**, *7*, 88-95.
51. Komersova, A.; Komers, K.; Cegan, A., New findings about Ellman's method to determine cholinesterase activity. *Z Naturforsch C* **2007**, *62* (1-2), 150-154.

52. Willig, S.; Hunter, D. L.; Dass, P. D.; Padilla, S., Validation of the use of 6,6'-dithiodinitrotinic acid as a chromogen in the Ellman method for cholinesterase determinations. *Vet Hum Toxicol* **1996**, *38* (4), 249-253.
53. Chow, C. M.; Islam, M. F., Colorimetric Determination of Red Blood Cell Acetylcholinesterase Activity. *Clin Biochem* **1970**, *3* (4), 295-&.
54. Worek, F.; Mast, U.; Kiderlen, D.; Diepold, C.; Eyer, P., Improved determination of acetylcholinesterase activity in human whole blood. *Clin Chim Acta* **1999**, *288* (1-2), 73-90.
55. Forsberg, A.; Puu, G., Kinetics for the inhibition of acetylcholinesterase from the electric eel by some organophosphates and carbamates. *Eur J Biochem* **1984**, *140* (1), 153-6.
56. Hart, G. J.; O'Brien, R. D., Recording spectrophotometric method for determination of dissociation and phosphorylation constants for the inhibition of acetylcholinesterase by organophosphates in the presence of substrate. *Biochemistry* **1973**, *12* (15), 2940-5.
57. Aldridge, W. N., Some properties of specific cholinesterase with particular reference to the mechanism of inhibition by diethyl p-nitrophenyl thiophosphate (E 605) and analogues. *Biochem J* **1950**, *46* (4), 451-60.
58. Herkert, N. M.; Schulz, S.; Wille, T.; Thiermann, H.; Hatz, R. A.; Worek, F., Pre- and post-treatment effect of physostigmine on soman-inhibited human erythrocyte and muscle acetylcholinesterase in vitro. *Toxicol Appl Pharmacol* **2011**, *253* (1), 7-13.
59. Thiermann, H.; Worek, F.; Kehe, K., Limitations and challenges in treatment of acute chemical warfare agent poisoning. *Chem Biol Interact* **2013**, *206* (3), 435-43.
60. Hobbiger, F., Protection against the lethal effects of organophosphates by pyridine-2-aldoxime methiodide. *Br J Pharmacol Chemother* **1957**, *12* (4), 438-46.
61. Hobbiger, F., Reactivation of phosphorylated acetylcholinesterase by pyridine-2-aldoxime methiodide. *Biochim Biophys Acta* **1957**, *25* (3), 652-4.
62. Clement, J. G., Toxicology and pharmacology of bispyridium oximes--insight into the mechanism of action vs Soman poisoning in vivo. *Fundam Appl Toxicol* **1981**, *1* (2), 193-202.
63. Worek, F.; Widmann, R.; Knopff, O.; Heyes, G.; Szinicz, L., Reactivation of organophosphorus - Inhibited human erythrocyte-acetylcholinesterase by oximes in vitro. *Nato Sci S I Disarm* **1999**, *25*, 219-227.
64. Mercey, G.; Verdelet, T.; Renou, J.; Kliachyna, M.; Baati, R.; Nachon, F.; Jean, L.; Renard, P. Y., Reactivators of acetylcholinesterase inhibited by organophosphorus nerve agents. *Acc Chem Res* **2012**, *45* (5), 756-66.
65. Childs, A. F.; Davies, D. R.; Green, A. L.; Rutland, J. P., The reactivation by oximes and hydroxamic acids of cholinesterase inhibited by organo-phosphorus compounds. *Br J Pharmacol Chemother* **1955**, *10* (4), 462-5.
66. Iyer, R.; Iken, B.; Leon, A., Developments in alternative treatments for organophosphate poisoning. *Toxicol Lett* **2015**, *233* (2), 200-6.
67. Wilson, I. B., ACETYLCHOLINESTERASE: XIII. REACTIVATION OF ALKYL PHOSPHATE-INHIBITED ENZYME. *Journal of Biological Chemistry* **1952**, *199* (1), 113-120.
68. Askew, B. M., Oximes and Hydroxamic Acids as Antidotes in Anticholinesterase Poisoning. *Brit J Pharm Chemoth* **1956**, *11* (4), 417-423.

69. Davies, D. R.; Green, A. L., The chemotherapy of poisoning by organophosphate anticholinesterases. *British journal of industrial medicine* **1959**, *16* (2), 128-134.
70. Hobbiger, F., Effect of nicotinhydroxamic acid methiodide on human plasma cholinesterase inhibited by organophosphates containing a dialkylphosphato group. *Br J Pharmacol Chemother* **1955**, *10* (3), 356-62.
71. Wilson, I. B.; Ginsburg, B., A powerful reactivator of alkylphosphate-inhibited acetylcholinesterase. *Biochim Biophys Acta* **1955**, *18* (1), 168-70.
72. Wilson, I. B.; Ginsburg, S., Reactivation of acetylcholinesterase inhibited by alkylphosphates. *Arch Biochem Biophys* **1955**, *54* (2), 569-71.
73. Poziomek, E. J.; Hackley, B. E.; Steinberg, G. M., Pyridinium Aldoximes¹. *The Journal of Organic Chemistry* **1958**, *23* (5), 714-717.
74. Hobbiger, F.; O'Sullivan, D. G.; Sadler, P. W., New potent reactivators of acetylcholinesterase inhibited by tetraethyl pyrophosphate. *Nature* **1958**, *182* (4648), 1498-9.
75. Heilbronn, E.; Tolagen, B., Toxogonin in Sarin, Soman and Tabun poisoning. *Biochem Pharmacol* **1965**, *14* (1), 73-77.
76. O'Leary, J. F.; Kunkel, A. M.; Jones, A. H., EFFICACY AND LIMITATIONS OF OXIME-ATROPINE TREATMENT OF ORGANOPHOSPHORUS ANTICHOLINESTERASE POISONING. *Journal of Pharmacology and Experimental Therapeutics* **1961**, *132* (1), 50.
77. Hackley, B. E.; Steinberg, G. M.; Lamb, J. C., Formation of Potent Inhibitors of Ache by Reaction of Pyridinaldoximes with Isopropyl Methylphosphonofluoridate (Gb). *Archives of Biochemistry and Biophysics* **1959**, *80* (1), 210-214.
78. Hobbiger, F.; Sadler, P. W., Protection against lethal organophosphate poisoning by quaternary pyridine aldoximes. *Br J Pharmacol Chemother* **1959**, *14* (2), 192-201.
79. Bajgar, J.; Patocka, J.; Jakl, A.; Hrdina, V., Antidotal Therapy and Changes of Acetylcholinesterase Activity Following Isopropyl Methylphosphonofluoridate Intoxication in Mice. *Acta Biol Med Ger* **1975**, *34* (6), 1049-1055.
80. Harris, L. W.; Anderson, D. R.; Lennox, W. J.; Woodard, C. L.; Pastelak, A. M.; Vanderpool, B. A., Evaluation of Several Oximes as Reactivators of Unaged Soman-Inhibited Whole-Blood Acetylcholinesterase in Rabbits. *Biochem Pharmacol* **1990**, *40* (12), 2677-2682.
81. Koplovitz, I.; Stewart, J. R., Efficacy of Oxime Plus Atropine Treatment against Soman Poisoning in the Atropinesterase-Free Rabbit. *Drug Chem Toxicol* **1992**, *15* (2), 117-126.
82. Luettringhaus, A.; Hagedorn, I., [Quaternary Hydroxyiminomethylpyridinium Salts. The Dischloride of Bis-(4-Hydroxyiminomethyl-1-Pyridinium-Methyl)-Ether (Lueh6), a New Reactivator of Acetylcholinesterase Inhibited by Organic Phosphoric Acid Esters]. *Arzneimittelforschung* **1964**, *14*, 1-5.
83. Erdmann, W. D.; Von, C., [a New Esterase Reactivator for the Treatment of Alkylphosphate Poisonings]. *Dtsch Med Wochenschr* **1963**, *88*, 2201-6.
84. Hagedorn, I.; Gundel, W. H.; Schoene, K., Reactivation of Phosphorylated Acetylcholin Esterase by Oxims - Contribution to Study of Course of Reaction. *Arznei-Forschung* **1969**, *19* (4), 603-&.
85. Oldiges, H.; Schoene, K., Antidotal Effects of Pyridinium Salts and Imidazolium Salts on Soman and Paraoxon Poisoning in Mice. *Arch Toxikol* **1970**, *26* (4), 293-&.

86. Eyer, P.; Hagedorn, I.; Klimmek, R.; Lippstreu, P.; Löffler, M.; Oldiges, H.; Spohrer, U.; Steidl, I.; Szinicz, L.; Worek, F., Hlo-7 Dimethanesulfonate, a Potent Bispyridinium-Dioxime against Anticholinesterases. *Arch Toxicol* **1992**, *66* (9), 603-621.
87. Clement, J. G., Efficacy of Mono-Pyridinium and Bis-Pyridinium Oximes Versus Soman, Sarin and Tabun Poisoning in Mice. *Fund Appl Toxicol* **1983**, *3* (6), 533-535.
88. Jokanovic, M.; Prostran, M., Pyridinium oximes as cholinesterase reactivators. Structure-activity relationship and efficacy in the treatment of poisoning with organophosphorus compounds. *Curr Med Chem* **2009**, *16* (17), 2177-88.
89. Melchers, B. P. C.; Philippens, I. H. C. H. M.; Wolthuis, O. L., Efficacy of HI-6 and HLö-7 in preventing incapacitation following nerve agent poisoning. *Pharmacology Biochemistry and Behavior* **1994**, *49* (4), 781-788.
90. Bartosova, L.; Kuca, K.; Kunesova, G.; Jun, D., The acute toxicity of acetylcholinesterase reactivators in mice in relation to their structure. *Neurotox Res* **2006**, *9* (4), 291-6.
91. Boskovic, B.; Kovacevic, V.; Jovanovic, D., PAM-2 Cl, HI-6, and HGG-12 in soman and tabun poisoning. *Fundam Appl Toxicol* **1984**, *4* (2 Pt 2), S106-15.
92. Allgardsson, A.; Berg, L.; Akfur, C.; Hornberg, A.; Worek, F.; Linusson, A.; Ekstrom, F. J., Structure of a prereaction complex between the nerve agent sarin, its biological target acetylcholinesterase, and the antidote HI-6. *Proc Natl Acad Sci U S A* **2016**, *113* (20), 5514-9.
93. Kovarik, Z.; Radic, Z.; Berman, H. A.; Simeon-Rudolf, V.; Reiner, E.; Taylor, P., Mutant cholinesterases possessing enhanced capacity for reactivation of their phosphonylated conjugates. *Biochemistry* **2004**, *43* (11), 3222-9.
94. Ekstrom, F.; Hornberg, A.; Artursson, E.; Hammarstrom, L. G.; Schneider, G.; Pang, Y. P., Structure of HI-6*sarin-acetylcholinesterase determined by X-ray crystallography and molecular dynamics simulation: reactivator mechanism and design. *PLoS One* **2009**, *4* (6), e5957.
95. Su, C. T.; Wang, P. H.; Liu, R. F.; Shih, J. H.; Ma, C.; Lin, C. H.; Liu, C. Y.; Wu, M. T., Kinetic studies and structure-activity relationships of bispyridinium oximes as reactivators of acetylcholinesterase inhibited by organophosphorus compounds. *Fundam Appl Toxicol* **1986**, *6* (3), 506-14.
96. Green, A. L.; Smith, H. J., The reactivation of cholinesterase inhibited with organophosphorus compounds. 2. Reactivation by pyridinealdoxime methiodides. *Biochem J* **1958**, *68* (1), 32-5.
97. Worek, F.; Eyer, P.; Szinicz, L., Inhibition, reactivation and aging kinetics of cyclohexylmethylphosphonofluoridate-inhibited human cholinesterases. *Arch Toxicol* **1998**, *72* (9), 580-7.
98. Maxwell, D. M.; Koplovitz, I.; Worek, F.; Sweeney, R. E., A structure-activity analysis of the variation in oxime efficacy against nerve agents. *Toxicol Appl Pharmacol* **2008**, *231* (2), 157-64.
99. Reiter, G.; Muller, S.; Hill, I.; Weatherby, K.; Thiermann, H.; Worek, F.; Mikler, J., In vitro and in vivo toxicological studies of V nerve agents: molecular and stereoselective aspects. *Toxicol Lett* **2015**, *232* (2), 438-48.
100. Worek, F.; Aurbek, N.; Wille, T.; Eyer, P.; Thiermann, H., Kinetic analysis of interactions of paraoxon and oximes with human, Rhesus monkey, swine, rabbit, rat and guinea pig acetylcholinesterase. *Toxicol Lett* **2011**, *200* (1-2), 19-23.

101. Worek, F.; Reiter, G.; Eyer, P.; Szinicz, L., Reactivation kinetics of acetylcholinesterase from different species inhibited by highly toxic organophosphates. *Arch Toxicol* **2002**, *76* (9), 523-9.
102. Sussman, J. L.; Harel, M.; Frolow, F.; Oefner, C.; Goldman, A.; Toker, L.; Silman, I., Atomic structure of acetylcholinesterase from *Torpedo californica*: a prototypic acetylcholine-binding protein. *Science* **1991**, *253* (5022), 872-9.
103. Ollis, D. L.; Cheah, E.; Cygler, M.; Dijkstra, B.; Frolow, F.; Franken, S. M.; Harel, M.; Remington, S. J.; Silman, I.; Schrag, J.; et al., The alpha/beta hydrolase fold. *Protein Eng* **1992**, *5* (3), 197-211.
104. Dvir, H.; Silman, I.; Harel, M.; Rosenberry, T. L.; Sussman, J. L., Acetylcholinesterase: from 3D structure to function. *Chem Biol Interact* **2010**, *187* (1-3), 10-22.
105. Wiesner, J.; Kriz, Z.; Kuca, K.; Jun, D.; Koca, J., Acetylcholinesterases--the structural similarities and differences. *J Enzyme Inhib Med Chem* **2007**, *22* (4), 417-24.
106. Greenblatt, H. M.; Dvir, H.; Silman, I.; Sussman, J. L., Acetylcholinesterase: a multifaceted target for structure-based drug design of anticholinesterase agents for the treatment of Alzheimer's disease. *J Mol Neurosci* **2003**, *20* (3), 369-83.
107. Dvir, H.; Jiang, H. L.; Wong, D. M.; Harel, M.; Chetrit, M.; He, X. C.; Jin, G. Y.; Yu, G. L.; Tang, X. C.; Silman, I.; Bai, D. L.; Sussman, J. L., X-ray structures of *Torpedo californica* acetylcholinesterase complexed with (+)-huperzine A and (-)-huperzine B: structural evidence for an active site rearrangement. *Biochemistry* **2002**, *41* (35), 10810-8.
108. Raves, M. L.; Harel, M.; Pang, Y. P.; Silman, I.; Kozikowski, A. P.; Sussman, J. L., Structure of acetylcholinesterase complexed with the nootropic alkaloid, (-)-huperzine A. *Nat Struct Biol* **1997**, *4* (1), 57-63.
109. Bourne, Y.; Grassi, J.; Bougis, P. E.; Marchot, P., Conformational Flexibility of the Acetylcholinesterase Tetramer Suggested by X-ray Crystallography. *Journal of Biological Chemistry* **1999**, *274* (43), 30370-30376.
110. Bourne, Y.; Taylor, P.; Bougis, P. E.; Marchot, P., Crystal structure of mouse acetylcholinesterase. A peripheral site-occluding loop in a tetrameric assembly. *J Biol Chem* **1999**, *274* (5), 2963-70.
111. Bourne, Y.; Taylor, P.; Radic, Z.; Marchot, P., Structural insights into ligand interactions at the acetylcholinesterase peripheral anionic site. *Embo J* **2003**, *22* (1), 1-12.
112. Harel, M.; Kryger, G.; Rosenberry, T. L.; Mallender, W. D.; Lewis, T.; Fletcher, R. J.; Guss, J. M.; Silman, I.; Sussman, J. L., Three-dimensional structures of *Drosophila melanogaster* acetylcholinesterase and of its complexes with two potent inhibitors. *Protein Sci* **2000**, *9* (6), 1063-72.
113. Cheung, J.; Mahmood, A.; Kalathur, R.; Liu, L.; Carlier, P. R., Structure of the G119S Mutant Acetylcholinesterase of the Malaria Vector *Anopheles gambiae* Reveals Basis of Insecticide Resistance. *Structure (London, England : 1993)* **2018**, *26* (1), 130-136.e2.
114. Bourne, Y.; Renault, L.; Marchot, P., Crystal structure of snake venom acetylcholinesterase in complex with inhibitory antibody fragment Fab410 bound at the peripheral site: evidence for open and closed states of a back door channel. *J Biol Chem* **2015**, *290* (3), 1522-35.

115. Franklin, M. C.; Rudolph, M. J.; Ginter, C.; Cassidy, M. S.; Cheung, J., Structures of paraoxon-inhibited human acetylcholinesterase reveal perturbations of the acyl loop and the dimer interface. *Proteins* **2016**, *84* (9), 1246-56.
116. Bourne, Y.; Taylor, P.; Marchot, P., Acetylcholinesterase inhibition by fasciculin: crystal structure of the complex. *Cell* **1995**, *83* (3), 503-12.
117. Harel, M.; Kleywegt, G. J.; Ravelli, R. B.; Silman, I.; Sussman, J. L., Crystal structure of an acetylcholinesterase-fasciculin complex: interaction of a three-fingered toxin from snake venom with its target. *Structure* **1995**, *3* (12), 1355-66.
118. Radic, Z.; Quinn, D. M.; Vellom, D. C.; Camp, S.; Taylor, P., Allosteric control of acetylcholinesterase catalysis by fasciculin. *J Biol Chem* **1995**, *270* (35), 20391-9.
119. Hornberg, A.; Artursson, E.; Warne, R.; Pang, Y. P.; Ekstrom, F., Crystal structures of oxime-bound fenamiphos-acetylcholinesterases: reactivation involving flipping of the His447 ring to form a reactive Glu334-His447-oxime triad. *Biochem Pharmacol* **2010**, *79* (3), 507-15.
120. Hornberg, A.; Tunemalm, A. K.; Ekstrom, F., Crystal structures of acetylcholinesterase in complex with organophosphorus compounds suggest that the acyl pocket modulates the aging reaction by precluding the formation of the trigonal bipyramidal transition state. *Biochemistry* **2007**, *46* (16), 4815-25.
121. Carletti, E.; Colletier, J. P.; Dupeux, F.; Trovaslet, M.; Masson, P.; Nachon, F., Structural evidence that human acetylcholinesterase inhibited by tabun ages through O-dealkylation. *J Med Chem* **2010**, *53* (10), 4002-8.
122. Benschop, H. P.; Konings, C. A.; Van Genderen, J.; De Jong, L. P., Isolation, anticholinesterase properties, and acute toxicity in mice of the four stereoisomers of the nerve agent soman. *Toxicol Appl Pharmacol* **1984**, *72* (1), 61-74.
123. Hall, C. R.; Inch, T. D.; Inns, R. H.; Muir, A. W.; Sellers, D. J.; Smith, A. P., Differences between some biological properties of enantiomers of alkyl S-alkyl methylphosphonothioates. *J Pharm Pharmacol* **1977**, *29* (9), 574-6.
124. Berjanskii, M.; Wishart, D. S., NMR: prediction of protein flexibility. *Nat Protoc* **2006**, *1* (2), 683-8.
125. Bernetti, M.; Masetti, M.; Rocchia, W.; Cavalli, A., Kinetics of Drug Binding and Residence Time. *Annu Rev Phys Chem* **2019**.
126. Kristensen, S. M.; Kasimova, M. R.; Led, J. J., The Use of NMR in the Studies of Highly Flexible States of Proteins: Relation to Protein Function and Stability. In *Modern Magnetic Resonance*, Webb, G. A., Ed. Springer Netherlands: Dordrecht, 2006; pp 1369-1376.
127. Sargsyan, K.; Grauffel, C.; Lim, C., How Molecular Size Impacts RMSD Applications in Molecular Dynamics Simulations. *J Chem Theory Comput* **2017**, *13* (4), 1518-1524.
128. Newmark, J., CHAPTER 56 - Nerve Agents. In *Clinical Neurotoxicology*, Dobbs, M. R., Ed. W.B. Saunders: Philadelphia, 2009; pp 646-659.
129. Weigelt, J.; van Dongen, M.; Uppenberg, J.; Schultz, J.; Wikström, M., Site-Selective Screening by NMR Spectroscopy with Labeled Amino Acid Pairs. *Journal of the American Chemical Society* **2002**, *124* (11), 2446-2447.
130. Weigelt, J.; Wikström, M.; Schultz, J.; van Dongen, M., Site-Selective Labeling Strategies for Screening by NMR. *Combinatorial Chemistry & High Throughput Screening* **2002**, *5* (8), 623-630.

APPENDIX A
SUPPLEMENTARY MATERIAL FOR CHAPTER 2

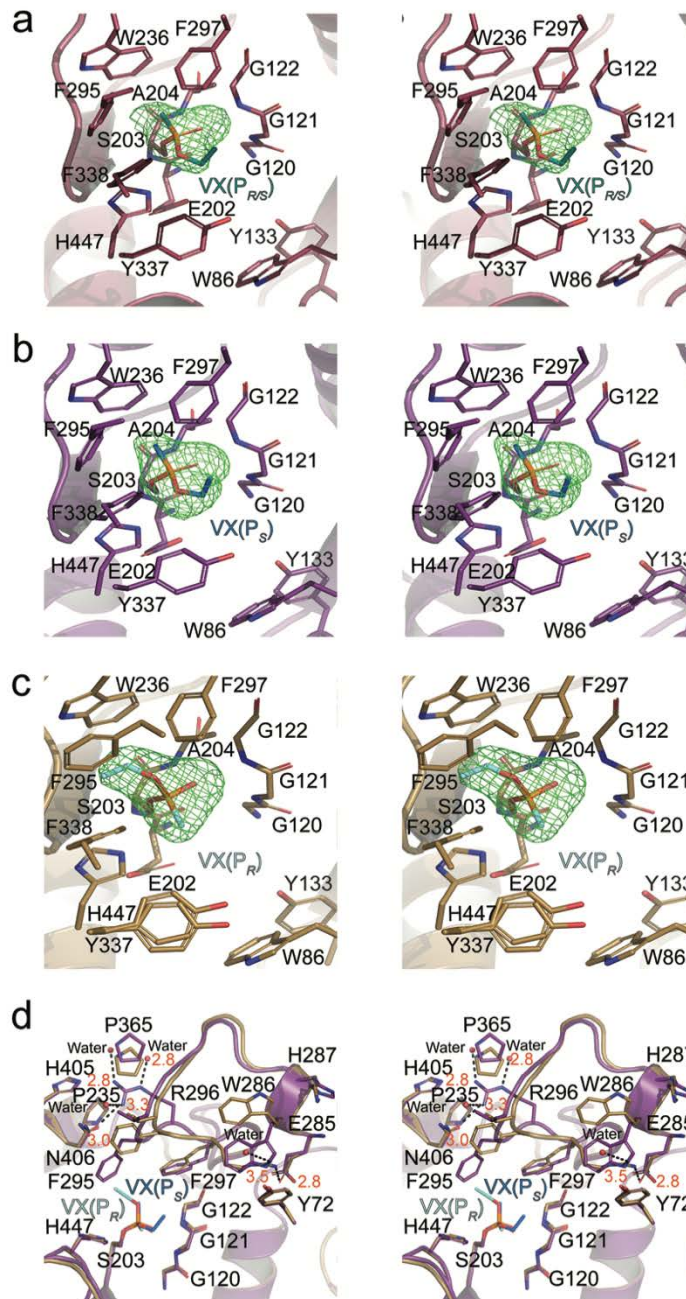


Figure S2.1. Crystal Structures of Human Acetylcholinesterase in complex with Stereoisomers of Nerve Agent, VX. (a) Wall-eyed stereoview of $P_{R/S}$ -VX (dark teal) bound to the active site of hAChE (dark pink) with hAChE $F_o - F_c$ density scaled to 3σ (green mesh) (PDB 6CQZ). (b) Wall-eyed stereoview of P_S -VX (marine blue) bound to the active site of hAChE (violet purple) with hAChE $F_o - F_c$ density scaled to 3σ (green mesh) (PDB 6CQT). (c) Wall-eyed stereoview of P_R -VX (aquamarine) bound to the active site of hAChE (sand) with hAChE $F_o - F_c$ density scaled to 3σ (green mesh) (PDB 6CQX). (d) Wall-eyed stereo view of an overlay of the acyl loop of hAChE with P_R -VX (sand brown) and P_S -VX (violet purple). The black dashed lines represent hydrogen bonds. The AChE residues are represented by black letters, while the red letters are the distances.

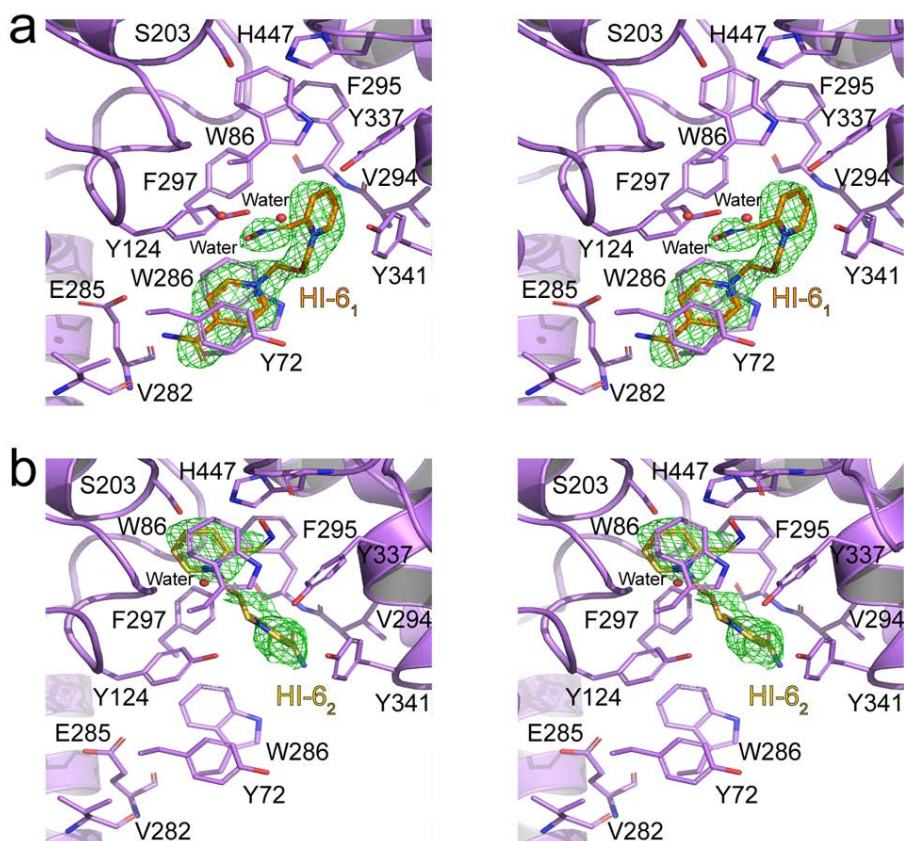


Figure S2.2. Crystal structures of HI-6 bound in the active site of hAChE. (A/B) Wall-eyed stereoview of the active sites of hAChE (bright purple) on chains A & B bound to HI-6 (orange and dark yellow respectively). $F_o - F_c$ density scaled to 3σ (green mesh) (PDB 6CQU). Waters are shown as red spheres and black dashed lines indicate hydrogen bond interactions.

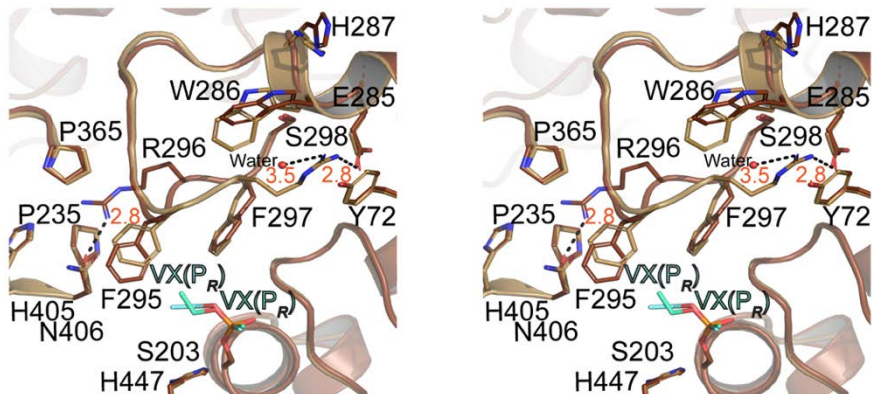


Figure S2.3. Overlay of the Acyl Loop Region of Human Acetylcholinesterase Inhibited by VX-PR. Wall-eyed stereo view of an overlay of the acyl loop of hAChE chain B (sand brown) and Chain A (chocolate) inhibited by P_R -VX (aquamarine; seafoam green). The black dashed lines represent hydrogen bonds. The AChE residues are represented by black letters, while the red letters are the distances.

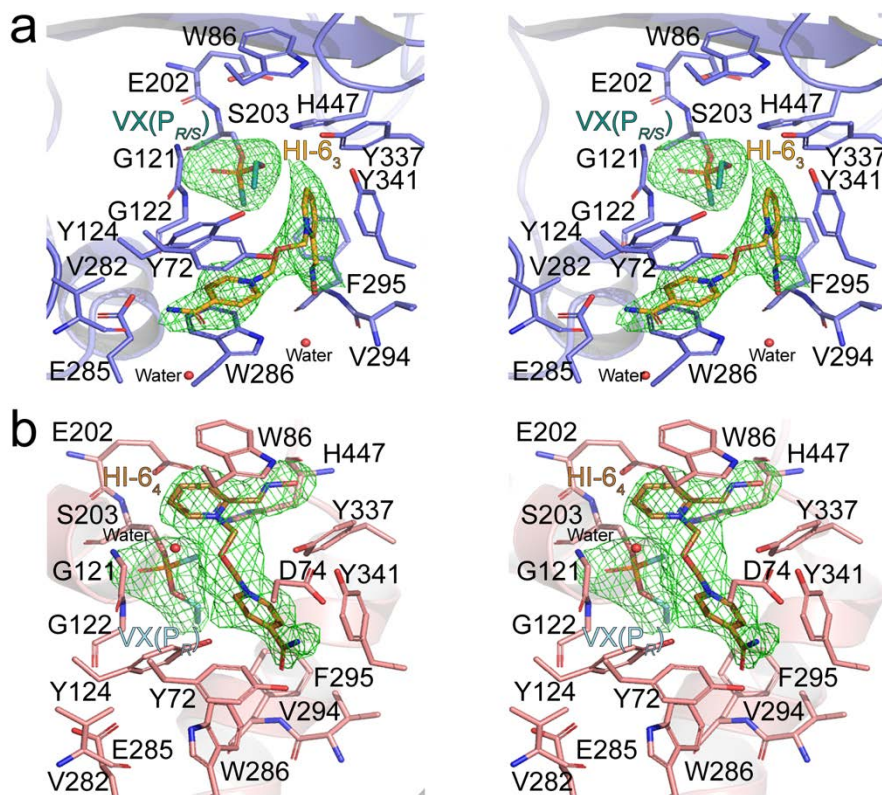


Figure S2.4. The Active Site of human Acetylcholinesterase with Stereoisomers of VX and the Reactivator, HI-6. (a) Wall-eyed stereoview of $P_{R/S}$ -VX (dark teal) with reactivator HI-6 (bright orange) bound to the active site of hAChE (slate) with hAChE $F_o - F_c$ density scaled to 3σ (green mesh) (PDB 6CQW). (b) Wall-eyed stereoview of P_R -VX (aquamarine) with the reactivator HI-6 (copper-colored) bound to the active site of hAChE (salmon pink) with hAChE $F_o - F_c$ density scaled to 3σ (green mesh) (PDB 6CQV).

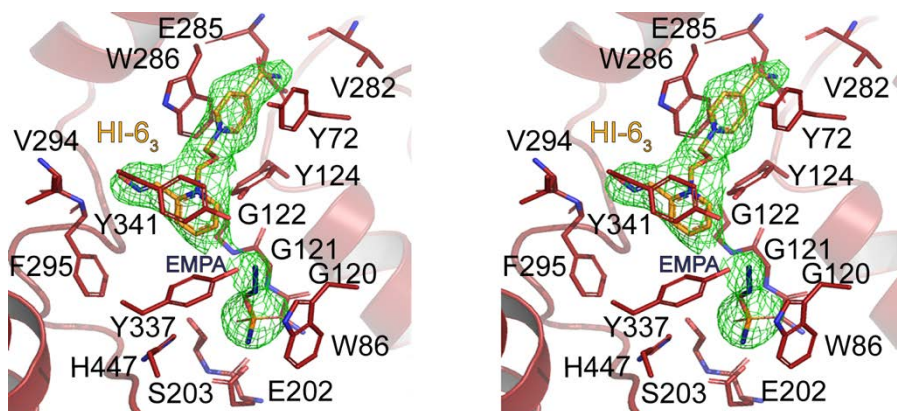


Figure S2.5. The Active Site of human Acetylcholinesterase with Post-Catalysis HI-6 and a by-product, EMPA. Wall-eyed stereoview of hAChE active site with reactivator, HI-6 (bright orange), and unbound VX (indigo), with hAChE $F_o - F_c$ density scaled to 3σ (green mesh) (PDB 6CQY).

APPENDIX B

SUPPLEMENTARY MATERIAL FOR CHAPTER 3

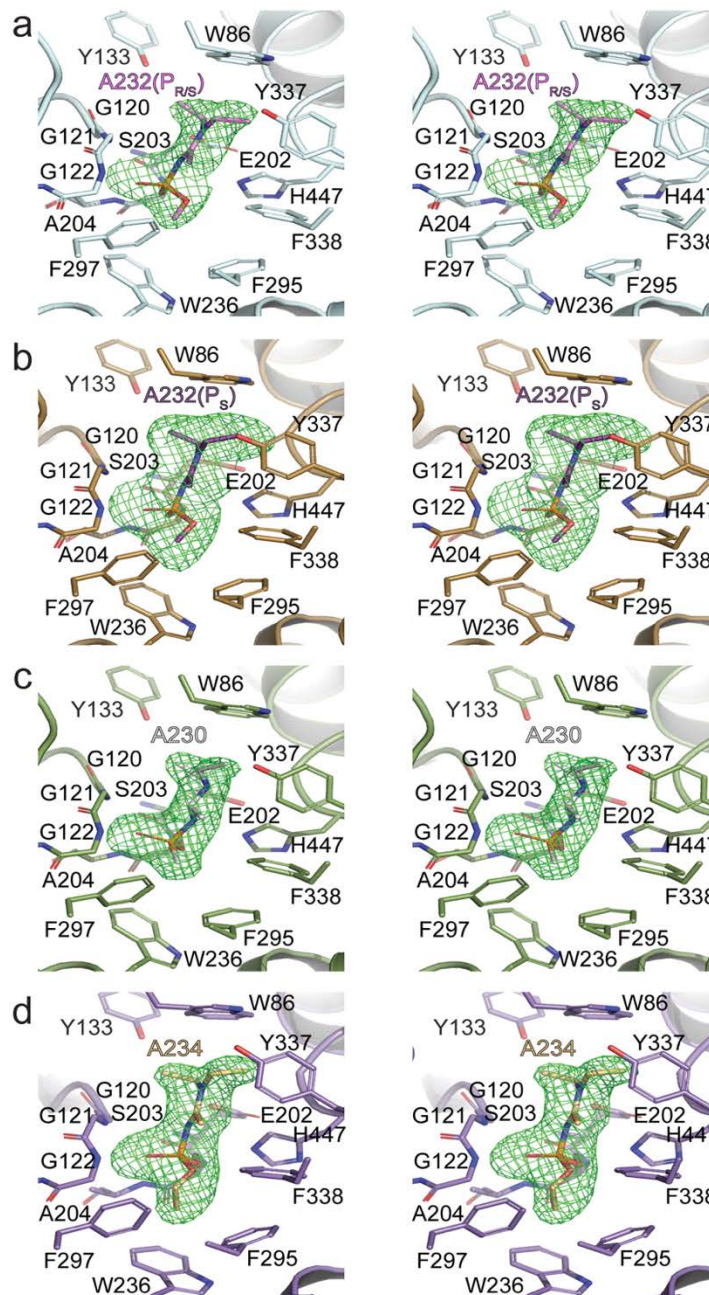


Figure S3.1. Comparison of Crystal Structures of Human Acetylcholinesterase in complex with A-series agents. (a) Wall-eyed stereoview of A232 Pr/S adduct (violet pink) bound to the active site of hAChE (light cyan) with $F_o - F_c$ density scaled to 3σ (green mesh) (PDB 6NTK). (b) Wall-eyed stereoview of A232 Ps adduct (dark purple) bound to the active site of hAChE (sand) with $F_o - F_c$ density scaled to 3σ (green mesh). (PDB 6NTH). (c) Wall-eyed stereoview of A230 Pr/S adduct (light grey) bound to the active site of hAChE (fern green) with $F_o - F_c$ density scaled to 3σ (green mesh) (PDB 6NTO). (d) Wall-eyed stereoview of A234 Pr/S adduct (light orange) bound to the active site of hAChE (light purple) with $F_o - F_c$ density scaled to 3σ (green mesh). (PDB 6NTL). The black lines represent hydrogen bonds. The AChE residues are represented by black letters, while the red letters are the distances.

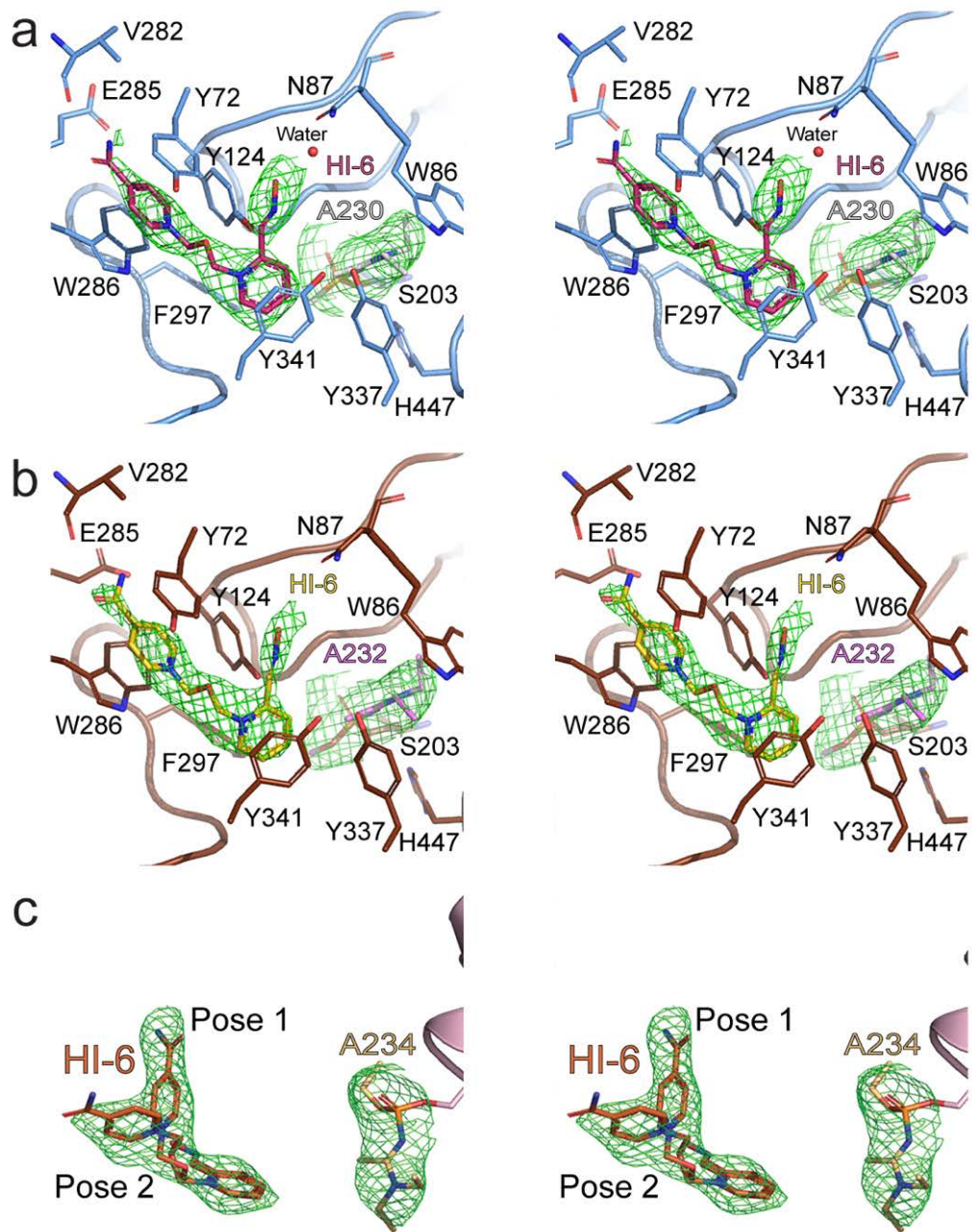


Figure S3.2. Crystal Structures of Human Acetylcholinesterase in complex with A-series agents and HI-6. (a) A wall-eyed stereoview of HI-6 (hot pink) bound to the active site of hAChE-A230 (baby blue; light grey) with $F_o - F_c$ density scaled to 3σ (green mesh) (PDB 6NTN). (b) A wall-eyed stereoview of HI-6 (golden yellow) bound to the active site of hAChE-A232 (chocolate; violet pink) with $F_o - F_c$ density scaled to 3σ (green mesh) (PDB 6NTM). (c) A wall-eyed stereoview of $F_o - F_c$ density scaled to 3σ (green mesh) for HI-6 (dark orange) and A234 (light orange) bound to hAChE (light pink) (PDB 6NTG). The black lines represent hydrogen bonds and the red spheres denote waters. The AChE residues are represented by black letters, while the red letters are the distances.

APPENDIX C

SUPPLEMENTARY MATERIAL FOR CHAPTER 4

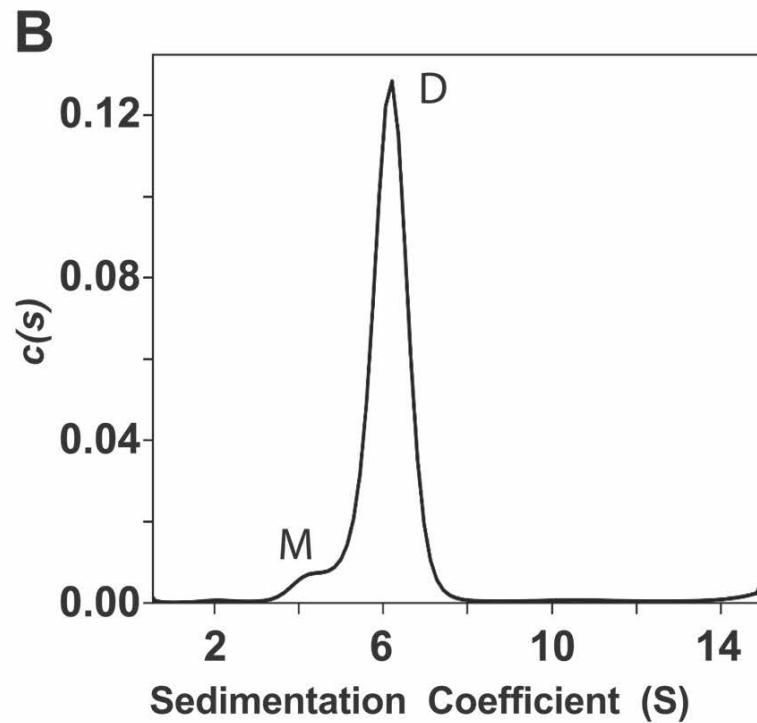
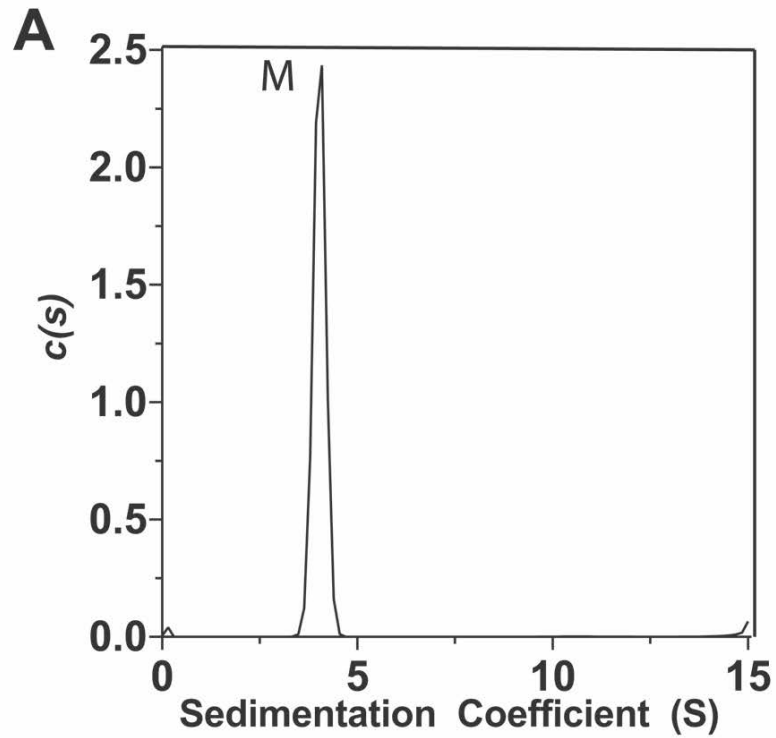


Figure S4.1. Sedimentation velocity analysis studying the oligomeric state of hAChE L380R/F535K and hAChE in solution. The $c(s)$ distribution shows hAChE L380R/F535K is entirely monomeric (M) in (A) whereas hAChE is predominantly dimeric in nature (B).

APPENDIX D

ADDITIONAL MATERIAL ON THE ENZYME KINETICS OF INHIBITION

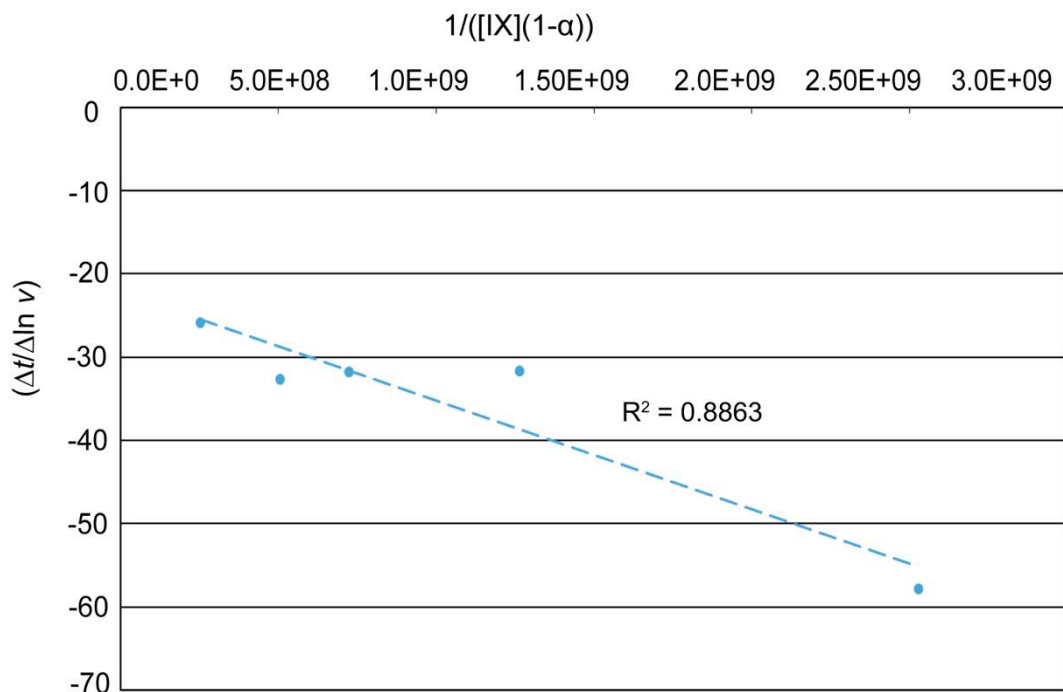


Figure A2.1. Double reciprocal plot for the inhibition of hAChE by racemic VX. The slope was determined by the least-squares method and provides the absolute value of $(k_2/K_d)^{-1} = k_i$, while the y- and x-intercepts yield the value of $(k_2)^{-1}$ and $(K_d)^{-1}$, respectively.

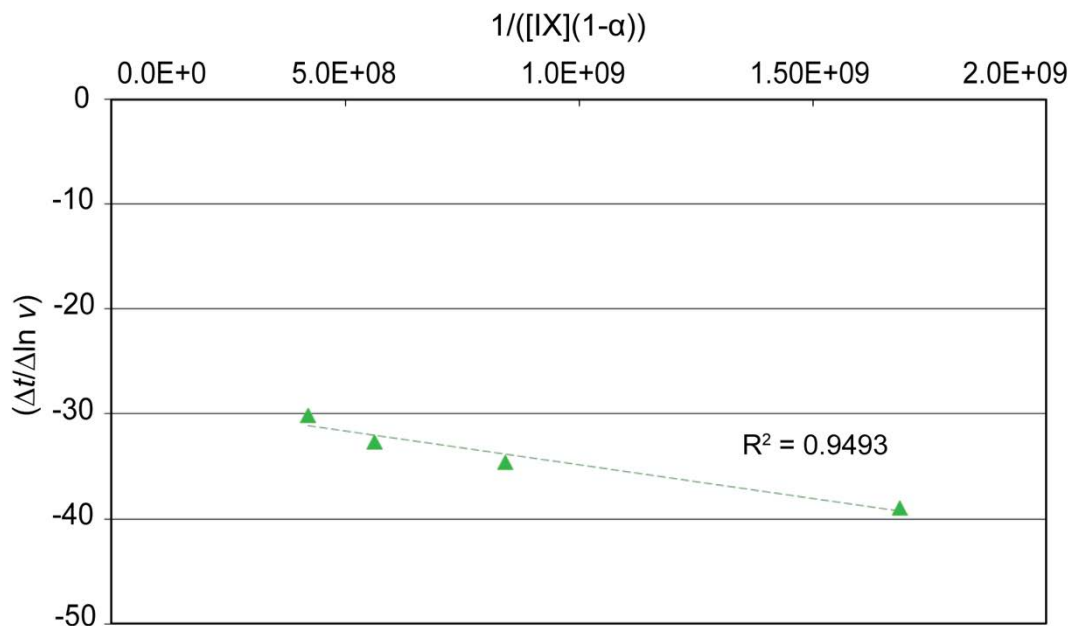


Figure A2.2. Double reciprocal plot for the inhibition of hAChE by P₅-VX. The slope was determined by the least-squares method and provides the absolute value of $(k_2/K_d)^{-1} = k_i$, while the y- and x-intercepts yield the value of $(k_2)^{-1}$ and $(K_d)^{-1}$, respectively.

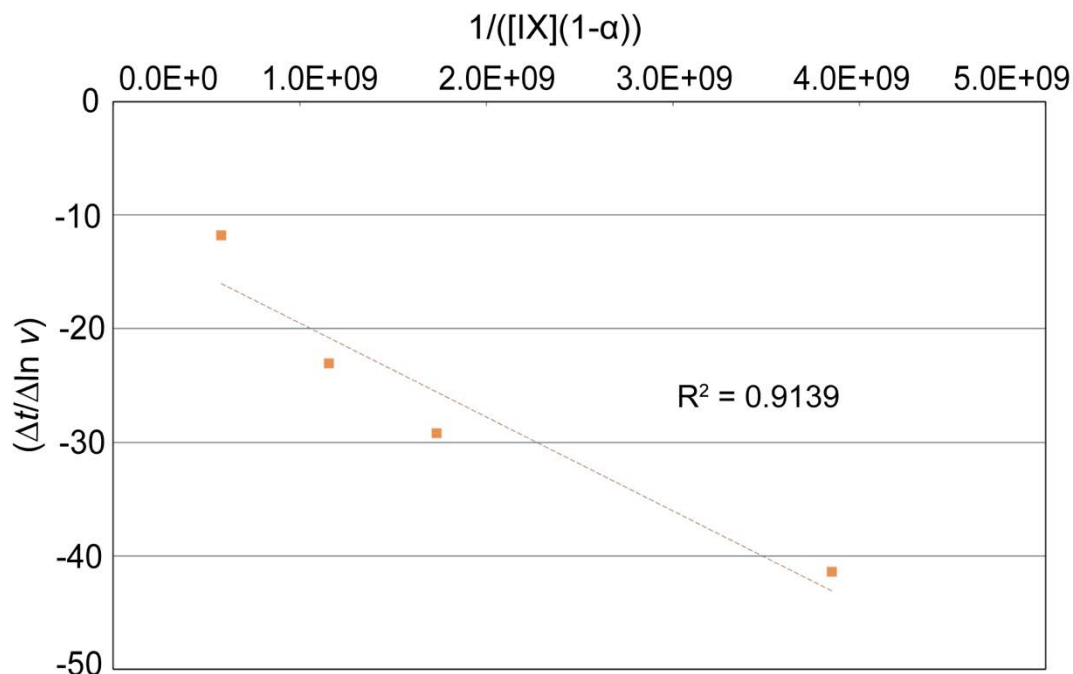


Figure A3.1. Double reciprocal plot for the inhibition of hAChE by racemic A-232. The slope was determined by the least-squares method and provides the absolute value of $(k_2/K_d)^{-1} = k_i$, while the y- and x-intercepts yield the value of $(k_2)^{-1}$ and $(K_d)^{-1}$, respectively.

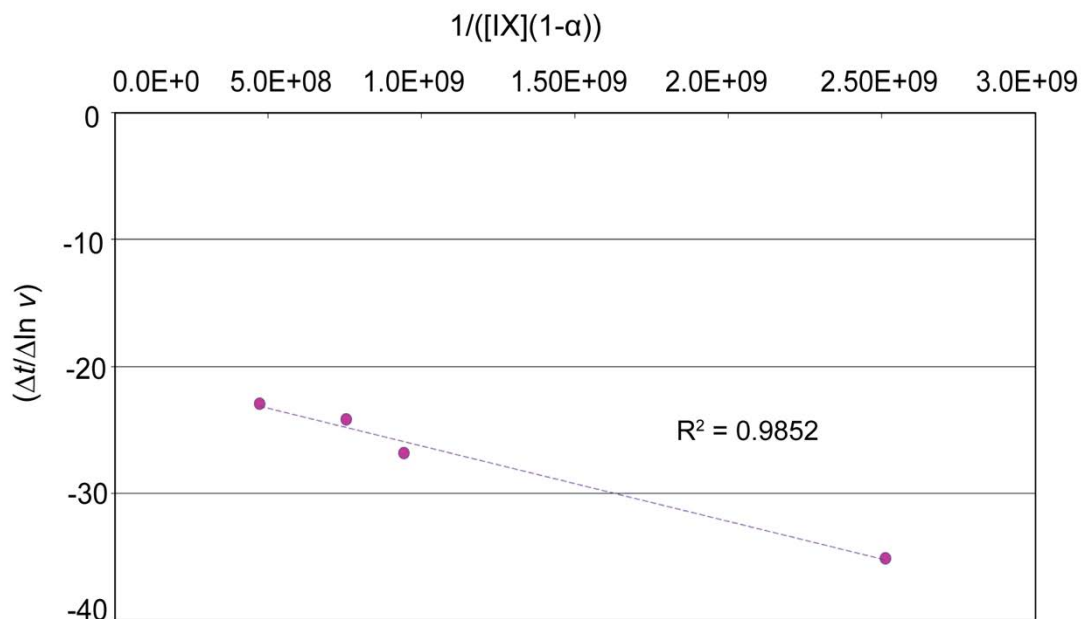


Figure A3.2. Double reciprocal plot for the inhibition of hAChE by P_S-A-232. The slope was determined by the least-squares method and provides the absolute value of $(k_2/K_d)^{-1} = k_i$, while the y- and x-intercepts yield the value of $(k_2)^{-1}$ and $(K_d)^{-1}$, respectively.

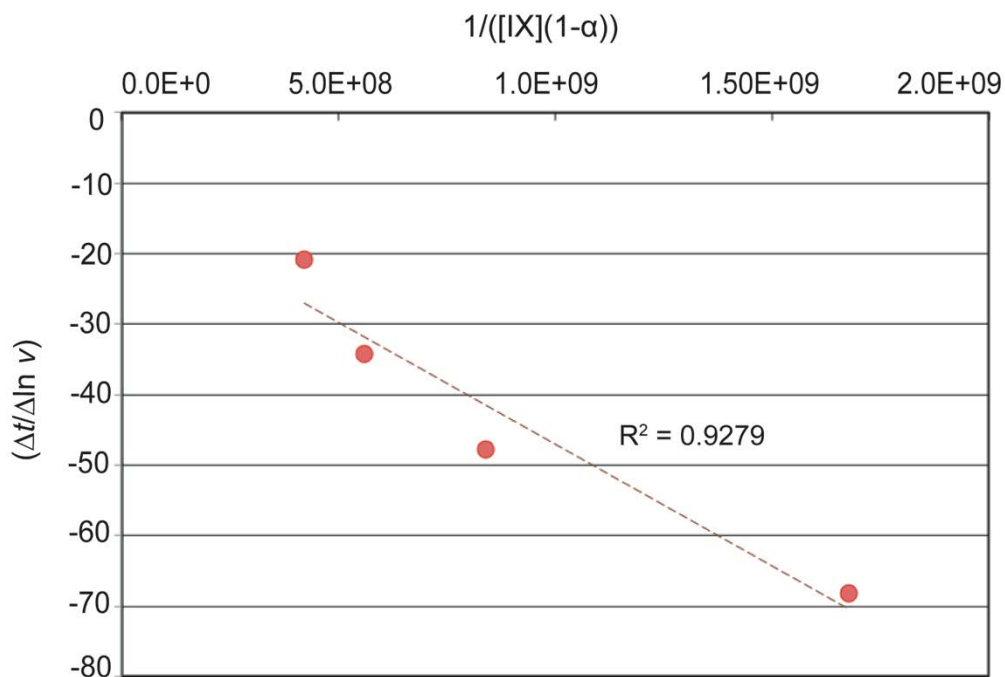


Figure A3.3. Double reciprocal plot for the inhibition of hAChE by racemic A-230. The slope was determined by the least-squares method and provides the absolute value of $(k_2/K_d)^{-1} = k_i$, while the y- and x-intercepts yield the value of $(k_2)^{-1}$ and $(K_d)^{-1}$, respectively.

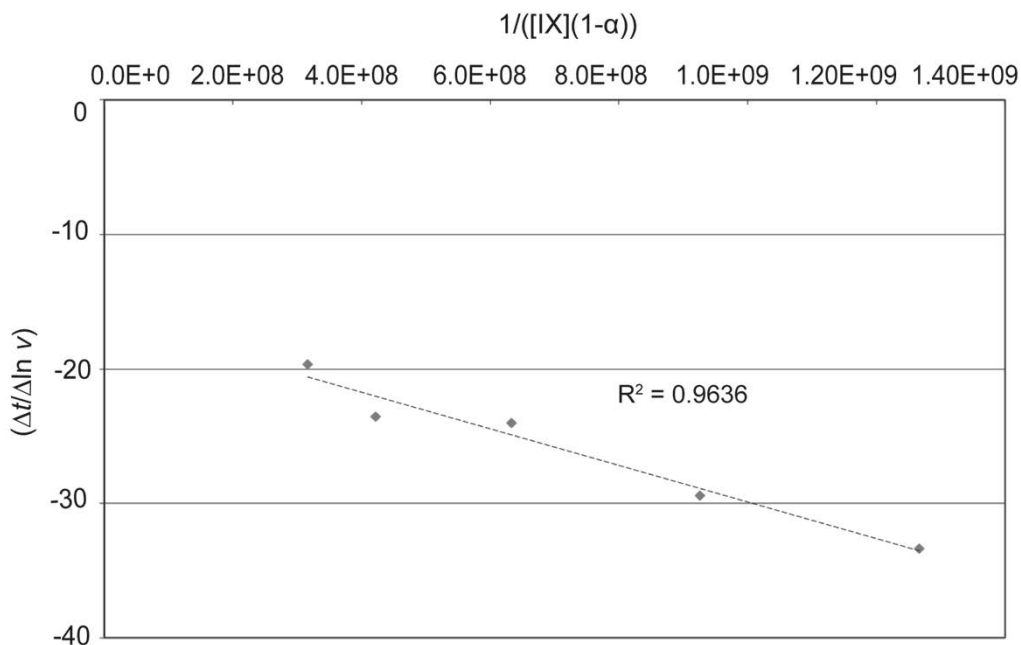


Figure A3.4. Double reciprocal plot for the inhibition of hAChE by racemic A-234. The slope was determined by the least-squares method and provides the absolute value of $(k_2/K_d)^{-1} = k_i$, while the y- and x-intercepts yield the value of $(k_2)^{-1}$ and $(K_d)^{-1}$, respectively.

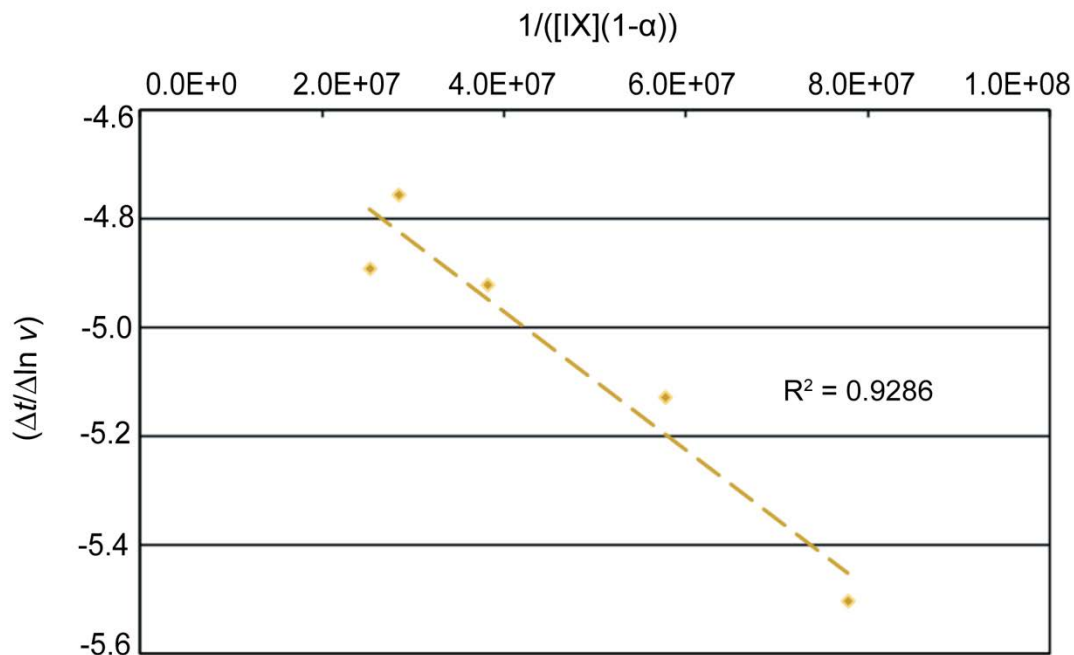


Figure A4.1. Double reciprocal plot for the inhibition of hAChE L380R/F535K by racemic VX. The slope was determined by the least-squares method and provides the absolute value of $(k_2/K_d)^{-1} = k_i$, while the y- and x-intercepts yield the value of $(k_2)^{-1}$ and $(K_d)^{-1}$, respectively.